Dosimetry for the MR-linac

Colophon:
This text was set using the freely available LaTeX 2_ε typesetting and text formatting system.

Cover:
An artistic impression of dose measurements in an MR-linac bore. The markings show that a obtaining a PhD is not always sunshine and roses, but if you put in some extra work the celebration is completely worth all the effort (and you deserve a party).

ISBN: 978-90-393-6369-0
Print: Gildeprint Drukkerijen

Dosimetry for the MR-linac

Dosimetrie voor de MR-linac

(met een samenvatting in het Nederlands)

Proefschrift

ter verkrijging van de graad van doctor aan de
Universiteit Utrecht op gezag van de rector magnificus,
prof.dr. G.J. van der Zwaan,
ingevolge het besluit van het college voor promoties
in het openbaar te verdedigen
op donderdag 9 juli 2015 des middags te 2.30 uur

door
Kimmy Smit
geboren op 29 mei 1986 te Alkmaar

Promotoren: Prof. dr. ir. J.J.W. Lagendijk
Prof. dr. B.W. Raaymakers

Contents

1 Introduction **3**
- 1.1 General introduction . . . 3
- 1.2 Radiotherapy treatment . . . 3
- 1.3 Imaging in radiotherapy . . . 5
- 1.4 MRI in radiotherapy . . . 7
- 1.5 MRI guided radiotherapy designs . . . 8
- 1.6 Radiation dose and the magnetic field . . . 10
- 1.7 Dosimetry . . . 10
- 1.8 Outline of the thesis . . . 16

2 Towards reference dosimetry for the MR-linac: magnetic field correction of the ionisation chamber reading **19**
- 2.1 Introduction . . . 21
- 2.2 Materials and methods . . . 23
- 2.3 Results . . . 30
- 2.4 Discussion . . . 34
- 2.5 Conclusion . . . 36

3 Relative dosimetry in a 1.5 T magnetic field: an MR-linac compatible prototype scanning water phantom **37**
- 3.1 Introduction . . . 39
- 3.2 Materials and methods . . . 40
- 3.3 Results . . . 45
- 3.4 Discussion . . . 49
- 3.5 Conclusion . . . 51

4 Performance of a multi-axis ionisation chamber array in a 1.5 T magnetic field **53**
- 4.1 Introduction . . . 54

4.2 Materials and methods 55
4.3 Results 60
4.4 Discussion 64
4.5 Conclusion 65

5 Performance of the STARCHECK^{TM} multi-axis ionization chamber array in a 1.5 T magnetic field 67
5.1 Introduction 69
5.2 Materials and methods 70
5.3 Results 72
5.4 Discussion 74
5.5 Conclusion 75

6 Integrated MegaVoltage portal imaging with a 1.5 T MRI linac. 77
6.1 Introduction 78
6.2 Methods 78
6.3 Results 81
6.4 Discussion 83
6.5 Conclusion 86

7 Performance of the ArcCHECK-MR QA system in a transverse 1.5 T magnetic field 87
7.1 Introduction 88
7.2 Materials and methods 88
7.3 Results 92
7.4 Discussion 94
7.5 Conclusion 97

8 The impact of beam transmission through a closed bore MRI on several beam characteristics for a prototype MR-linac system 99
8.1 Introduction 101
8.2 Materials and methods 102
8.3 Results 104
8.4 Discussion 107
8.5 Conclusion 109

9 Summary and general discussion 111
9.1 Reference dosimetry in the MR-linac 111

9.2 Radiation beam commissioning 115
9.3 Routine radiation beam quality assurance 115
9.4 Machine quality assurance 117
9.5 Patient treatment plan quality assurance 118
9.6 On-line quality assurance for adaptive radiotherapy 119
9.7 MR-linac design 121
9.8 Concluding remarks 122

References **123**

10 Publications **129**

11 Nederlandse Samenvatting **131**

12 Dankwoord **135**

1

Introduction

1.1 General introduction

In radiotherapy, the aim is to eradicate malignant cells by exposing them to a high dose of ionising radiation. The external beam radiotherapy used in this thesis uses high energy photons as ionizing radiation. When these photons encounter matter they can interact with the atoms in the matter. Given the mega voltage (MV) photon energy used in external beam radiotherapy and the tissue densities found in a human, the Compton effect is the dominant process of interaction. In the Compton interaction, the photon gives part of its energy to an electron in the electron cloud surrounding the nucleus of the atom. The photon is deflected and can travel on, the energy of the photon is diminished by dislodging the electron from its energy band and giving it kinetic energy. The freed electrons continue to interact with matter along their track until all their energy has been deposited by ionizing or exciting large molecules e.g. nucleic acid and proteins [1]. This may cause changes in the molecular structures which then affect the function and metabolism of the cells. When irreparable damage has been done, the body will eliminate the damaged cells. Most healthy cells have mechanisms to repair some radiation damage, but these mechanisms are often impaired in tumorous cells. This makes the tumorous tissues more sensitive to radiation damage than the healthy cells.

1.2 Radiotherapy treatment

During radiation treatment the goal is to maximize the dose to the tumour while minimizing the dose to the surrounding healthy tissue structures. To customize the dose delivered to the patient, typically a Computed Tomography (CT)

scan is made to visualize the patient anatomy, delineate relevant anatomical structures and to define the material properties of the tissue needed for the dose calculations [2]. Other imaging modalities, such as Magnetic Resonance Imaging (MRI) or Positron Emission Tomography (PET) can be used to aid the delineation. The delineation of specific organs and volumes is described in many reports and papers (e.g. [3] [4]). The radiation oncologist manually delineates the Gross Tumour Volume (GTV), which is the macroscopic part of the tumour. Tumours often have invisible microscopic invasions in the surrounding healthy tissue, therefore the GTV can be expanded to the Clinical Target Volume (CTV). To compensate for the geometric inaccuracies and uncertainties, the CTV is expanded with a margin to the Planning Target Volume (PTV). The margin between the CTV and the PTV depends on the radiation treatment modality used, the tumour site and the applied patient fixation [2] and [3]. Based on the delineation and a prescription, a treatment plan is derived that aims to deliver a designated dose to the PTV while minimizing the dose to the organs at risk (OARs). The dose calculations are performed by specific treatment planning systems using the density information obtained in the pre-treatment CT-scan. Since healthy tissues can recover from a radiation dose better than tumerous cells, the total dose is typically not delivered at once. Fractionated radiotherapy can be used to allow healthy tissue recovery between fractions of treatment and thereby decrease the normal tissue complication rate [5].

For example, prostate cancer is typically treated with 35 fractions of 2.2 Gy dose, spread out over a period of 7 weeks. Before delivery of each fraction, the patient is positioned on the treatment couch using fiducial markers, to reproduce the state of the anatomy represented by the pre-treatment CT. Inaccuracies that arise from patient positioning, organ motion during each fraction and between fractions, or changes in organ sizes; are included in the PTV margins. These margin sizes can be derived from population statistics [6] [7]. Although these margins prevent under-dosing of the tumour, it results in irradiation of regions containing mainly healthy tissue. This increases the risk of complications and thus limits the dose that can safely be delivered to the tumour.

1.3 Imaging in radiotherapy

Image guidance plays a vital role in reducing geometrical uncertainties associated with tumour shape and position ([8]). The purposes of imaging in relation to radiation treatment can be subdivided into the following 4 categories.

1.3.1 Treatment volume definition and characterisation

The ideal imaging modality for treatment volume definition and characterisation can depict the tumour in high contrast to its surroundings in 3D, with a high spatial resolution. Currently, several types of imaging are available in the pre-treatment phase. Examples of such modalities are, CT [9], positron emission tomography (PET) [10], single photon emission tomography (SPECT) [11], ultrasound [12] and magnetic resonance imaging [13]. In addition to being used for tumour positioning, these modalities may be employed to visualize tumour tissue characteristics, like cell density, hypoxia and perfusion. Based on this information the dose can be prescribed heterogeneously onto the tumour, giving a higher dose to high risk regions. By applying this 'dose painting' based on tumour characteristics the treatment of different kinds of malignancies may be improved [14] [15].

1.3.2 Setup correction

Online imaging of the patient in the treatment position can be used to verify patient setup and, wherever necessary, correct for daily variation to ensure a more accurate dose delivery. The resulting increase in precision enables reduction of the PTV margin and therefore decreases the dose to healthy tissues allowing for an increase of dose to the tumour volume. A flat panel imager, mounted on the accelerator gantry opposite to the MV radiation source, enables acquisition of MV transmission images [16]. This type of imaging is called portal imaging. Due to the high energy radiation used, this type of imaging has low soft tissue contrast. But it is possible to distinguish bones and implanted markers from soft tissue and match these markers to pre-treatment images [17] [18]. Another commonly available option is a kV radiation source that is mounted on the accelerator gantry, often orthogonal to the MV source, in combination with a flat panel detector on the opposite side of the patient. When the gantry is rotated around the patient, backprojection can be used to reconstruct a CT-like image [19] [20]. This type of imaging is called Cone Beam CT (CBCT) because of the fanned out kV radiation beam. CBCT facilitates set-up correction based on bony anatomy and fiducial markers, but the lower energy of the photons

allows for a limited use of soft tissue landmarks as well [20]. Less common modalities for set-up corrections are for example, ultrasound (mainly used for prostate treatment, e.g. [21]), radio frequency (RF) beacons e.g. Calypso 4D localization system (Varian Medical Systems, Palo Alto, CA, USA) and plain radiographs. The dynamic setup corrections can also be used to characterise the position of the tissues over a period of time and then predict the motion of the tumour during radiation treatment. This information can be used for updating the position verification protocols on a patient specific basis [22].

1.3.3 Treatment plan adaptation

Currently, the patient position is adapted to mimic the planned situation in the best possible way. For some situations the patient anatomy surrounding the tumour can change significantly for a longer period of time, e.g. due to patient weight loss, tumour shrinkage or inflamed tissue. In this case a new CT scan can be made on which a new treatment plan is calculated.

Ideally the treatment should always be adapted to the patient, not the other way around. However, this is a more challenging situation. A possible solution is to prepare a set of treatment plans for the most likely possible anatomies in preparation for the treatment, this approach is often called 'library of plans'. The online imaging provides images of the anatomy at the moment of treatment, the best suited treatment can then be selected from the pre-calculated and approved set [23] and [24]. The obvious drawback to this approach is the limited amount of available plans for anatomical variations. A more extensive planning set can minimize this problem, but will require increasing amount of resources. Alternatively, instead of preparing a set of plans in advance, a plan may be generated just before the fraction delivery takes place [25] [26]. This 'plan of the day' approach brings high flexibility and adaptivity but it puts high demands on the on-line imaging modalities and the timescale on which a full plan must be adapted or even created and approved.

1.3.4 Intra-fraction motion compensation

Radiation treatment for the abdominal organs such as kidney, pancreas, stomach and liver, but also for the lungs is hampered by respiratory motion since it causes the target to make a large semi-periodic movement. [27] and [28]. This motion can be accounted for by including a margin to the CTV, creating the internal target volume (ITV) or mid-ventilation solutions (e.g. [29]).

Additionally, motion compensated radiation delivery based on markers outside the patient's body, is available [30]. Using this technique gated radiation delivery can be used to minimize motion errors by employing the target position signal to switch the treatment beam on when the target is in a favourable location, and off when the target moves away from this position. This strategy has proven to be useful for margin reduction by diminishing target motion induced errors [31] but can cause patient throughput issues because the beam can be off for a large portion of the treatment time. Voluntary or involuntary breath hold, as well as audiovisual feedback [32] may be applied to optimise the patient throughput. A more time efficient option would be to shape the beam, using the multi leaf collimator (MLC) leaves, to follow the tumour motion [33] However, these methods are limited by the capacity of the external motion to predict the internal motion, and therefore by the accuracy of the motion/position models.

The previously mentioned Calypso 4D localization system can use implanted RF beacons for real time image guidance of the radiation treatment. This option increases the target position verification but still OARs cannot be visualised individually. The best solution is to depict the internal organ motion itself, during the course of the treatment. It would provide images of the internal patient anatomy with sufficiently high soft-tissue contrast to distinguish the tumour from its surrounding and to detect translations, rotation and deformations. These images must have an adequate spatial resolution and give a complete picture to compensate in all three dimensions. Temporal resolution must be sufficiently high to follow the process under investigation.

1.4 MRI in radiotherapy

Compared to other commonly used imaging modalities in radiotherapy, MRI provides superior soft-tissue contrast and thus a clear view of both tumorous tissue and OARs. Magnetic resonance (MR) sequences have numerous parameters that can be varied to obtain a multitude of contrasts reflecting various tissue characteristics, e.g. tissue oxygenation, cell density and tissue perfusion. Using MRI; volumetric 3D, 2D and 1D data sets can be obtained in arbitrary orientation. MR imaging uses no ionising radiation and can therefore be repeated without increasing the patient radiation burden. These properties make MRI an excellent image guidance candidate for the purposes stated in the pre-

vious section. Therefore, the integration of an MRI in a radiotherapy system has been an area of interest for some time.

Karlsson et. al. [34] have proposed a next door MRI scanner for the radiotherapy clinic; a 1.5 T MRI system installed close to a linear accelerator. Patients will be transported on a custom made trolley from the treatment couch to the imaging device and back. A more sophisticated solution (installed in Toronto, Canada) is the IMRIS inc. (Winnipeg, Canada) system [35]. This is a rail-mounted MRI system that moves in and out of the treatment room. Although having an in-room MRI scanner is an attractive concept, these systems do not provide feedback during radiation delivery. Raaymakers et. al. [36] have proposed to integrate a linear accelerator with an MRI scanner for online image guidance during radiotherapy.

1.5 MRI guided radiotherapy designs

There are several designs to integrate a radiotherapy modality with an MR imaging modality.

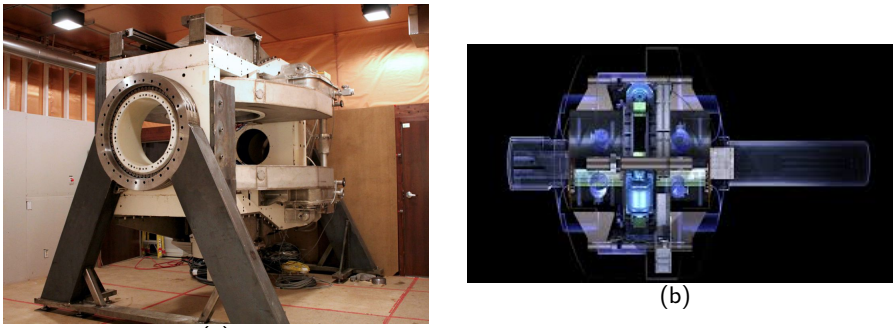

(a) (b)

Figure 1.1: Visualizations of the hybrid MR imaging and radiation treatment modalities developed by the Cross Cancer institute (a) and Viewray.

The team at the Cross Cancer Institute has designed a hybrid system that comprises a 6MV linac mounted on the open end of a biplanar MRI magnet, with both the linac and magnet sited on a gantry that rotates around the patient. In this "rotating-biplanar" geometry, the magnetic field vector is fixed with respect to the beam direction. The first prototype, composed of a biplanar 0.2

T MR system with a 27 cm square opening coupled to a 6 MV linac, was used for proof of principle [37]. In 2013, an upgraded version comprised of a 0.5 T MRI and a 60 cm diameter opening was installed [38], this set up is visulalized in figure 1.1(a).

Viewray (Viewray, Ohio, United States of America) has developed the MRIdian system. This system combines 3 Cobalt-60 teletherapy heads, each with their own multi leaf collimator (MLC), with a split-magnet 0.35T MRI system [39]. This system, figure 1.1(b) has been in clinical use since September of 2014.

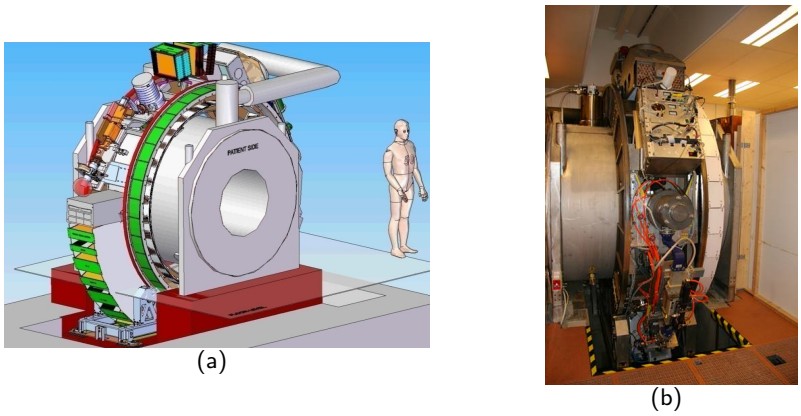

(a) (b)

Figure 1.2: Visualizations of the hybrid MR imaging and radiation treatment modality (MR-linac) developed by the University Medical Center Utrecht. A schematic visualization of the MR-linac (a) and a picture of the prototype set up (b).

The UMC Utrecht in collaboration with Elekta (Elekta AB, Stockholm, Sweden) and Philips (Philips Medical Systems, Best, The Netherlands) have given proof of concept of the MR-linac, visualized in figure 1.2, a 6 MV linear accelerator combined with a closed bore 1.5 T MRI scanner [40]. The MRI scanner is optimized to allow beam passage to the isocenter of the MRI scanner with a maximum field size of 24 cm in the feet head direction. It can obtain MR images of similar quality as diagnostic 1.5 T MRI scanners simultaneously delivering radiation. Recently a new design of the Utrecht MR-linac has been installed. This design integrates a 8 MeV linear accelerator with a 1.5 T MRI scanner.

1.6 Radiation dose and the magnetic field

The combination of an MRI scanner with a irradiation modality creates the opportunity for on-line image guided radiotherapy, but the fact that the isocenters coincide means the radiation dose will be delivered in a magnetic field. The photons in the irradiation beam will not be affected by the magnetic field because they are uncharged energy packets. However, the photons release a cascade of secondary electrons. When in a magnetic field, these moving charged particles will be influenced by the Lorentz force. This creates a curvature in the track of the electrons [41]. Since the radiation damage is done throughout the entire electron track, the dose distribution will be affected by the presence of a magnetic field [42] [43] [44].

Monte Carlo simulations have been performed to predict the influence of the magnetic field on the dose distribution for a transverse magnetic field of 0.35 T [45] or 1.5 T [46] [47] or a magnetic field parallel to the irradiation beam [48]. These simulations found that the influence of the magnetic field is largest for the longest electron track i.e. the lowest density medium. In clinical practice this means the effect is most noticeable for tissue-air interfaces. Without a magnetic field the electrons generated in the last few centimetres of tissue can leave the body. When inside the 1.5 T magnetic field of the MR-linac, the electron track in air is long enough to facilitate a full 180° turn. This causes the electrons to return to the tissue and deposit their energy, the so-called electron return effect (ERE) described by Raaijmakers et al. [41].

1.7 Dosimetry

Dosimetry at a clinical radiotherapy department is generally subdivided into two categories. Reference dosimetry, which characterizes the 'absolute' amount of dose given at a specific point of interest, and relative dosimetry which investigates the dose distribution relative to a reference point. A combination of these two allow determination of the 'absolute' dose for each measured point.

1.7.1 Reference dosimetry

Reference dosimetry is nearly always performed with an air filled ionization chamber. This ionization chamber measures the amount of ionizations in the measuring volume by capturing the charged particles that are produced in the ionizations. In order to capture the charged particles, an ionization chamber has two electrodes with a voltage difference between them. An electrometer

can be used to read the number of electrons (i.e. electric current) that are collected by the ionization chamber.

There are widely used (inter)national protocols to calculate the deposited dose from the ionization chamber reading [49] [50]. All protocols are based on the same principle where a national standards laboratory uses a calibration set-up. In this set-up absolute dosimetry can be performed, e.g. using calorimetric measurements, to determine the absolute amount of energy deposited in the volume of interest. A secondary standard ionization chamber, provided by a radiotherapy institute, will be calibrated in this set-up. Since the exact amount of dose applied is known the calibration factor for the secondary standard can be calculated. The secondary standard is then used at the institute to calibrate all ionization chambers used for reference dosimetry measurements in clinical practice.

1.7.2 Reference dosimetry and the magnetic field

In previous paragraphs we have explained that the influence of the magnetic field on the charged particle track is increased for low density materials. Therefore we expect the dose response of an air filled ionization chamber to be influenced by the magnetic field. Meijsing et. al. [51] have shown that the influence of the magnetic field on the ionization chamber reading is directly related to the number of ionized particles entering the measuring volume and the average track length of the particles inside the sensitive volume. With this in mind, we can hypothesize the factors that determine the influence of the magnetic field on the ionization chamber dose response.

- Ionization chamber geometry
- Magnetic field strength
- Orientation of the ionization chamber relative to the magnetic field and the irradiation beam

The track length of the charged particles is influenced by the magnetic field strength and the ionization chamber geometry. The orientation of the ionization chamber relative to the B-field and the irradiation beam determines the number of particles in the ionization chamber and further influences their average track length inside the air cavity of the ionization chamber.

1.7.3 Relative dosimetry

The goal of relative dosimetry is to measure the dose in many positions, normalized to the dose at a reference point. Relative dosimetry can be performed

using a wide variety of methods using a wide variety of detectors. Firstly, a single detector can be moved e.g. in a scanning water phantom [52], to measure the dose in many positions. For this method the dose distribution needs to remain stable for the duration of the measurement. Scanning water phantoms simulate the treatment conditions well because they generally have a large volume with a density close to human tissues.

Another method is to use many detectors at once. These detectors can be arranged in one line, e.g. for the LA-48 (Physikalische Technische Werkstätten, Freiburg, Germany) or in 2D on a panel. Some relative dosimetry panels use a star formation to measure two perpendicular dose profiles and two diagonal profiles at once e.g. IC PROFILER^{TM} (Sun Nuclear Corporation, Melbourne, FL USA) or the STARCHECK^{TM} (Physikalische Technische Werkstätten, Freiburg, Germany). The detectors can also be distributed evenly over a surface on the panel e.g. the Matrixx (IBA Dosimetry, Schwarzenbruck, Germany) and the Octavius detector series (Physikalische Technische Werkstätten, Freiburg, Germany). The detectors can also be arranged in a 3D configuration in a phantom e.g. the ArcCHECK (Sun Nuclear Corporation, Melbourne, FL USA) or the Delta^4 phantom (Scandidos AB, Uppsala, Sweden).

Relative dosimetry is vital for checking and calibrating critical radiation treatment characteristics.

1.7.4 Descriptors of dose distribution

Two types of common dose profiles measured during radiation beam commissioning will be discussed into more detail below.

Percentage depth dose

The percentage depth dose (PDD) profile shows the development of the dose over the depth of the phantom [1]. This profile is usually measured in a homogeneous phantom on the central axis of the irradiation beam, the central beam axis. The measurement results are then normalized to the maximum measured dose. The energy spectrum of the irradiation beam is verified using this type of profile measurement. Several important defining properties of the profile will be explained.

From the surface of the medium to the depth where the maximum dose is reached (d_{max}) the dose increases quickly. Photons are interacting with

the matter and releasing electrons which in turn deposit their energy to the medium. In this region there is no charged particle equilibrium and the dose gradient is relatively steep. After the d_{max} the dose steadily decreases due to beam attenuation and divergence.

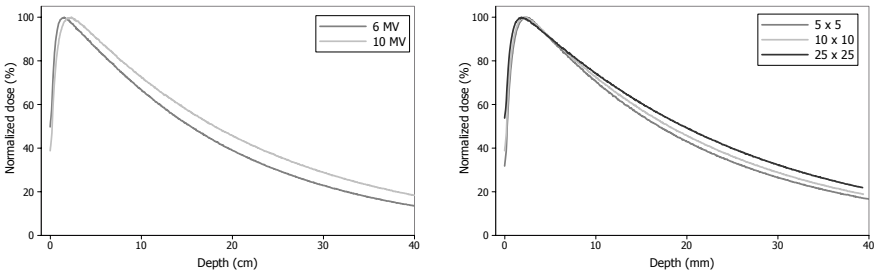

(a) (b)

Figure 1.3: Percentage depth dose profiles for several radiation beam energies (a) and field sizes (b).

Figure 1.3(a) shows PDD profiles for the same irradiation field size for several beam energies. For a high irradiation energy the photons are less likely to interact with the medium, this results in a larger d_{max} and a less steep slope of the profile after d_{max}. Additionally the irradiation field size influences the PDD shape, figure 1.3(b) a smaller field will have a steeper slope because in smaller fields more of the photons are scattered away from the central beam axis.

The SSD in the MR-linac is 143.5 cm, instead of the standard 100 cm, this creates a difference in beam divergence at the point of measurement. This effect is especially noticeable in the PDD measurements, where it creates a less steep decline of the PDD after the dose maximum.

Lateral dose profiles

The variation of dose occurring on a line perpendicular to the central beam axis at a certain depth is known as the lateral dose profile. The measured doses are normalized to the maximum measured dose. Lateral dose profiles can be measured in any direction perpendicular to the central beam axis. Generally the dose profiles are measured along the two principal directions, the resulting dose profiles are called inline and crossline profiles. The lateral dose profiles can be used to determine the beam symmetry, the ratio of dose at a pair of

points located opposite each other from the central beam axis. The AAPM recommends that the dose at these two points should vary by less than 2% Some clinical systems include a flattening filter, a cone shaped high density metal component, that creates a homogeneous dose throughout the field for a specific measurement depth and field size. For these types of systems the lateral dose profile can be used to determine the radiation beam flatness, the variation in the beam strength across the central part of the beam. In the MR-linac the flattening filter is omitted to increase the delivered dose and decrease the scatter contribution from the radiation head.

There are typically three parts in a lateral dose profile:

- The central region which is usually flat and generally includes doses over 80% of the central beam axis
- The penumbra region where dose falls off rapidly at the beam edge, between a dose of 20-80% of the central beam axis
- The umbra region where dose is minimal (under 20% of the central beam dose)

Examples of dose profiles for radiation beams with flattening filters as measured on a clinically used linac, are presented in figure 1.4

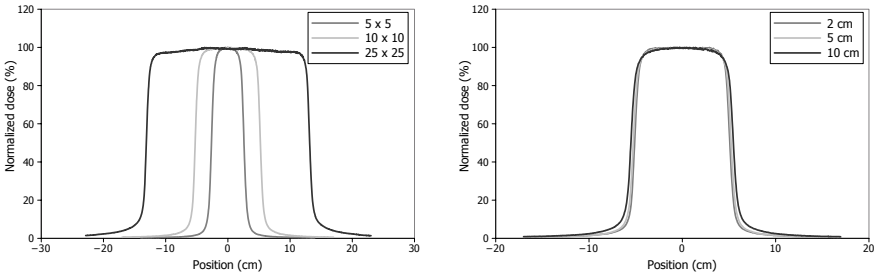

Figure 1.4: Lateral dose profiles for several different field sizes (a) and a fixed field size of 10 x 10 cm^2 for several measurement depths (b).

Since the higher energy photons and electrons are more likely to travel forward [1], the energy spectrum changes along the lateral dose profile, with the low energy photons more prominently present in towards the edges of the field. Since lower energy photons are more likely to interact with matter, the field shape becomes more rounded with increasing depth. The penumbra region of the

lateral dose profile gives information about the linac geometry, the shape and location of the MLC leaves and the spot size of the accelerated electron beam on the target. The dose in the umbra region is determined by the scatter in the setup. This scatter can originate in the radiation head, or the patient/phantom.

1.7.5 Radiation beam commissioning

Radiation beam commissioning is executed prior to using a linac for clinical practice. During this extensive measurement process the beam characteristics e.g. percentage depth dose profiles and lateral dose profiles, that characterize the dose distribution [53] are investigated. The beam characteristics are then imported into the treatment planning system to be taken into account in the calculations of the patient treatment plan. During the radiation beam commissioning, many of the dosimetry methods are used. The scanning water phantom is used extensively for this type of measurements, since this is the most versatile of the relative dosimetry methods.

1.7.6 Routine radiation beam quality assurance

Quality assurance (QA) in radiation therapy includes those procedures that ensure a consistent and safe fulfilment of the dose prescription to the target volume, with minimal dose to normal tissues and minimal exposure to personnel [54] [55]. During this procedure several PDD's and lateral profiles are measured. These profiles can be compared to the profiles acquired during beam commissioning and implented into the treatment planning system. If the deviation between the profiles is too large e.g. due to a decrease in field symmetry or beam energy, the linac settings can be adjusted accordingly.

Routine radiation beam quality assurance is performed regularly [56], e.g. every 6 weeks at our department . For a quick radiation beam check an ionization chamber array panel can be used. This panel is easy and quick to set up and gives instant information about the lateral dose profiles in all array orientations. When a more extensive test needs to be performed, e.g. PDD measurements or lateral dose profile measurent at several measurement depths, a scanning water phantom can be used. This phantom requires more set-up time, but is more versatile in the measurement options than the ionization chamber array panels.

1.7.7 Patient treatment plan quality assurance

Before commencing a radiation treatment the planned dose can be compared to the measured dose for each individual patient treatment plan, in a process

called patient treatment plan quality assurance. For this test the patient plan is delivered to a phantom in which dose detectors are positioned. The phantom has been implemented into the treatment planning system, to enable direct evaluation of the dose delivered to each location in the phantom. The measured dose is compared to the dose predicted for each location by the treatment planning system.

Conventionally, this process was done using a film placed between a slab phantom. This method provides detailed dose distribution in a single plane, but the process is labour intensive. New dedicated phantoms, e.g. ArcCHECK, Delta^4 or the Octavius 4D can measure the dose in many different locations allowing for a 3D evaluation of the radiation dose. Since these phantoms can be connected directly to a computer, the process is much less labour intensive than the film based process. Additionally, radiation sensitive gels can be used for 3D dose distribution measurements.

1.8 Outline of the thesis

The purpose of this thesis is to investigate the influence of the MR scanner on dosimetry for the radiation modality, and to investigate the possible solutions for the dosimetric measurements discussed in section 1.7.

Chapter 2 investigates the feasibility to use a standardized national reference dosimetry protocol for the MR-linac. Firstly, the feasibility of using an ionisation chamber in an MR-linac was assessed by investigating possible influences of the magnetic field on an NE2571 Farmer type ionisation chamber characteristics: linearity, repeatability, orientation in the magnetic field; and AAPM TG51 correction factor for voltage polarity and ion recombination. Secondly, the influence of the permanent 1.5 T magnetic field on the NE2571 chamber reading was quantified.

Chapter 3 presents the design and performance of a prototype MR-linac compatible scanning water phantom. In order to use a scanning water phantom, the performance of air filled ionisation chambers in the magnetic field must be characterised. The performance of the scanning water phantom will be validated at a clinical set-up in a 0 T magnetic field. Inside the MR-linac set-up, the performance of the MR-linac scanning water phantom is validated using radiographic film.

Chapter 4 investigates the performance of the IC PROFILER^{TM}, a multi-axis ionisation chamber array, in a 1.5 T magnetic field. The influence of the magnetic field on the IC PROFILER^{TM} reproducibility, dose response linearity, pulse rate frequency dependence, power to electronics, panel orientation and ionisation chamber shape are investigated. IC PROFILER^{TM} dose profiles were compared with film dose profiles obtained simultaneously in the MR-linac.

Chapter 5 investigates the feasibility of using the STARCHECK^{TM} multi-axis ionisation chamber array panel, in a transverse 1.5 T magnetic field. The method of investigation is similar to that used for the IC PROFILER^{TM} in chapter 4. The investigated characteristics are short term reproducibility, dose response linearity, accuracy of output factor measurements and the influence of the magnetic field on a purposefully introduced misalignment. As a validation of feasibility, STARCHECK^{TM} measurements were compared with film measurements simultaneously obtained in the MR-linac.

Chapter 6 investigates the feasibility of using an MV portal imager in an MR-linac set-up. MV imaging integrated with the MR-linac has the potential to provide an independent position verification tool, a field edge check and a calibration for alignment of the coordinate systems of the MRI and the accelerator. A standard aSi MV detector panel is added to the system and both qualitative and quantitative performance are determined.

Chapter 7 examines the performance characteristics of the ArcCHECK-MR QA system in a transverse 1.5 T magnetic field. This ArcCHECK-MR system is used for QA of patient treatment plans. To this end, the short-term reproducibility, dose linearity, dose rate dependence, field size dependence, dose per pulse dependence and inter-diode variation of the ArcCHECK-MR diodes were evaluated on a conventional linac and on the MR-linac.

Chapter 8 investigates the influence of the closed bore MRI scanner structures on several radiation beam characteristics for squared fields of sizes 5.6, 9.8 and 23.8 cm^2. The MR-linac set-up will be implemented into a Monte Carlo simulation environment facilitating dose profile simulations in a 1.5 T magnetic field with and without MRI scanner structures. The results of the Monte Carlo simulations will be validated against scanning water phantom measurement results obtained in the MR-linac for the PDD and lateral profiles.

2

Towards reference dosimetry for the MR-linac: magnetic field correction of the ionisation chamber reading

This chapter has been published as:
K. Smit, B. van Asselen, J.G.M. Kok, A.H. Aalbers, J.J.W. Lagendijk and B.W. Raaymakers. Towards reference dosimetry for the MR-linac: magnetic field correction of the ionization chamber reading. *Physics in Medicine and Biology*. 2013. **58**(17):5945–57.

Abstract
In the UMC Utrecht a prototype MR-linac has been installed. The system consists of a 6 MV Elekta (Crawley, UK) linear accelerator and a 1.5 T Philips (Best, The Netherlands) Achieva MRI system. This paper investigates the feasibility to correct the ionisation chamber reading for the magnetic field within the dosimetry calibration method described by [50].
Firstly, the feasibility of using an ionisation chamber in an MR-linac was assessed by investigating possible influences of the magnetic field on an NE2571 Farmer type ionisation chamber characteristics: linearity, repeatability, orientation in the magnetic field; and AAPM TG51 correction factor for voltage polarity and ion recombination. We found that these AAPM correction factors for the NE2571 chamber were not influenced by the magnetic field.
Secondly, the influence of the permanent 1.5 T magnetic field on the NE2571 chamber reading was quantified. The reading is influenced by the magnetic field, therefore a correction factor has been added. For the standardised setup used in this paper, the

NE2571 chamber reading increases by 4.9% ($\pm$ 0.2%) due to the transverse 1.5 T magnetic field.
Dosimetry measurements in an MR-linac are feasible, if a setup specific magnetic field correction factor ($P_{1.5\ T}$) for the charge reading is introduced. For the setup investigated in this paper, the $P_{1.5\ T}$ has a value of 0.953.

2.1 Introduction

The University Medical Center Utrecht, The Netherlands, has demonstrated proof of concept of the MR-linac [40], visualised in figure 2.1. The MR-linac is an integrated system consisting of a 1.5 T Philips Achieva MRI scanner with a closed bore magnet and an Elekta 6 MV linear accelerator. The goal of such integration is to use the soft-tissue contrast of MR-imaging for high precision image-guided radiotherapy to be able to escalate the dose to the tumour while sparing surrounding healthy tissues [57]. Therefore the setup allows simultaneous, independent irradiation and imaging of the patient. In this design, the irradiation beam axis is perpendicular to the permanent 1.5 T B_0 field of the MRI scanner, with the isocentre at 143.5 cm from the source, inside the bore of the imaging modality. The MR-linac uses an Elekta Agility based MLC, consisting of 160 leaves, with a projected leaf width of 7 mm at the isocentre.

In clinical practice, clinical reference dosimetry measurements of linear accelerators are performed by measuring the dose with a calibrated air-filled ionisation chamber, in a reference measurement setup. The dose delivered at the point of measurement for a certain beam quality (D_w^Q), can then be calculated from the detector reading using equations 2.1 and 2.2.

Firstly, the raw measurement value (M_{raw}) is corrected for several parameter variations using equation 2.1.

$$M = M_{raw} \times P_{TP} \times P_{ion} \times P_{pol} \times P_{elec} \qquad [C] \tag{2.1}$$

The M_{raw} value is corrected for variations in ambient conditions including temperature and air pressure (P_{TP}), and non-ambient influences including incomplete ion collection (P_{ion}), polarity effects (P_{pol}) and electrometer calibration factor (P_{elec}).

The corrected measured value, in C, is converted to dose using an absorbed-dose calibration coefficient obtained for reference conditions in a ^{60}Cobalt beam ($N_{D,w}^{^{60}Co}$ [Gy/C]). The quality conversion factor k_Q converts the absorbed-dose to water calibration coefficient for the ^{60}Co beam into the calibration coefficient for an arbitrary beam of quality Q.

$$D_w^Q = M k_Q N_{D,w}^{^{60}Co} \qquad [Gy] \tag{2.2}$$

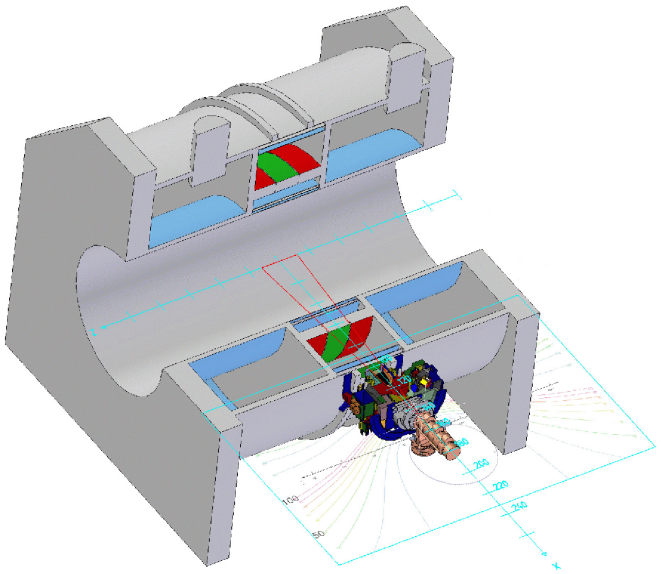

Figure 2.1: A schematic overview of the MR-linac prototype setup. The linear accelerator is shown horizontally next to the MRI. The electron gun and part of the waveguide are positioned in a low magnetic field zone around the MRI. Transmission of the radiation through the closed bore MRI is facilitated by a beam portal.

Equations 2.1 and 2.2 were taken from [50] a clinical reference dosimetry protocol based on the use of ionisation chambers calibrated in terms of absorbed dose to water in a ^{60}Co beam. Similar equations can be found in the IAEA report 398 [58] or in reports of national codes of practice for dosimetry [49]. Other reports (e.g. [59]) use protocols with ionisation chambers calibrated in linear accelerator beams, this does not change the structure of the protocols.

In this study we investigate the influence of the magnetic field on the response of traceable calibrated ionisation chamber by applying the dose formalism as described by the AAPM [50] and given in equation 2.2. For the calibrated dosimeter (ionisation chamber combined with an electrometer) used in this feasibility study the product $N_{D,w}^{^{60}Co}k_Q$ is constant for any given photon beam. Any change in the response of the dosimeter may be treated as a change in the charge reading M (see equation 2.1).

Although the photon beam is not affected by the magnetic field, the secondary electrons depositing the dose are deflected by the Lorentz force when travelling in a magnetic field. The effect of the deflected electrons [41] [42] is most noticeable at tissue-air interfaces.

In a homogeneous medium, where there is a charged particle equilibrium, the dose is affected little by the presence of a magnetic field [36].

However, an air-filled ionisation chamber used for dose measurements introduces a small air cavity inside the surrounding wall material and the phantom material. The effect of the magnetic field on the electrons will not be negligible inside the air cavity. Since the M_{raw} depends directly on the number of electrons entering the chamber and the electron track length, the dose response of the ionisation chamber is expected to be influenced by the magnetic field [51].

Firstly, we will assess the impact of the magnetic field on the performance of the NE2571 chamber and the electrometer. This measurement set will focus on the linearity and repeatability of the dosimeter as well as the influence of the ionisation chamber orientation, with respect to the magnetic field, on the response of the chamber.

When correct functioning of the ionisation chamber is established, the influence of the magnetic field on correction factor P_{ion} and P_{pol} mentioned in equation 2.1 will be investigated.

Finally, we will investigate the influence of the magnetic field on the ionisation chamber response. We will introduce a magnetic field correction factor for the ionisation chamber reading within the context of the previously described protocol.

2.2 Materials and methods

Unless mentioned otherwise, the following standardised measurement descriptions apply. Measurements were performed with NE2571 Farmer type ionisation chambers (NE Technology Limited, Berkshire RG7 5PR, England). The general measurement setup is visualised in figure 8.1. In this figure points A, B and C are located on the surface of the respective phantoms.

The ionisation chambers were placed in a 30 x 30 x 20 cm^3 polystyrene slab phantom with a mass density of 1.03 g/cm^3. The point of measurement was

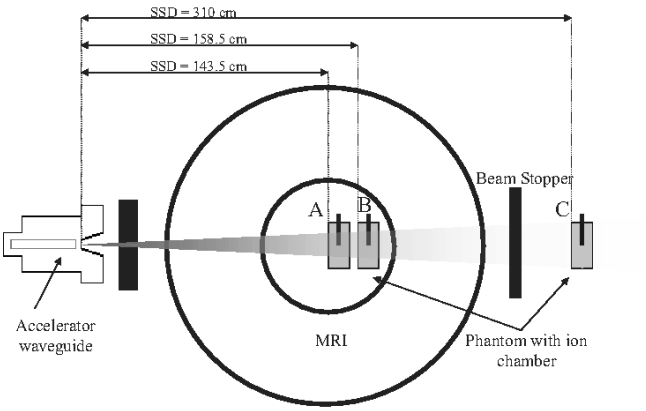

Figure 2.2: A schematic overview of the general measurement setup in the MR-linac. Three locations are used for measurements. Point A and B are situated in the bore of the MR-linac at a 1.5 T magnetic field with SSD of 143.5 cm and 163.5 cm, respectively. Point C is located behind the MR-linac where the magnetic field is approximately 0 T and the SSD is 310 cm.

located in the centre of the phantom at a depth of 10 cm to attain electron equilibrium for the 6 MV irradiation beam and rule out electron contamination.

Irradiation took place along the horizontal axis, perpendicular to the detector axis. As will be described in section 5.3.4 this orientation, with the detector axis perpendicular to the magnetic field, is the preferable measurement orientation. The ionisation chamber phantom was placed at point A, the front surface of the phantom is placed at the isocentric plane, with a source to surface distance (SSD) of 143.5 cm. When a reference chamber was included, this chamber would be placed in the phantom at point B or C. Point C was inside the region around the MR-linac where the magnetic field strength was lower than 1 mT when the MR-linac was at operational magnetic field strength [40].

A field size of 9.8 x 9.8 cm^2 at the isocentric plane was used and the applied number of monitor units (MU) are mentioned per measurement type. The dose per 100 MU is approximately 0.33 Gy at the depth of the maximum dose, for

this described measurement setup.

In total four ionisation chambers of the same type were investigated: serial number (sn) 1315, 2854, 3626 and 3628 were investigated. An Unidos E electrometer (PTW, Freiburg GmbH, Germany) was used to measure the charge collected, in nC. Before commencing any of the measurements, the ionisation chambers were pre-irradiated with a dose of 1 Gy and the ionisation chamber and electrometer were left in stand-by mode for at least 10 minutes. Leakage measurements were performed regularly during measurements. When leakage during the measurement exceeded 0.1% of the estimated measurement value, a new leakage measurement was obtained and used for signal correction. Results obtained between leakage measurements were then discarded.

Each of the described measurements were performed with and without the 1.5 T magnetic field, to determine the influence of the magnetic field.

2.2.1 Linearity and repeatability

For accurate dose measurements it is essential that the ionisation chamber has a steady response that directly reflects the applied dose. There are two main aspects to this. Firstly, the ionisation chamber readout should be proportional to the applied dose, this will be referred to as the linearity of the system. Secondly, the repeatability of the system should be determined.

The linearity of the system was investigated for the range from 200 to 1000 MU in steps of 200 MU. A total of 4 measurements were performed per step, the average readout value is determined per step and normalised to a reference of 200 MU.

To determine the repeatability, a series of 10 measurements were performed consecutively. For each measurement 200 MU was applied to the ionisation chamber. The repeatability is defined as the relative standard deviation of a measurement series and can be calculated from the measurements using equation 2.3.

$$Repeatability = \frac{100}{\overline{R}} \sqrt{\sum_{i=1}^{n} \frac{(\overline{R} - R_i)^2}{n-1}} \tag{2.3}$$

In this equation R_i represents a single readout value, and $\overline{R}$ the average readout value of all measurements in the series (n).

2.2.2 Influence of ionisation chamber orientation

[51] showed that orientation of the NE2571 chamber with respect to the magnetic field of the MR-linac influences the dose response. When a small change in ionisation chamber orientation significantly influences the dose response, it would make the correct positioning of the setup more critical in a transverse 1.5 T magnetic field. Therefore the influence of orientation on the ionisation chamber (sn 1315) reading in the MR-linac, was investigated. The optimal chamber orientation, for which a change in orientation had little effect on the chamber reading, was determined from these results.

An in-house developed PMMA phantom, see figure 2.3, was used for these measurements. The phantom consisted of a squared 8 x 8 x 8 cm^3 mounting part and an 7.5 cm high cylinder with a diameter of 7 cm. A cavity with the exact shape of the ionisation chamber was carved out of the PMMA cylinder. The effective point of measurement of the detector, calculated using a method described by Tessier et. al [60] to be at 1.5 mm, resided in the centre of the phantom at a depth of 4 cm. This phantom allowed rotation around the effective point of measurement of the ionisation chamber. For these measurements a field size of 23.8 x 23.8 cm^2 was used.

Rotation took place around the central beam axis (CAX) of the irradiation beam. During this rotation, irradiation orientation remains constant, therefore any change in dosimeter response will be due to a change in orientation with the magnetic field. The orientation was varied between 0° and 180° in steps of 10°. The 0° and 180° orientations represented the positions where the axis of the ionisation chamber was parallel to the B_0 magnetic field.

2.2.3 Ion recombination

The factor P_{ion} in equation 2.1 corrects for the incomplete ion collection in the ionisation chamber. Because the magnetic field influences the trajectory of ions, ion collection efficiency may be influenced by the magnetic field.

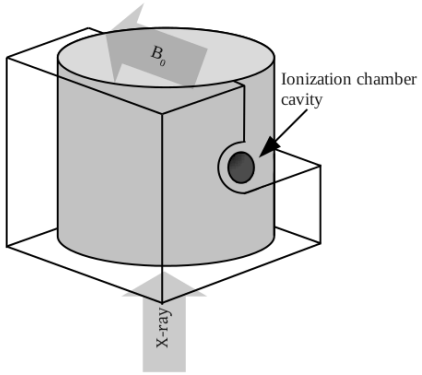

Figure 2.3: A schematic view of the PMMA phantom used for measuring the influence of the orientation in a magnetic field on the ionisation chamber reading. A cylindrical insert allows for rotation around the central beam axis (CAX). The phantom is visualised in the 0° orientation. The direction of the magnetic field(B_0) and irradiation (γ) are included.

The ion collection efficiency of an ionisation chamber can be determined by varying the polarising voltage difference between the two electrodes of the ionisation chamber [61]. The polarising voltage was varied from 25 V to 400 V. In the lower voltage range, from 25 V to 150 V, the polarising voltage was varied in steps of 25 V to increase accuracy. From 150 V to 400 V the polarising voltage was increased in steps of 50 V. After each alteration of the voltage, the setup was left idle for at least 15 minutes to reach an equilibrium before commencing a measurement series of 5 measurements with that polarising voltage.

The correction factor for incomplete ion recombination can be calculated using equation 2.4 ([50]). Where V_H and V_L represent the high (250 V) and low (50 V or 25 V) values of the polarising voltages, and M^H and M^L the ionisation chamber readings for the respective polarising voltages.

$$P_{ion}(V_H) = \frac{1 - V_H/V_L}{M^H_{raw}/M^L_{raw} - V_H/V_L} \tag{2.4}$$

A reference chamber was positioned at point B (see figure 8.1). The behaviour of the ion recombination in a magnetic field will be investigated for ionisation chamber (sn 3628).

2.2.4 Polarity corrections

The influence of the voltage polarity on the measured value is accounted for in equation 2.1 by the correction factor P_{pol}. When the polarising voltage of an ionisation chamber is reversed, the electrons released in the sensitive volume of the ionisation chamber will be attracted to the other electrode. The magnetic field influences the path of the electrons, and can therefore influence the polarity correction factor.

The influence of polarity on the dose response of the ionisation chamber was measured in two series of 10 measurements each. For each series the polarising voltage was reversed and the setup was left long enough to equilibrate before starting measurements. The average of each of the two series is determined as well as the maximum spread within a series.

The correction factor for the polarising voltage can then be calculated using equation 2.5, where M^{+}_{raw} and M^{-}_{raw} are the chamber readings obtained when the polarising voltage of the ionisation chamber is positive or negative, respectively. The chamber reading M_{raw} is the collected charge for the voltage polarity applied to the ionisation chamber during the measurement.

$$P_{pol} = \left| \frac{M^{+}_{raw} - M^{-}_{raw}}{2M_{raw}} \right| \tag{2.5}$$

2.2.5 Photon fluence distribution

The stray magnetic field of the MRI can affect the electron path inside the waveguide of the accelerator, which in turn creates a difference in energy fluence and therefore in the dose distribution. In a perfect implementation of the setup described in figure 8.1, the primary ionisation chamber (point A) and reference chamber (point C) will be perfectly aligned on the central axis. In this case the reference ionisation chamber will correct for changes in output of the linac without being influenced by changes in energy fluence.

However, because of the distance and structures between the primary and reference ionisation chambers, a possible misalignment can arise. This misalignment

can influence the determination of the magnetic field correction factor if there is a difference in fluence between the situations with and without the magnetic field. In this section we will investigate the sensitivity for a lateral misalignment up to $\pm$0.5 cm at isocentric distance.

To detect possible differences in 2D dose distribution, film measurements were performed with and without the presence of a magnetic field. For these measurements two Gafchromic EBT2 (ISP, Wayne, USA) films were wedged between two polystyrene plates of 29.8 x 29.8 x 3.75 cm^3. The phantom was positioned at point A in the setup in figure 8.1 at an SSD of 143.5 cm and a measuring depth of 3.75 cm.

The films were scanned 24 hours after irradiation, on an Epson 10000XL flatbed scanner (Epson Seiko Corporation, Nagano, Japan) using the associated software Epson Scan v3.04s.

To improve the reproducibility of the film placement, a dark template was fitted to the scanner surface. Each film was scanned prior to the irradiation to facilitate individual background correction. In-house developed software was used for analysis and correction of the image. The red-channel of the optical density (OD) images was used for dose information and the blue signal for local polymer density correction. A polynomial fit of a calibration curve was used to convert the OD images to dose, a second polynomial fit of OD values at lateral positions corrected for the lateral scanner effect. Using this method, the precision of the scanner setup was estimated at 0.2% by performing 10 scans, including re-positioning and difference of the scanner warm up, of the exact same film.

2.2.6 Total influence of the 1.5 T magnetic field

[51] have shown that the magnetic field influences the response of an NE2571 ionisation chamber. If all ionisation chamber characteristics are favourable in the magnetic field, a magnetic field correction factor ($P_{1.5\ T}$) can be determined by calculating the ratio between the ionisation chamber reading with and without magnetic field. This correction factor will be specific for the setup, in particular ionisation chamber orientation, and magnetic field strength.

$$P_{1.5\ T} = \frac{M_{0T}}{M_{1.5T}} \tag{2.6}$$

In order to determine the correction factor for the 1.5 T magnetic field accurately, it is crucial that the dose applied to all NE2571 ionisation chambers was equal for the situation with and without magnetic field. Therefore, a reference chamber (at point C) is included in the measurement setup used to determine the correction factor for the 1.5 T magnetic field, visualised in figure 8.1. When the MRI magnet was downramped, the magnetic field at point A and B, was reduced from 1.5 T to less than 1 mT while the magnetic field at point C remains less than 1 mT [40].

Firstly, the $P_{1.5\ T}$ for one ionisation chamber was determined. Ionisation chamber 1315 was positioned at point A while ionisation chamber 2854 was used as a reference chamber at point C. Measurements were performed with and without the 1.5 T magnetic field. In this setup the beam stopper was not installed.

Secondly, the $P_{1.5\ T}$ for three ionisation chambers (sn 3628, 3626 and 2854) was determined. The phantom was positioned at point A (CAX, SSD of 143.5 cm), in one PMMA 20 x 20 x 13 cm^3 three ionisation chambers were placed with measuring depths of 3.6, 7.4 and 10.8 cm, respectively. A 30cc ionisation chamber type 2530/3 (NE Technology Limited, Berkshire RG7 5PR, England) was positioned on the CAX at point C, at an SSD of 310 cm as a reference to monitor output variations. For this measurement set, the beam stopper was mounted therefore an ionisation chamber with a larger volume was chosen to increase the measured signal.

Readout of all ionisation chambers was performed simultaneously. All measurement series were performed under similar temperature and air pressure conditions as the first series, such that the difference between the two P_{TP} correction factors is less than 0.1%. No influence of the magnetic field on the temperature measurement is expected due to the very low magnetic susceptibility of the thermometer device at room temperature [62].

2.3 Results

An overview of the measurement results, is given in table 2.1. For each discussed measurement, the average result of all ionisation chambers and largest deviation from average values are included.

Table 2.1: Overview of measurement results for the ionisation chamber characteristics with and without magnetic field.

	Without magnetic field		With magnetic field	
Characteristic	Average value	Maximum deviation	Average value	Maximum deviation
Linearity	100.1%	0.4%	100.1%	0.2%
Repeatability	0.1%	<0.1%	0.1%	<0.1%
P_{ion}			1.001	<0.001
P_{pol}	1.000	<0.001	1.000	<0.001
$P_{1.5T}$			0.953	0.002

2.3.1 Linearity and Reproducibility

Figure 4.2 shows the normalised linearity chamber measurement results for all ionisation chambers, in the situations with and without the magnetic field. Without the magnetic field, the maximum deviation from the ideal linear values is 0.4%, while this value is 0.2% with the magnetic field.

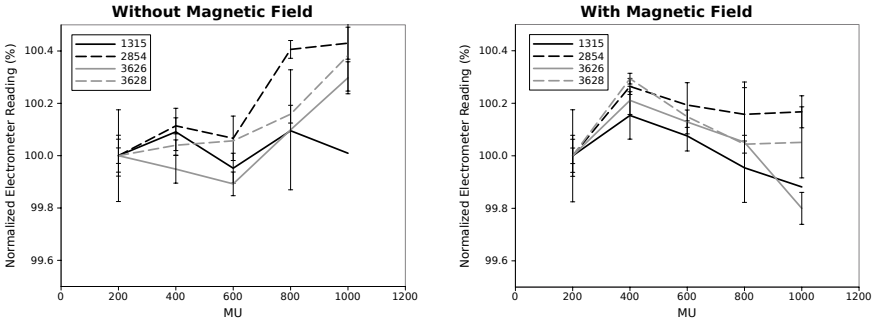

Figure 2.4: Dosimeter measurements for each applied amount of Monitor Units (MU), normalised to a reference of 200 MU. Measurements performed with and without the presence of a transverse 1.5 T magnetic field. The error bars represent the measured value range for each point of measurement.

The reproducibility was determined for each ionisation chamber, for the situation with and without the magnetic field. The results are displayed in table 2.1. The reproducibility of each ionisation chamber was well within the 0.5% target

stated in the methods section. The 1.5 T magnetic field does not appear to influence the linearity or reproducibility of the ionisation chambers.

2.3.2 Influence of ionisation chamber orientation

Figure 2.5 shows the influence of the orientation on the reading of the ionisation chamber.

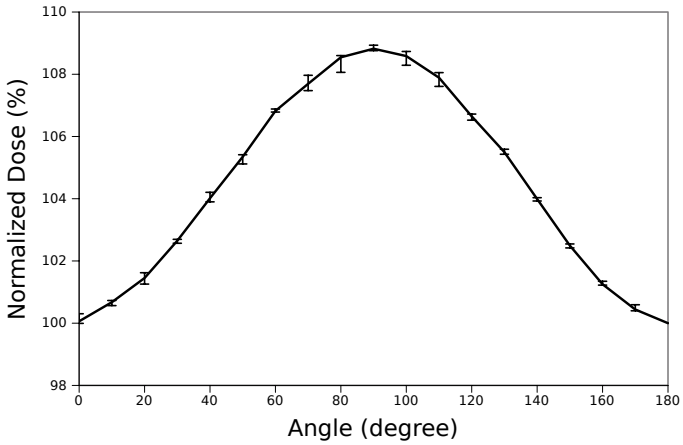

Figure 2.5: Influence of orientation inside magnetic field on the reading of the dosimeter. Rotation took place around the Central Beam Axis (CAX).

As can be seen in figure 2.5, the total change in ionisation chamber response was 8.8% for an orientation change from 0° to 90° where the ionisation chamber axis moves from parallel to perpendicular to the magnetic field. However, the smallest change in response was less than 0.2% for 10° rotations between 80° and 100°. Because of the small influence of a change in orientation in this region, the 90° orientation would be preferable for dosimetry measurements.

2.3.3 Ion recombination

Figure 2.6 shows the normalised dosimeter readings (Q) of the recombination measurements. The error bars represent the minimum and maximum measured value for each point of measurement.

The correction factor P_{ion} was calculated twice using equation 2.4, using a high polarising voltage of 250 V and a low polarising voltage of 50 and 25 V, respectively. The value of P_{ion} was 1.001 for both voltage differences, this is

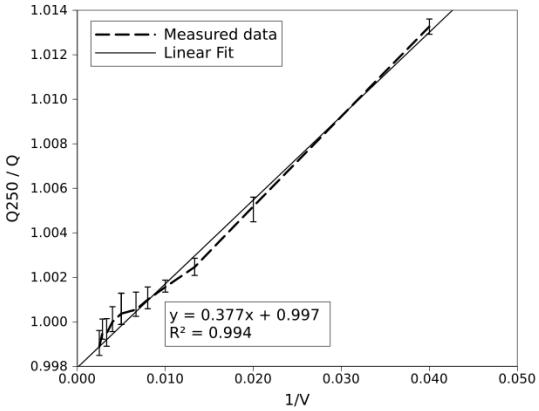

Figure 2.6: Dosimeter readings for varying polarising voltages. A linear fit is included.

equal to the ion recombination correction factor used in the clinic without a magnetic field.

2.3.4 Polarity corrections

For each ionisation chamber the correction factor P_{pol} was calculated for the measurements with and without a magnetic field. The results can be found in table 2.1.

The largest change in P_{pol} due to the magnetic field was less than 0.15% for the ionisation chamber 2854. For the other ionisation chambers tested, the influence of the magnetic field is less than 0.1%.

2.3.5 Photon fluence distribution

Figure 2.7 shows normalised dose profiles in two directions acquired with and without the 1.5 T magnetic field.

The measurement values in the profiles are normalised to the total dose inside the radiation field. The point of measurement for the ionisation chamber lies inside the square. The difference in the area of interest, in which the ionisation chambers are positioned, is 0.5%. The observed difference near the radiation field edge in figure 2.7(b) is due to the influence of the Lorentz force acting on the electrons. A more detailed description of this effect can be found in [36].

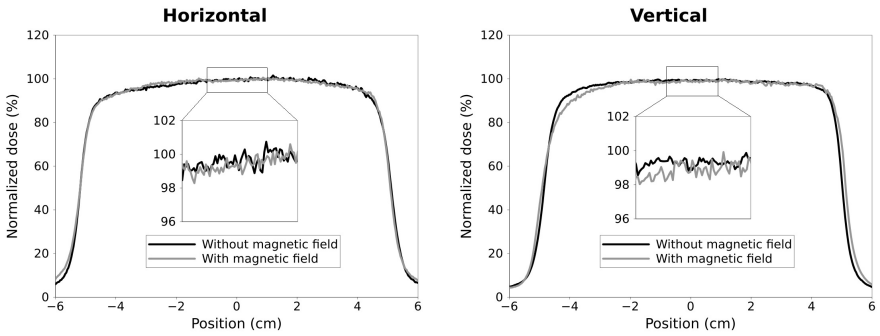

Figure 2.7: Dose profiles with and without magnetic field in two directions through the centre of the field. The horizontal profile is displayed in figure a, and vertical profile in figure b. Dose values are normalised to the total area under the curve within the radiation field. Area of measurement of the NE2571 ionisation chambers, represented with a rectangle, is magnified.

2.3.6 Total influence of the 1.5 T magnetic field

For the setup described in section 2.2.6, the 1.5 T magnetic field of the MRI increases the reading of the NE2571 ionisation chamber by an average of 4.9%. The largest and smallest influence of the magnetic field measured were 5.1% and 4.7%, respectively. The correction factor for the 1.5 T magnetic field ($P_{1.5\ T}$) will therefore be 0.953.

2.4 Discussion

For the measurements performed in this study, the dosimeter signal is reproducible and linearly related to the applied dose inside a 1.5 T magnetic field. The results of the orientation measurements in this paper have shown that although the ionisation chamber is sensitive to orientation change, the standard dosimetry setup described in section 2.2.6 can be used reliably for measurements.

The influence of the magnetic field on the polarisation and recombination effects was investigated, and found to be negligible. The ion collection efficiency was expected to be affected by the magnetic field, because the longer electron trajectories of the ions inside the sensitive volume of the chamber allow for more ion recombination. To estimate the order of magnitude of this effect we

will assume that the increase in recombination scales linearly with the track length of the electrons. The contribution of recombination is estimated to be a few tenths of a percent, at 0 T ([63], [64] and [65]). In a 1.5 T magnetic field the length of electron trajectories will increase approximately 5% on average [51]. Therefore an increase in recombination of 5% is expected. This means that a 1.5 T magnetic field leads to a 0.005% decrease in reading due to the recombination effect. This effect is smaller than can be measured in the current setup, indeed the results in section 3.3.1 show no significant change in ion recombination due to placing the chamber in the magnetic field. Since the advised polarising voltage of 250 V is still in the linear area of the curve in figure 2.6, charge multiplication will not affect the reading significantly and the advised polarising voltage can be used in the transversal 1.5 T magnetic field.

The influence of the magnetic field on the air-pressure and temperature has not been investigated in this study. This ambient condition influences the amount of air particles inside the sensitive volume of the chamber, and therefore the amount of interactions. The magnetic field influences the path and therefore the track length of a charged particle in an ionisation chamber, not the chance of interaction for a certain path length. Therefore the influence of the magnetic field on this correction factor is expected to be negligible.

The transverse 1.5 T magnetic field, increases the ionisation chamber reading by 4.9%, for the standardised output dosimetry setup conditions. This influence of the magnetic field is explained qualitatively by Meijsing et. al. [51], as a combination of the number of electrons and the average path length in the sensitive volume of the ionisation chamber. In that same study, Monte Carlo simulations were used to predict a reading increase of a NE2571 Farmer type ionisation chamber of 4.9% $\pm$ 2.5% (1 sd). The simulated increase predicted by Meijsing *et al* is in agreement with the measured increase in ionisation chamber response.

Based on this information we propose that the corrected reading calculation (equation 2.1) should be expanded to equation 2.7 by adding a correction factor $P_{1.5\ T}$, for dosimetry calibration measurements in the MR-linac.

$$M_{corr} = M_{raw} \times P_{TP} \times P_{ion} \times P_{pol} \times P_{elec} \times P_{1.5T} \qquad [C] \qquad (2.7)$$

where $P_{1.5T}$ has a value of 0.953 for the standard dosimetry setup described in section 2.2.6. A preliminary estimation of the uncertainty is $\pm$ 1% (2 sd), based solely on the measurement data presented in this paper. Of importance for this uncertainty are the results of the linearity, reproducibility and magnetic field correction factor ionisation chamber measurements as well as the photon fluence measurements. More experimental data are necessary to estimate a full uncertainty budget for $P_{1.5T}$.

2.5 Conclusion

It is feasible to use an NE2571 Farmer type ionisation chamber for reference dosimetry measurements at an MR-linac. Due to the 1.5T magnetic field, the reading of the NE2571 chamber increases by 4.9%. To account for the influence of the 1.5 T magnetic field of the MRI on the NE2571 chamber, an extra correction factor for the magnetic field can be included in the calculations of the corrected measurement value. The value obtained for the correction factor holds only for the specific measurement setup and magnetic field conditions described in this paper. To apply the AAPM TG51 Code of practice or equivalent protocols in full for the absorbed dose determination, the various parameters investigated in this study have to be re-assessed according to all conditions required by the Code of practice. The influence of the magnetic field on the correction factors (i.e. P_{pol}, P_{ion}) is negligible.

Acknowledgements

Part of this research is financially supported by the Dutch Technology Foundation STW.

3

Relative dosimetry in a 1.5 T magnetic field: an MR-linac compatible prototype scanning water phantom

This chapter has been published as:
K. Smit, J. Sjöholm, J.G.M. Kok, J.J.W. Lagendijk and B.W. Raaymakers. Relative dosimetry in a 1.5 T magnetic field: an MR-linac compatible prototype scanning water phantom *Physics in Medicine and Biology*. 2014. **59**(15):4099–4109.

Abstract
The MR-linac is a hybrid MRI radiotherapy system allowing dose delivery in a 1.5 T magnetic field. This paper presents the design and performance of a prototype MR-linac compatible scanning water phantom. Since a scanning water phantom requires dose detectors, the performance air filled ionisation chambers in the magnetic field was characterised.
We have found that the linearity and reproducibility of an ionisation chamber are unaffected by the magnetic field. Also, moving the ionisation chambers in a magnetic field during irradiation does not affect the dose response. When scanning in-plane profiles, the change in irradiation orientation can influence the ionisation chamber dose response by up to 0.4%. However this effect can be eliminated by rotating the ionisation chamber by 90° before measuring the in-plane profile.

The performance of the total scanning water phantom was validated at a clinical setup in a 0 T magnetic field. There was no significant difference between the dose profiles measured with a standard clinical scanning water phantom and the profiles measured

with the MR-linac compatible scanning water phantom. The performance of the MR-linac scanning water phantom in the MR-linac was validated using Gafchromic EBT2 film. There was no significant difference in dose profiles between the MR-linac scanning water phantom and the radiochromic film. These results indicate that automated scanning water phantom measurements using ionisation chamber detectors are possible in the MR-linac.

3.1 Introduction

The University Medical Center Utrecht, The Netherlands, has developed a prototype MR-linac [40] in collaboration with Elekta (Elekta AB, Stockholm, Sweden) and Philips (Best, The Netherlands). The MR-linac consists of a modified 1.5 T Philips Achieva MRI scanner and a ring mounted Elekta 6 MV linear accelerator which share a common isocentre. The superior soft-tissue contrast of MR-imaging can be used for high precision image-guided radiotherapy. The setup allows simultaneous, independent irradiation and imaging of the patient enabling escalation of the dose to the tumour while sparing surrounding healthy tissues [57].

The irradiation beam axis is perpendicular to the permanent 1.5 T field of the MRI scanner. The linac is equipped with a 160 leaf Elekta Agility based MLC, with a projected leaf width of 7 mm at the isocentre. In the direction of the leaf travel, the irradiation field is restricted to a maximum field size of 24 cm by MRI scanner structures. Since the isocentre of the linac coincides with the isocentre of the MRI scanner, the dose is delivered in the presence of a lateral 1.5 T magnetic field.

Although the photon beam is not affected by the magnetic field, the secondary electrons depositing the dose are deflected by the Lorentz force when travelling in a magnetic field [41]. The effect of the deflected electrons on the dose distribution is most noticeable at tissue-air interfaces [41] [42].

The dose response of an ionisation chamber in a magnetic field is directly related to the number of electrons and their average path length ([51]). Therefore the dose response of an air-filled ionisation chamber is influenced by the ionisation chamber shape, orientation in the magnetic field and irradiation orientation, amongst others.

Smit et. al. [66] have investigated the influence of the transverse magnetic field on dose response of an NE2571 Farmer type ionisation chamber. These studies have shown that reference dosimetry using this type of ionisation chamber is still possible because important ionisation chamber characteristics [50] like linearity and reproducibility are not affected by the magnetic field.

Another common use of ionisation chambers in dosimetry is relative dosimetry using scanning water phantoms. In clinical practice, scanning water phantoms

are often used for commissioning and periodical control measurements. The requirements for equipment used for beam data commissioning can be found in [53] or similar reports. Scanning water phantoms are a valuable tool for beam commissioning because, the dose at virtually any point within the scanning volume of the water phantom can be measured using an ionisation chamber. An MR-linac compatible scanning water phantom would be a valuable tool to investigate the beam characteristics of the MR-linac [54]. However, the clinically used scanning water phantoms are incompatible with the MR-linac setup due to their size, magnetic components and the use of electric motors. Moreover, the impact of the magnetic field on the ionisation chambers should be investigated.

This paper presents a prototype MR-linac compatible scanning water phantom and validates the performance. Firstly, the design and modifications of the scanning water phantom are explained. Secondly, the performance of the air filled ionisation chambers in the magnetic field is characterised. Lastly, the performance of the total scanning water phantom inside and outside a magnetic field is investigated.

3.2 Materials and methods

The basis of the MRL scanning water phantom, henceforth referred to as the MRL water tank, is a PTW-MP3T (PTW, Freiburg GmbH, Germany) scanning water phantom. This clinical scanning water phantom was designed for the TomoTherapy system (TomoTherapy Inc, Madison, Wisconsin). The MRL water tank has 3 axes along which movement can take place. A specific measurement arm was designed in order to ensure that the centre of the measurement volume coincides with the isocentre. The MRL water tank can be transported from a trolley onto the table, or table bridge, of the MRL, the trolley contains the control unit of the system, and will remain outside the MRL but in the magnetic fringe field. In addition to automated driving, a hand held control is available for manual driving of the MRL water tank.

3.2.1 Water tank modifications

Size

The current MRL prototype has a bore diameter of 60 cm with the table placed in the same position as the standard clinical Philips Achieva imaging modalities. To facilitate this relatively small bore diameter, the MP3T water

tank is rotated 90 degrees, such that the longest axis of the water tank will be parallel to the permanent B_0 field of the MRL i.e. the feet-head (FH) direction of the patient.

In order to fit into the MRL in this orientation the height, anterior-posterior (AP) direction, of the water tank had to be lowered 9 cm. Additionally, the electric motors and driving axes had to be shifted 7 cm towards the centre of the water tank in the left-right (LR) direction.

This new configuration, visualised in figure 3.1(a), creates a scanning volume of 24 x 40 x 11.5 cm^3 (LR x FH x AP) centred around the isocentre of the MR-linac. The dimensions of the total water scatter volume are 41.5 x 61.5 x 22 cm^3.

Ferromagnetic components

The standard MP3-T water tank contains some ferromagnetic components which will have to be replaced by non-ferromagnetic components before the water tank can be used in the magnetic field. For all three axes the driving spindles are replaced by aluminium components. The motion is conferred from the spindles to the ionisation chamber carriage using nuts, which were replaced by magnetic field compatible nylon versions. Fibre sensors (Keyence FU-38 + amplifiers) were installed as position reference sensors.

Electric motors

The standard design motors are stepper motors using a permanent magnet. The performance of this type of electric motor design will be affected by the magnetic field. Therefore the standard MP3-T electric motors are replaced by magnetic field compatible ultrasonic motors (Shinsei corporation, Japan) visualised in figure 3.1(b). These ultrasonic motors work in the magnetic field in any orientation and have been used in the Philips MRI guided High Intensity Focused Ultrasound system to move the ultrasound transducers in the 1.5 T magnetic field [67].

The ultrasonic motors are equipped with relative encoders. The electronics box of the MP3-T water tank has been replaced and now contains the motor power supply, three Shinsei motor drivers and a Galil DMC-2250 motion controller (Galil Motion Control, Rocklin CA, USA) and software. Translator software is made to translate commands from the standard Mephysto software (PTW, Freiburg, Germany) to the Galil motion controller. This means that all the

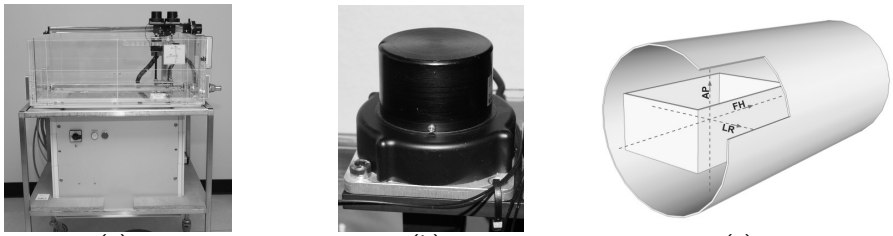

(a) (b) (c)

Figure 3.1: Pictures of the MRL water tank on the transportation cart containing the control unit (a) and an ultrasonic motor mounted on the water tank(b). Figure (c) shows a schematic representation of the water tank and scanning directions in the MRL bore.

standard software can be used in its regular fashion, without limitations in function. The ultrasonic motors move slower than the original electric motors, the new maximum speed of the carriage is estimated to be 1.3 cm/s.

3.2.2 Ionisation chambers

Water tank dose measurements can only be successful if the ionisation chambers perform correctly in the magnetic field. Therefore, the performance of a selection of air filled ionisation chambers in a magnetic field has been investigated. Several sizes of air filled ionisation chambers have been tested, named CC01, CC04 and CC13; with volumes of 0.01 CC, 0.04 CC and 0.13 CC, respectively. These ionisation chambers, produced by IBA dosimetry (IBA dosimetry, Germany), are currently used for treatment planning commissioning measurements at our department. An NE2571 Farmer type reference ionisation chamber (NE Technology Limited, Berkshire, England) was included in these measurements to correct for possible linac output variations. Smit et. al. [66] has shown that the NE2571 can be used as a reference without the need for any magnetic field correction. The performance of ionisation chambers in a magnetic field was investigated for the following characteristics.

Reproducibility

The reproducibility of the ionisation chamber is of vital importance to the precision of the measurement. To test the short term reproducibility 100 measurements of 1 second were performed consecutively. The relative standard deviation and the maximum deviation from the average measured value were used to assess the reproducibility of the ionisation chambers.

Linearity

The dose response linearity of the ionisation chambers was determined by varying the integration time over a range from 0.2 to 10 seconds. For each integration time, 5 consecutive measurements were performed. The measurement results were normalised to a reference integration time of 1 second. The obtained results will be used to estimate an optimal integration time for the dose profile measurements, based on measurement time and reproducibility of the measurement.

Orientation in a magnetic field

When measuring a dose profile in the MR-linac, the orientation of the ionisation chamber in the magnetic field will remain constant. Because of the varying location in the MR-linac combined with the beam divergence, the irradiation orientation will vary slightly.

For a profile measurement of the maximum field size in the transversal direction, the cross-plane direction, the ionisation chamber is rotationally symmetric and directed along the magnetic field. Therefore, no geometrical difference in irradiation orientation is present.

For the in-plane profiles, the orientation will vary around an axis perpendicular to the ionisation chamber axis. The irradiation beam is limited to 24 cm in this direction, when taking into account an overscan of 5 cm on either side, the irradiation orientation varies between -8° and +8°. Within this window, the magnetic field should not influence the ionisation chamber reading by more than 0.5%.

The exact irradiation orientation change found when measuring in-plane profiles cannot be investigated without changing either the ionisation chamber location or orientation with respect to the magnetic field. Therefore, we will assume that the total effect of the change in irradiation orientation and the orientation change in the magnetic field, is a summation of the individual effects.

Firstly, we investigated the influence of an orientation change in the magnetic field, without a change in irradiation orientation. Secondly, we investigated the influence of an orientation change in the magnetic field, and a change in irradiation orientation. From the combined results of these measurements, we determined the influence of a change in irradiation orientation found when measuring in-plane profiles on the ionisation chamber dose response.

Varying orientation measurements could be performed using an in-house developed PMMA phantom [66]. A rotating cylinder in this phantom allows rotation around the ionisation chamber effective point of measurement, without changing the phantom geometry.

Moving in a magnetic field

When using a scanning water phantom in a magnetic field, the ionisation chambers will measure dose during, or directly after, moving in the magnetic field. We investigated the impact of this motion on the dose response of the ionisation chambers. Because the radiation beam of the MR-linac setup is unflattened, the delivered dose is dependent on the location in the irradiation beam. A change in dose response can therefore be due to the movement or to the different dose at the new location.

Therefore the influence of movement in a magnetic field on the ionisation chamber reproducibility was investigated at our clinical MRI HDR brachytherapy facility, using a microselectron v2 (Nucletron, Netherlands) as a radiation source. The estimated air-kerma strength of the Iridium source at the time of measurement was 44.25 mGy/h at 1 m distance. Dose is measured over fixed time intervals of 30 seconds, 10 measurements were performed per setup condition.

To ascertain a constant dose delivery, the distance between the radiation source and the ionisation chamber must remain constant. Therefore, a dedicated phantom was designed to contain the irradiation source and the ionisation chamber.

Firstly, the dose was measured outside the magnetic field, to establish a baseline reproducibility for the setup. Secondly, 5 measurements were performed in the magnetic field, without movement of the phantom. Finally, the applied dose was measured while moving the phantom in a magnetic field. During this movement, there was no change in orientation of the phantom.

3.2.3 Water tank performance

Geometrical accuracy and precision

The geometrical precision of the MRL water tank inside and outside the magnetic field was investigated by driving the probe to the isocentre 10 times from random positions in the water tank [68].

The accuracy of the water tank was investigated by driving the probe from the isocentre to the point 10 cm along the axis parallel to the permanent B_0 field.

A needle was placed in the ionisation chamber position on the carriage, and at the desired location to more accurately determine the position variations. The absolute difference in position was determined by measuring the distance with a vernier caliper. In addition the position of the water tank was extracted from the software and compared to the set position.

Performance at a clinical linac

The performance of the MRL water tank was benchmarked against an IBA Blue phantom^2 (IBA Dosimetry, Germany) at an Elekta Axesse. In-plane and cross-plane dose profiles of 5 x 5 cm^2 and 10 x 10 cm^2 fields at a depth of 5 cm were measured using the CC01, CC04 and CC13 ionisation chambers in the IBA water tank and the MRL water tank. Both water tanks were positioned at an SSD of 100 cm, with the centre of the scanning volume on the central axis of the linac. The water tank positioning was identical, only the scanning volume and the total volume of the water tank differ.

Performance in the MR-linac

Since a clinical water tank cannot be used at the MR-linac, the performance of the MRL water tank in a magnetic field was benchmarked against Gafchromic EBT2 (ISP, Wayne, USA) radiographic film measurements. A 30 x 30 cm^2 piece of film was suspended in the water tank at a depth of 5 cm. This film acquires a 2 dimensional dose distribution of a 10 x 10 cm^2 field, from which the dose profiles will be extracted. Subsequently the dose profiles of the 10 x 10 cm^2 field were measured using the CC01, CC04 and CC13 ionisation chambers in the MRL water tank.

3.3 Results

3.3.1 Ionisation chambers

Reproducibility

The relative standard deviations, maximum relative standard deviation and maximum deviation from average, for all investigated ionisation chambers are visualised in table 4.1.

The magnetic field does not increase or decrease the CV significantly ($p = 0.05$). As expected from theory [1] the CV were largest for the smallest ionisation chamber and decreased as the ionisation chamber volume increased.

Table 3.1: Overview of the reproducibility measurements results for the various ionisation chambers inside and outside the magnetic field.

	CC01		CC04		CC13	
Magnetic field	No	Yes	No	Yes	No	Yes
Mean CV (%)	0.22	0.20	0.16	0.15	0.13	0.12
Max deviation (%)	0.67	0.87	0.47	0.69	0.45	0.40

Linearity

The results of the linearity measurements for all three chambers are visualised in figure 4.2. The maximum average deviation from linearity for the normalised dose is less than 0.2% for all ionisation chambers and all investigated integration times.

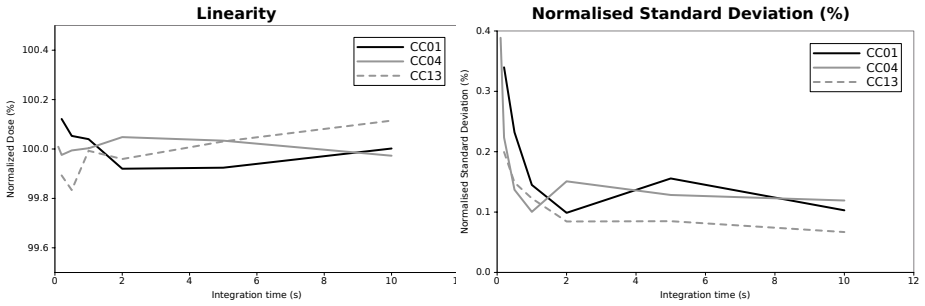

(a) (b)

Figure 3.2: Results of the linearity measurements. Figure a shows the normalised dose measurements per integration time. Figure b shows the standard deviation of the measurements per integration time.

The normalised standard deviation per integration time is visualised in figure 3.2(b). For all ionisation chambers the largest normalised standard deviation is found for the smallest integration time. All ionisation chambers show a lowering of the standard deviation for increasing integration times. When taking into account the increase in total measurement time due to longer integration times, an integration time of 1 second was chosen as optimal integration time for future profile measurements.

Orientation in a magnetic field

The influence of the ionisation chamber orientation in the magnetic field on the dose response is visualised in figure 3.3.

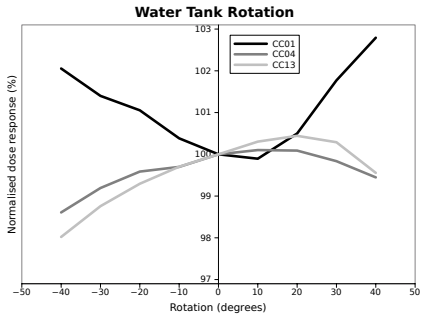

Figure 3.3: Results of the orientation change measurements, normalised to the irradiation orientation used when the ionisation chamber is placed on the central beam axis.

An orientation change of 10° induces a maximum change in dose response of 0.4% for the CC01 ionisation chamber. For the CC04 and CC13 ionisation chambers, a largest deviation of 0.3% was found. The deviation at 10° is less than the 0.5% accepted maximum for all ionisation chambers.

The CC01, the ionisation chamber with the most oblong geometry, shows the largest influence of orientation in the magnetic field. This change in dose response for the individual ionisation chambers coincides qualitatively with the expected change based on the theory [51] [1], and the specific ionisation chamber geometry.

Moving in a magnetic field

The relative standard deviations for each measurement set are displayed in table 3.2.

For all ionisation chambers the relative standard deviation is larger for the static situation outside the magnetic field, than for the movement in the magnetic field. As expected, the absolute dose response of the ionisation chambers is affected by the presence of the magnetic field, but this will not affect the relative standard deviation measurements.

Table 3.2: Overview of the relative standard deviation for the measurements with and without movement in the magnetic field.

	CC01	CC04	CC13
0 T without movement	0.06	0.05	0.06
1.5 T without movement	0.05	0.04	0.05
1.5 T with movement	0.03	0.04	0.06

3.3.2 Water tank performance

Geometrical accuracy and precision

The geometrical accuracy and the precision of the water tank were less than 0.2 mm. It was not possible to measure more accurately using the Vernier caliper. The water tank probe positions reported by the software never varied more than 0.01 mm from the requested positions.

Performance at a clinical linac

The cross-plane profiles measured for a 10 x 10 cm^2 field using an IBA Blue phantom^2 water tank and the MR-linac prototype water tank, are visualised in figure 3.4.

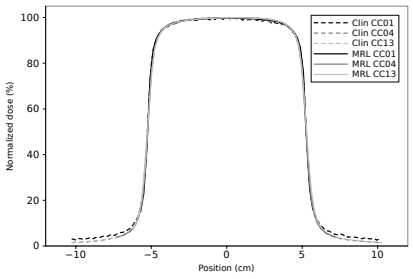

Figure 3.4: Results of water tank measurements at the Elekta Axesse for the three types of ionisation chambers. Dashed lines represent the results obtained with the clinical water tank. Solid lines represent the measurements in the MR-linac prototype water tank.

The average difference between the clinical and MRL water tank is 0.3% for the CC01 and less than 0.2% for the CC04 and CC13. As can be seen in section

3.3.1, this difference originates in ionisation chamber signal noise rather than a systematic difference due to water tank performance.

Performance in the MR-linac

Figure 3.5 shows the profiles measured in the water tank using the ionisation chambers and the EBT2 films.

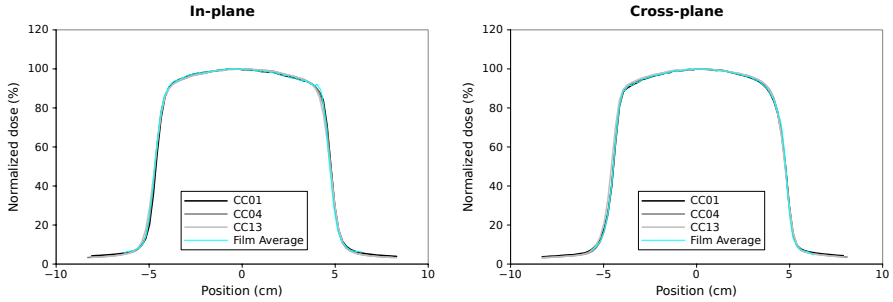

Figure 3.5: Results of water tank and EBT2 film measurements in the MR-linac, in-plane (a) and cross-plane (b) profiles.

The average deviations between the profiles measured using the ionisation chambers and the film are; 0.36, 0.18 and 0.13 for the CC01, CC04 and CC13, respectively. There is no visible spacial dependency in the deviation between the film and ionisation chamber profiles.

3.4 Discussion

We have shown that the MRL water tank prototype functions correctly inside and outside a magnetic field. The mechanical stability and precision appear to be uninfluenced by the modifications made to the water tank.

The investigated ionisation chambers can be used for relative dosimetry in the magnetic field, because they have a reproducible response that is linearly related to the applied dose. Moving the ionisation chambers in a magnetic field while irradiating does not influence the dose response of the ionisation chambers. Only movement in the magnetic field without change in orientation of the ionisation chamber with respect to the magnetic field have been investigated, since this is the type of movement used in the water tank.

As explained in section 3.2.2 and 3.3.1, the change in irradiation orientation can influence the dose measurement by up to 0.4% for the smallest ionisation chamber at the edge of the measurement volume. This irradiation orientation change is solely due to the divergence of the beam, not to a misalignment of the ionization chamber. The irradiation orientation effect can be eliminated in the in-plane direction by mounting the ionisation chamber under a 90° angle, such that the situation of the original cross-plane profile is created. In this orientation there is no geometrical difference in irradiation orientation over the profile, due to the rotational symmetry of the ionisation chamber. Section 3.3.2 does not show the expected 0.2% difference in the edges of the dose in-plane dose profile, indicating that this change in ionisation chamber mounting is not necessary in every type of measurement.

The measurement results obtained using the MR-linac water tank are comparable to measurement results obtained with the clinical IBA water tank. The translation software is functional, but not yet optimised. The software induces a delay of approximately 0.5 seconds per measurement step. Additionally, the ultrasonic motors intrinsically move slower than the standard design electric motors. This decreases the maximum measurement speed, increasing the measurement time when performing continuous profile measurements. We estimate that the combination of these two effects slows the measurements by a factor of 2 for the current water tank design. Further research will be performed to optimise the measurement speed.

There are some intrinsic design differences between the standard clinical water tank and the MR-linac water tank. The MR-linac water tank volume is smaller because of the size limitations by the MRI bore size. Additionally, the current water tank was a modification of an existing water tank and therefore had limited options for size modifications. This caused the third axis, used for PDD measurements in standard convention, to be limited to a maximum depth of 11.5 cm. The PDD measurements could be extended to 24 cm by irradiating horizontally and measuring along the LR-axis. For this type of measurements an irradiation window would need to be installed in the water tank, to ascertain correct measurement of the dose maximum. For a new water tank, the dimensions of the water tank will be chosen to fit the available space more optimally, creating a larger scanning volume.

This prototype scanning water phantom has proven that scanning ionisation chamber water tank measurements are possible inside the 1.5 T magnetic field

of the MR-linac. We expect the water tank can be used not just in the MR-linac, but also in other radiation treatment combinations which incorporate a magnetic field, e.g. Renaissance^{TM} System (ViewRay, Oakwood Village, Ohio, USA) [37] [48]. For all of these modalities, the water tank can be of great importance for dosimetry measurements as performed for e.g. beam commissioning.

3.5 Conclusion

Scanning water phantom measurements are possible inside an MR-linac. Some dedicated modifications are necessary to a standard scanning water phantom for usage in a magnetic field. These modifications can be done without influencing the accuracy and precision of the scanning water phantom. For the evaluated ionisation chambers, the important characteristics i.e. linearity and reproducibility are unaffected by the magnetic field. Therefore, these ionisation chambers can be used as dose detectors in the water tank. Dose profiles measured with the MR-linac scanning water phantom coincide with profiles measured with a standard scanning water phantom.

Acknowledgements

Part of this research is financially supported by the Dutch Technology Foundation STW. The authors would like to thank PTW for their technical support and for supplying the TANDEM electrometer. The technical support from Wilfred de Vries and Bernhard Klok is greatly appreciated.

4

Performance of a multi-axis ionisation chamber array in a 1.5 T magnetic field

This chapter has been published as:
K. Smit, J.G.M. Kok, J.J.W. Lagendijk and B.W. Raaymakers. Performance of a multi-axis ionisation chamber array in a 1.5 T magnetic field. *Physics in Medicine and Biology*. 2014. **59**(7):1845–55.

Abstract
At the UMC Utrecht a prototype MR-linac has been installed. The system consists of an 8 MV Elekta linear accelerator and a 1.5 T Philips MRI system. This paper investigates the performance of the IC PROFILER^{TM}, a multi-axis ionisation chamber array, in a 1.5 T magnetic field.
The influence of the magnetic field on the IC PROFILER^{TM} reproducibility, dose response linearity, pulse rate frequency dependence, power to electronics, panel orientation and ionisation chamber shape were investigated. The linearity, reproducibility, pulse rate frequency dependence, panel orientation and ionisation chamber shape are unaffected by the magnetic field. When measurements results are normalised to the centre reference chamber, the measurements can commence unaltered. Orientation of the ionisation chambers in the magnetic field is of importance, therefore caution must be taken when comparing or normalising results from several different axes.
IC PROFILER^{TM} dose profiles were compared with film dose profiles obtained simultaneously in the MR-linac. Deviation between the film and the IC PROFILER^{TM} data was caused by the noise in the film, indicating correct performance of the IC PROFILER^{TM} in the transverse 1.5 T magnetic field.

Chapter 4

4.1 Introduction

The MR-linac is an Image Guided Radiotherapy device, a combination of a 1.5 T closed bore Philips MRI scanner (Best, The Netherlands) and an 8 MV Elekta (Crawley, UK) linear accelerator. This setup is an upgrade of the setup described by Raaymakers et. al. [40]. The goal of this combination is to use the superior soft tissue contrast of the imaging system for high precision image guidance. This will improve tumour position verification and thereby minimise the required tumour motion margins [57].

The presence of the homogeneous 1.5 T magnetic field affects the dose deposition, dosimetry measurements and quality assurance of the linac. The photons in the treatment beam are not affected by the magnetic field, yet the secondary electrons are deflected by the Lorentz force [36]. The effect of this is most noticeable at tissue-air interfaces, because of the longer electron trajectory in low density media [41]. As the reading of an ionisation chamber depends on the number of electrons and the electron trajectory inside the measuring volume [51], the dose response of air filled ionisation chambers changes in the magnetic field.

Smit et. al. [66] have shown that reliable measurements are still possible with an NE2571 air filled ionisation chamber. But a magnetic field correction factor must be taken into account for reference dosimetry. The magnitude of this magnetic field correction factor depends on several factors including, but not limited to; magnetic field strength, ionisation chamber geometry and orientation of the ion chamber inside the magnetic field.

When performing relative dosimetry measurements in a magnetic field, ionisation chamber arrays can be of great convenience for dose distribution measurements because of their easy handling and fast results [39]. However, before this sort of device can be used in a magnetic field, the influence of the magnetic field on the ionisation chambers in the array must first be characterised.

The ionisation chambers used for relative dosimetry generally have smaller sensitive volume than ionisation chambers used for reference dosimetry, and are therefore expected to be less affected by the magnetic field. But more importantly, for relative dosimetry the signal is generally normalised to a reference chamber. This can eliminate the need for a correction factor in a homogeneous magnetic field when the ionisation chamber geometry and orientation are identical.

Performance of a multi-axis ionisation chamber array in a 1.5 T magnetic field

The purpose of this study was to investigate the feasibility of using an IC PROFILER^{TM} (Sun Nuclear Corporation, Melbourne, FL USA) in the transverse 1.5 T magnetic field of the MR-linac. The influence of the magnetic field on the basic IC PROFILER^{TM} characteristics were investigated similarly to Simon et. al. [69]. The investigated characteristics were [54]: dose response linearity, reproducibility, start-up time before use and panel orientation. As a validation of feasibility, IC PROFILER^{TM} measurements were compared with film measurements simultaneously obtained in the MR-linac.

4.2 Materials and methods

The panel used in this study is the IC PROFILER^{TM} (Sun Nuclear Corporation, Melbourne, FL USA). This specific panel was modified for measurements inside a magnetic field by removing the power supply unit from the panel and replacing it by an external power supply.

The panel has 251 parallel plate ionisation chambers, with a sensitive volume of 0.05 cm^3 per chamber. The panel has an intrinsic build-up and backscatter thickness of 0.9 and 2.3 g/cm^2. The detectors are mounted in four arrays within an area of 32 x 32 cm^2, two arrays on the coordinate axis (referred to as X and Y) and two arrays on the positive and negative diagonals (referred to as PD and ND). The detector spacing is 0.5 cm on the coordinate axes and 0.71 cm on the diagonal axes. At the intersection of the arrays only the Y-axis has detectors, the other arrays each skip three detectors.
A picture of the panel surface is given in figure 5.1. The outline of the ionisation chambers are depicted on the surface of the panel. This figure illustrates the two types of ionisation chamber shapes, straight and curved conforming to the isodose lines in the penumbra regions associated with the orthogonal axes and diagonals of the fields.

Unless mentioned otherwise, the panel measurements were performed according to the following standard setup conditions.

The first set of measurements was obtained at an Elekta SL*i* (Crawley, UK) at an SSD of 100 cm, with a field size of 25 x 25 cm^2.

The second set of measurements were performed at the MR-linac, in a 1.5 T magnetic field. The isocentre of the linac coincides with the isocentre of the MRI. The linac is flattening filter free and can rotate around the MRI with the central beam axis (CAX) in the plane perpendicular to the magnetic field.

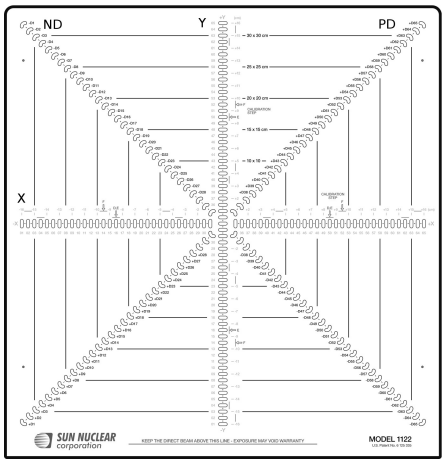

Figure 4.1: A beams eye view image of the IC PROFILER^{TM} panel provided by Sun Nuclear Corporation. The surface of the panel shows the the ionisation chamber positions and shapes. For clarity, the names of the ionisation chamber axes have been added.

The MR-linac uses an Agility (Elekta, Crawley, UK) based MLC, consisting of 160 leaves. Each leaf has a projected width of 7 mm at 143.5 cm isocentric distance. The field size is restricted in the MRI feet-head direction by scanner structures to a maximum of 24 cm at the isocentric plane. More information on the MR-linac design can be found in [40].

The panel was positioned with the central reference ionisation chamber at the CAX at an SSD of 153.5 cm. Irradiation took place with a 23.8 x 23.8 cm^2 field at isocentric distance, the largest square field size currently available at the MR-linac, this field projects to a 25.5 x 25.5 cm^2 field at the panel surface.

The panel calibration was performed at the Elekta SL*i* setup, no additional calibration was obtained for the situation with the magnetic field. The 174 detectors located in the centre 22 x 22 cm^2 region of the panel were used for analysis. A PMMA build-up plate of 36.7 x 35.3 x 1.9 cm^3 was placed on top of the panel surface for the measurements. Before commencing the measurements, the setup was left in stand by mode for 15 minutes and the panel was pre-irradiated with a dose of 1 Gy.

A NE2571 Farmer ionisation chamber (NE Technology Limited, Berkshire RG7 5PR, England) was used as a reference chamber. Smit et. al. [66] showed that the ionisation chamber dose response linearity and reproducibility are unaffected by the magnetic field. Therefore this ionisation chamber is suitable as an external reference detector to correct for possible linac output variations in a magnetic field. A Unidos E electrometer (PTW, Freiburg GmbH, Germany) was used to measure the charge collected by the Farmer ionisation chamber, in nC. The chamber was positioned on the CAX behind the panel in the centre of a 20 x 20 x 6 cm^3 PMMA phantom.

4.2.1 Data

The panel was controlled using software provided by the supplier, data was acquired in continuous mode or pulsed mode. The pulsed mode, used for dose measurements, is synchronised with the linear accelerator pulses by triggering diodes. The continuous mode was used solely for background current measurements.

For this study the raw data was exported in ASCII format and analysed using in-house developed MATLAB^{TM} (MathWorks, Natick, MA, USA) based software. The corrected counts (CC), proportional to chamber ionisation charge, were obtained as described by Simon et. al.[69] using equation 4.1.

$$CC_i = \frac{RawCount_i - TimeTic * bias_i}{gain} * P_{TP} * CF_i \tag{4.1}$$

For each detector (i), the raw detector data ($RawCount_i$) was corrected for leakage ($bias_i$) during the integration time ($TimeTic$), temperature and pressure dependency (P_{TP}), amplifier gain ($gain$) and by applying individual detector calibration factors (CF_i). Since the measurement data will be normalised to an internal or external reference ionisation chamber, a possible influence of the magnetic field on these correction factors can be neglected.

4.2.2 Reproducibility

The short term reproducibility was evaluated on the MR-linac and the Elekta SL*i* with 10 consecutive one minute deliveries. For the first type of analysis, only the last 45 seconds of saved data from each delivery was used to avoid possible start-up effects in the panel or beam. To correct for accelerator output variations per integration time, the centre chamber on the panel functioned

as reference chamber. The reproducibility was quantified by determining each detector's coefficient of variation (CV), which is the standard deviation normalised to the mean of the measurements, and the maximum deviation from the mean.

The second type of analysis investigated the detector response directly after start-up of the beam. A paired Students t-test was performed to determine if any of the measurement points from 0 to 15 seconds will differ significantly from the measurement points in the last 45 seconds.

4.2.3 Dose response linearity

The dose response linearity was determined over a range from 20 to 500 monitor units (MU). Individual ionisation chamber responses were normalised to a reference dose value of 100 MU. The NE2571 ionisation chamber was used in this setup as a reference. The panel's response was normalised to the reference chamber response as described by [69].

4.2.4 Output factors

The panel was used to determine output factors in a magnetic field, for field sizes of 5.6 x 5.6 cm^2 and 23.8 x 23.8 cm^2 and a reference field size of 9.8 x 9.8 cm^2. At the Elekta SL*i* the MLC leaves project to 1 cm at isocentre, therefore field sizes of 5 x 5 cm^2 and 25 x 25 cm^2 were chosen, to compare to a reference field size of 10 x 10 cm^2. To ascertain lateral charged particle equilibrium for all field sizes, only the ionisation chambers in the centre 3 cm of the panel were used. The output factor was determined for every individual ionisation chamber and compared to the output factor determined using the NE2571 ionisation chamber.

4.2.5 Pulse rate frequency dependence

The impact of a difference in pulse rate frequency (PRF) on the ionisation chamber response was determined for each individual ionisation chamber. The NE2571 chamber was used to correct for a possible change in linac output. In the magnetic field, the PRF dependence of the panel was determined by a halving of the PRF from 240 Hz to 120 Hz. At the Elekta SL*i*, without the magnetic field, the PRF was halved from 400 Hz to 200 Hz. The pulse lengths were 3.2μs and 4μs for the Elekta SL*i* and MR-linac, respectively. The ionisation chamber readings obtained with the lower PRF were normalised to the measurements obtained with the high PRF.

4.2.6 Power to electronics

The time required for the panel's electronics to reach equilibrium after applying power to the electronics was determined by taking background measurements using the continuous measuring mode. Before each measurement set, the panel was allowed to reach equilibrium in room conditions overnight. Leakage measurements commence directly after applying power to the electronics. One minute measurements were performed each minute for the first 5 minutes. After the first 5 minutes, one minute measurements were performed every 5 minutes for one hour.

Several setup conditions were investigated using this method. Firstly, a measurement set in the clinical accelerator treatment room, at earth magnetic field strength. Secondly, a measurement set after equilibrating the panel overnight at negligible magnetic field, and moving the panel into the 1.5 T magnetic field at the moment of applying power to the electronics. These two setup conditions were repeated, with the addition of a new background correction prior to the measurement at 15 minutes.

4.2.7 Influence of panel orientation

The influence of the ionisation chamber orientation in the magnetic field was determined by rotating the panel 5° in each direction around the CAX. If a slight panel rotation causes a large deviation in the measurements, it would seriously hamper the ease with which the panel can be used in the MR-linac. The resulting dose profiles were compared with the un-rotated profile after transforming it back to the original orientation.

4.2.8 Influence of ionisation chamber shape

The influence of the magnetic field on the measurement for the different shapes of ionisation chambers was investigated by rotating the panel 45° clockwise around the CAX. Because of this rotation ND-axis took the position of the Y-axis, therefore the same profile was measured with two different panel axes and thus two differently shaped ionisation chamber types. The profiles measured with the two different axes were compared.

4.2.9 Validation with film measurements

As a validation of feasibility, panel measurements were compared with Gafchromic EBT2 (ISP, Wayne, USA) film measurements obtained simultaneously in the

MR-linac. This type of film has previously been used for dose profile measurements inside the magnetic field [46]. If the ionisation chambers in the panel are affected significantly by the magnetic field, this will be visible as a difference between the film and panel dose profiles.

For these measurements films were placed between the build-up plate and the panel. Measurements were performed for field sizes of 5.6 x 5.6 cm^2, 9.8 x 9.8 cm^2 and 23.8 x 23.8 cm^2. The measured film profiles are projected onto the plane of the ionisation chamber to correct for the intrinsic build up distance of 0.9 cm. Analysis of the film took place according to the method described by Micke et. al. [70].

4.3 Results

4.3.1 Reproducibility

Table 4.1: Overview of the reproducibility measurements results.

	No magnetic field	Magnetic field
Mean CV (%)	0.287	0.230
Max CV (%)	0.522	0.490
Max deviation (%)	0.714	0.682

The reproducibility measurement results are summed in table 4.1. For the 10 repetitions of the one minute measurements without the magnetic field, the average CV is 0.29%, while the CV is 0.23% for the measurements inside the 1.5 T magnetic field. The distribution of the CV values is similar for both situations.

The student t-test shows no significant difference in measurement value (p=0.24), or CV, between the first 15 seconds after start up, and the last 45 seconds of the measurement.

4.3.2 Dose response linearity

The dose response linearity with and without magnetic field is summed in figure 4.2. The error bars represent the standard deviation of the results, per point of measurement.

The maximum average deviations from perfect linearity are 0.17% with and without magnetic field.

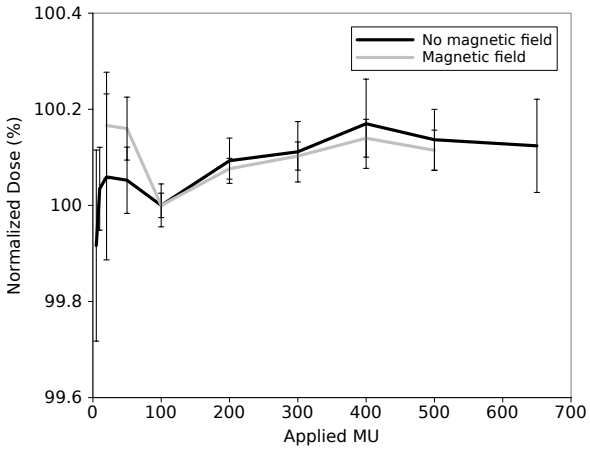

Figure 4.2: Dose response linearity for the setup at the situation with and without magnetic field. The results for each applied dose are normalised to a reference dose of 100 MU. The error bars represent the standard deviation per measurement point.

4.3.3 Output factors

The output factors determined by using the panel deviate less than 0.4%, from the factors determined using the NE2571 chamber. This deviation is independent of the presence of a magnetic field.

4.3.4 Pulse rate frequency dependence

Figure 4.3 shows the influence of a PRF halving on the dose response of the detectors on the X-axis and the PD-axis. The average change in dose response for the ionisation chambers is 0.5%, for the setup with and without magnetic field. The difference in detector response to the PRF halving was not significant, p=0.69 and p=0.10 for the X and PD axis, respectively.

4.3.5 Power to electronics

Figure 4.4 shows the average leakage of all ionisation chambers in the panel, and the standard deviation per measurement time. The average leakage after one hour is notably larger when the panel was placed into the magnetic field.

When a new background measurement is taken after 15 minutes in the magnetic field, followed by a new dark current correction, the average leakage and

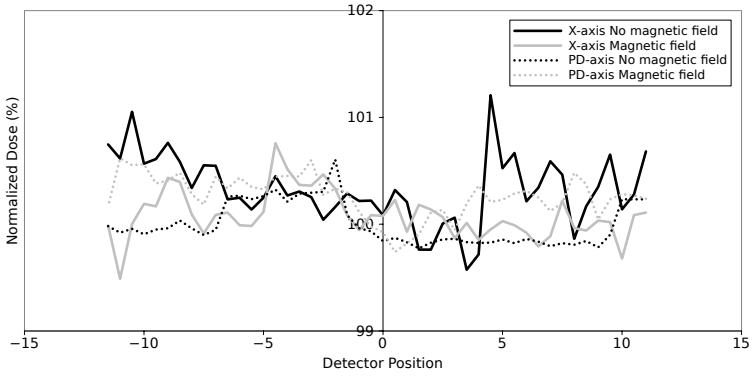

Figure 4.3: The change in ionisation chamber response due to halving of the PRF, for the detectors on the X-axis and PD-axis with and without the magnetic field.

the standard deviation over the ionisation chambers are minimised. The leakage 45 minutes after the second background measurement is less than 0.1% of the average expected CC per integration time for the lowest available dose rate.

A student t-test showed that there is no significant difference between the leakage of the chambers on the various axes, within a significance level of 5%.

4.3.6 Influence of panel orientation

Rotating the panel 5° in either direction affects the profile measurements by an average of less than 0.2% for the setup with and without the magnetic field. The largest deviation of 1% was found for the penumbra areas where the dose gradient is largest. This deviation is most likely due to a 0.1 mm shift in position of the panel, or an imperfect rotation around the CAX.

4.3.7 Influence of ionisation chamber shape

The dose profiles measured with both axes of the panel are visualised in figure 4.5. The largest deviation between the profiles is seen at the high dose gradient regions. This deviation is due to the difference in ionisation chamber placement between the profiles.

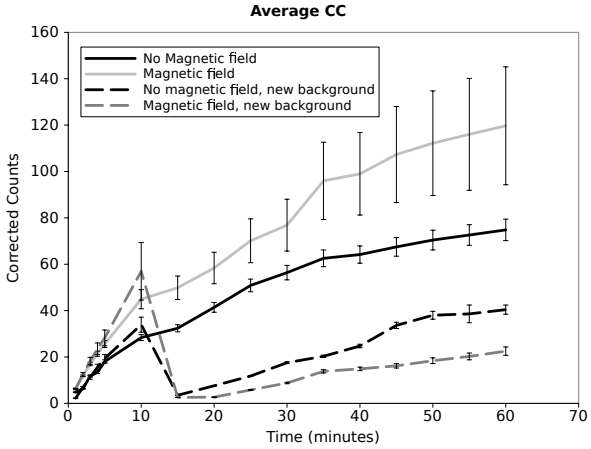

Figure 4.4: The one minute leakage measurements over a period of one hour starting the moment of applying power to the electronics. The error bars represent the standard deviation for each point of measurement.

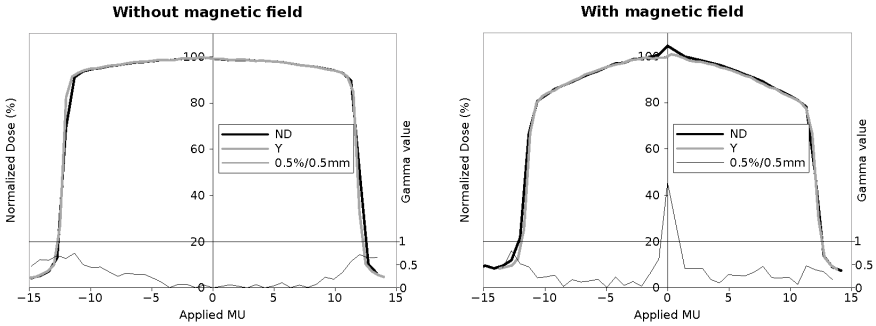

(a) (b)

Figure 4.5: Measurements of the same profile with the Y-axis and the ND-axis on the panel for the situation (a) without and (b) with magnetic field.

4.3.8 Validation with film measurements

Figure 5.3 shows the profiles measured with the panel and the EBT2 film. The extra series represents the γ 2%/2 mm for the film and panel measurements. For the X-axis, only 1% of all pixels have a gamma value larger than 2%/2 mm. For the ND-axis, 4% of all points have a gamma value larger than 2%/2 mm.

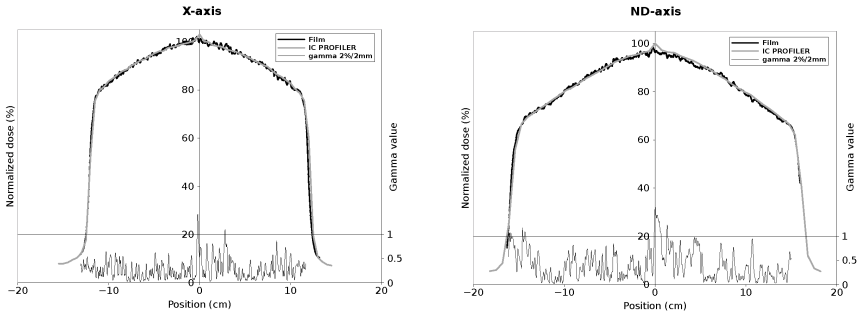

Figure 4.6: Normalised (a) X and (b) ND profiles measured with the IC PROFILER^{TM} and the Gafchromic EBT2 films. The gamma 2%/2mm is included, the horizontal line represents unity for the 2%/2mm comparison criterion.

4.4 Discussion

The dose response linearity and reproducibility of the ionisation chambers are not affected by the magnetic field. Additionally we have shown that the ionisation chamber shape and orientation in the magnetic field, does not affect the linearity and reproducibility. Therefore, the central ionisation chamber on the panel can be used to normalise the signal for ionisation chambers on all axes.

As can be seen in figures 5.3 and 4.5(b) shape and orientation of the ionisation chambers cannot be neglected completely. The X and ND-profiles show a slight peak in the centre of the profile, this peak is present in the X-axis, ND-axis and PD-axis. Each of these three axes do not have ionisation chamber at the centre, therefore the reading of the centre chamber on the Y-axis is used to complete the profiles. However, this chamber has a different orientation, and a different shape for the diagonal profiles, than the chambers on the other profiles.

When looking at the dose profiles, this peak is the only noticeable effect of the magnetic field. On both diagonal axes the ionisation chambers shape is

mirrored in the panel centre, but also the polarity of the chambers is mirrored. Because there is no visible effect in these profiles, we conclude that the polarity and ionisation chamber orientation in the magnetic field do not significantly influence the measurement results.

Since the leakage in the magnetic field is not significantly different for the various ionisation chamber orientations and shapes, the average leakage will be corrected by normalisation. This means that normalised array measurements, like profile measurements, can be performed when the standard deviation is considered acceptable.

Simon et. al. [69] showed that the panel can be used for measurements where the individual CC of the ionisation chambers are of interest, e.g. output factor measurements. Based on the results in section 4.3.5, we advise a stand by period of 15 minutes followed by a background correction, before commencing unnormalised measurements. In section 5.3.3 we showed that this statement is true for measurements inside and outside a 1.5 T magnetic field.

The validation with film measurement results, in figure 5.3, show that the panel performs well in a transverse 1.5 T magnetic field. This figure also clearly depicts the value of an ionisation chamber array. Film measurements have the advantage of measuring full 2 dimensional dose distributions with a high spatial resolution, but are time consuming and the results are less accurate than ionisation chamber measurements. Ionisation chamber array measurements have a short setup time, facilitate online feedback and provide enough information about the dose distribution for most purposes.

We expect the IC PROFILER^{TM} can be used not just in the MR-linac, but also in other radiation treatment combinations which incorporate a transverse magnetic field, e.g. [37] or [48].

4.5 Conclusion

The purpose of this study was to characterise the performance of the detector array IC PROFILER^{TM} in a 1.5 T magnetic field. We have shown that the IC PROFILER^{TM} is suited for profile measurements within a transverse 1.5 T magnetic field of the MR-linac. As expected from literature, the ionisation chambers are affected by the magnetic field, this affects the performance of the panel in a very limited manner. Not only can the IC PROFILER^{TM} be used for normalised profile measurements, the unnormalised measurement results

can also be used to determine output factors. Caution must be taken only when comparing the unnormalised values of ionisation chambers on more than one axis. The availability of a multi-axis ionisation chamber array greatly speeds up measurements in the MR-linac.

Acknowledgements

The authors would like to thank the Sun Nuclear Corporation for providing us with a magnetic field compatible IC PROFILER^{TM}. Part of this research is financially supported by the Dutch Technology Foundation STW.

5

Performance of the STARCHECK™ multi-axis ionization chamber array in a 1.5 T magnetic field

In preparation for submission
K. Smit, J.G.M. Kok, J.J.W. Lagendijk and B.W. Raaymakers.

Abstract Dosimetry for MRI-based image guided radiotherapy devices requires dosimetry devices compatible with a 1.5 T magnetic field. The purpose of this study was to investigate the feasibility of using a STARCHECK™ in a transverse 1.5 T magnetic field. The investigated characteristics were short term reproducibility, dose response linearity, accuracy of output factor measurements and the influence of the magnetic field on a purposefully introduced misalignment. As a validation of feasibility, STARCHECK™ measurements were compared with film measurements simultaneously obtained in the MR-linac.

The dose response linearity of the ionization chambers in the STARCHECK™ is not affected significantly by the magnetic field and output factor measurements can be performed using the panel. The reproducibility measurements show a significant 0.03% increase of the relative standard deviation due to the magnetic field, this increase is not considered to be clinically relevant. The orientation of the ionization chambers in the magnetic field is of importance, but it does not influence the required measurement setup accuracy requirements.

The difference in ionization chamber orientation between axes does not influence the individual measured dose profiles when the central ionization chambers are excluded

from analysis. From these results we conclude that the STARCHECK^{TM} is suited for dose profile measurements in a transverse 1.5 T magnetic field.

5.1 Introduction

The MR-Linac is an image guided radiotherapy device, a combination of a 1.5 T closed bore Philips MRI scanner (Best, The Netherlands) and an 8 MV Elekta (Crawley, UK) linear accelerator. This device is an upgraded version of the setup described in Raaymakers et. al. [40]. The goal of this combination is to use the superior soft tissue contrast of the imaging system for high precision image guidance of radiotherapy treatment delivery. The superior soft tissue contrast of the imaging system can be used to improve tumour position verification, and thereby minimize the required tumour motion margins [57].

The homogeneous 1.5 T magnetic field does not affect the photons in the treatment beam yet the secondary electrons are deflected by the Lorentz force [36]. The effect of this deflection on the deposited dose is most noticeable at tissue-air interfaces, because the longer electron trajectory in low density media allows the deflection to become more pronounced [41]. As the reading of an ionization chamber depends on the number of electrons and the electron trajectory inside the measuring volume, the dose response of air filled ionization chambers changes in the magnetic field [51]. Therefore, a magnetic field correction factor must be included for reference dosimetry with an air filled ionization chamber like the NE2571 [66]. The magnitude of this magnetic field correction factor depends on several factors e.g. magnetic field strength, ionization chamber geometry and orientation of the ion chamber inside the magnetic field.

Ionization chamber arrays are of great convenience for dose distribution measurements because of their easy handling and fast results [39]. However, before such a device can be used for dosimetry measurements in a magnetic field, the influence of the magnetic field on the ionization chambers in the array must be characterized [71].

The purpose of this study was to investigate the feasibility of using a STARCHECK^{TM} (Physikalische Technische Werkstätten, Freiburg, Germany) in a transverse 1.5 T magnetic field as for example found in the MR-linac and [37] or [48]. The influence of the magnetic field on the basic STARCHECK^{TM} characteristics were investigated similarly to Simon et. al. [69]. The investigated characteristics were short term reproducibility, dose response linearity and the accuracy of output factor measurements [54]. Additionally the influence of the magnetic field on a purposefully slight misalignment was investigated. As a validation of

feasibility, STARCHECK^{TM} measurements were compared with film measurements simultaneously obtained in the MR-linac.

5.2 Materials and methods

The panel used in this study is the STARCHECK^{TM} (Physikalische Technische Werkstätten, Freiburg, Germany). This specific panel was modified for measurements inside a magnetic field by removing all the ferromagnetic components.

The panel has 527 vented ionization chambers mounted in several arrays within an area of 25.2 x 25.2 cm^2. For this study the ionization chamber on the two arrays on the coordinate axes (referred to as inplane and crossplane) and two arrays on the positive and negative diagonals (referred to as first and second diagonals) were used. At the intersection of the arrays there is only one centre detector, that will be used as a reference detector for all arrays.
The ionization chamber positions are depicted on the surface of the panel, figure 5.1.

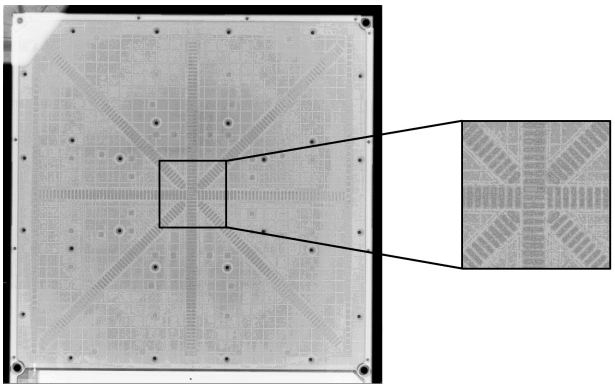

Figure 5.1: An mega voltage image of the surface of the STARCHECK^{TM} panel with a magnification of the panel centre showing the ionization chamber positions and orientations.

Unless mentioned otherwise, the panel measurements were performed according to the following standard setup conditions.

The baseline performance of the panel was assessed at an Elekta Synergy (Elekta AB, Stockholm, Sweden) at an SSD of 100 cm, a field size of 25 x 25 cm^2 was used.

The measurements in the 1.5 T magnetic field were performed at the MR-linac [40] at an SSD of 153.5 cm. In the MRI feet-head direction, the field size is restricted by scanner structures to a maximum of 24 cm at the isocentric plane. The MLC leaf width of the MR-linac is 0.7 cm, therefore irradiation took place with a 23.8 x 23.8 cm^2 field. At the STARCHECK^{TM} surface this field projects to 25.5 x 25.5 cm^2.

Both linacs are calibrated to deliver 1 Gy per 100 MU at dose maximum under reference conditions [50]. Before commencing the measurements, the setup was left in stand by mode for at least 15 minutes and the panel was pre-irradiated with a dose of 1 Gy.

For cumulative dose analysis, a NE2571 Farmer ionization chamber (NE Technology Limited, Berkshire RG7 5PR, England) was used as an external reference. A Unidos E electrometer (PTW, Freiburg GmbH, Germany) was used to measure the charge collected by the Farmer ionization chamber, in nC. The NE2571 was positioned on the CAX directly behind the panel in the centre of a 20 x 20 x 6 cm^3 PMMA phantom. Smit et. al. [66] showed that this ionization chamber is suitable as an external reference detector in a 1.5 T magnetic field.

The panel was controlled using software provided by the supplier. Data was acquired every 200 ms. The raw data was exported in ASCII format and analyzed using in-house developed MATLAB^{TM} (MathWorks, Natick, MA, USA) based software.

5.2.1 Reproducibility

The short term reproducibility of the panel was evaluated using 10 consecutive one minute measurements obtained under constant irradiation. The centre chamber on the panel funcioned as reference chamber per time point. All ionization chambers that received more than 80% of the reference chamber dose, were used for analysis. The reproducibility was quantified by determining each detectors coefficient of variation (CV), which is the relative standard deviation, and the maximum deviation from the mean.

5.2.2 Dose response linearity

The dose response linearity was determined over a range from 5 to 500 MU. All ionization chambers that received more than 80% of the reference chamber dose, were used for analysis. Individual ionization chamber responses were normalized to their response at 100 MU. These results were then normalized to the response of the NE2571 ionization chamber [69].

5.2.3 Output factors

The panel was used to determine output factors for field sizes between 5 x 5 cm^2 and 25 x 25 cm^2. To ascertain lateral charged particle equilibrium at the location of the ionization chambers for all field sizes, only the centre 9 ionization chambers of each axis were used for analysis. The output factors were determined for every individual ionization chamber and compared to the output factor determined using the NE2571 ionization chamber.

5.2.4 Influence of panel orientation

The influence of the magnetic field on the ionization chamber orientation was determined by rotating the panel 5° on purpose, in both directions around the CAX. The resulting dose profiles were compared with the perfectly aligned profile.

5.2.5 Validation with film measurements

As a validation of the panel performance, STARCHECK™ measurements were compared with Gafchromic EBT2 (ISP, Wayne, USA) film measurements obtained simultaneously in the MR-linac [46]. For these measurements films were placed between a 30 x 30 x 2 cm^3 build-up plate and the panel surface. Analysis of the film took place according to the method described by Micke et. al. [70].

5.3 Results

5.3.1 Reproducibility

The reproducibility measurement results are summed in figure 5.2(a). For the 10 repetitions of the one minute measurements the average CV are 0.19% and 0.22% with and without the 1.5 T magnetic field, respectively. A Student t-test shows that the difference between the CV distribution with and without the magnetic field is significant ($p<0.01$).

5.3.2 Dose response linearity

The dose response linearity with and without magnetic field is summed in figure 5.2(b). The average deviations from perfect linearity are 0.22 and 0.28% with and without magnetic field, respectively. The largest deviation was found for the lowest applied doses. The magnetic field does not have a significant effect on the average deviation from perfect linearity (p=0.35).

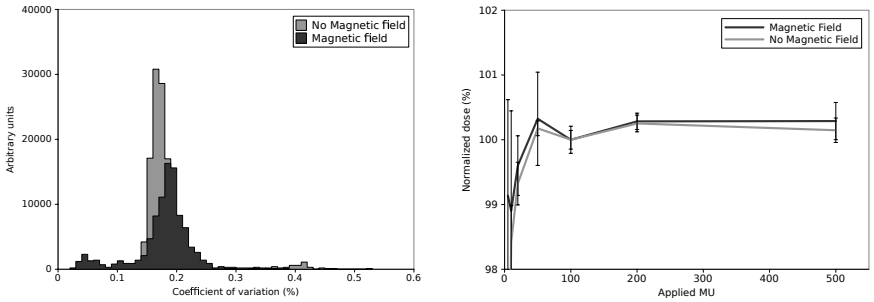

(a) (b)

Figure 5.2: Figure (a) shows the distribution of the calculated CV's, for the situations with and without the magnetic field. Figure (b) shows the dose response linearity for the setup at the situation with and without magnetic field. The results for each applied dose are normalized to a reference dose of 100 MU. The error bars represent the standard deviation per measurement point.

5.3.3 Output factors

The difference between the output factors determined using the STARCHECK^{TM} deviate less than 0.4% from the factors determined using the NE2571 ionization chamber, with and without the magnetic field.

5.3.4 Influence of panel orientation

Rotating the panel 5° in either direction affects the profile measurements by an average of 0.3% or 0.2% with and without the magnetic field, respectively. This deviation is not significantly different between any of the separate panel axes.

5.3.5 Validation with film measurements

Figure 5.3 shows the profiles measured with the panel and the EBT3 film. The extra series represents the γ 2%/2 mm for the film and panel measurements.

Approximately 5% of all pixels have a gamma value larger than 2%/2 mm. Nearly all these pixels are found in the centre 2 cm of the panel, where the 4 axes coincide.

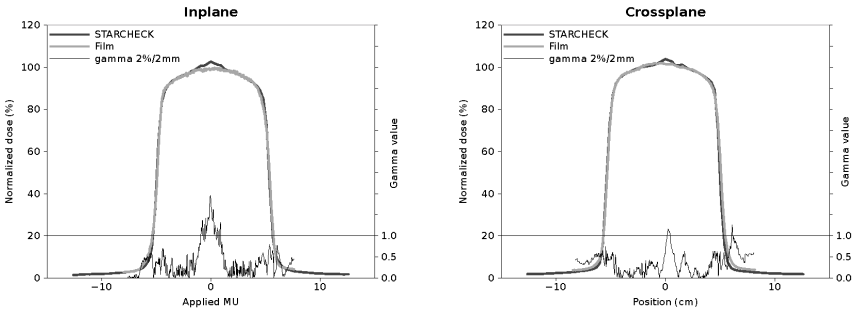

(a) (b)

Figure 5.3: Figure a shows two dose profiles measured using the STARCHECK^{TM} and the EBT3 films.

5.4 Discussion

The dose response linearity of the ionization chambers in the STARCHECK^{TM} is not affected by the magnetic field. Additionally, the panel can be used to perform output factor measurements with and without a magnetic field. The absolute difference in average CV with and without the magnetic field is 0.03%. A Student t-test showed that this difference is significant but it is not considered clinically relevant. The slightly higher average CV is possibly caused by the lower dose rate of the MR-linac prototype compared to the Elekta Synergy.

Meijsing et. al. [51] have shown that the orientation of an ionization chamber is of importance in a magnetic field. If a slight rotation causes a large deviation in the measurement results it would seriously hamper the ease with which an ionization chamber array panel can be used in the magnetic field. The 5° rotation evaluated in this study was easily discerned as a mis-position. Yet, this large mis-position does not affect the measurement results.

The effect of ionization chamber orientation in a magnetic field can also be seen in figure 5.3. The axes that do not have an ionization chamber in the centre position use the measured value of the centre ionization chamber. The different orientation of the reference detector compared to the other detectors

in the array causes a discontinuity in the profile. For the inplane direction, the ionization chamber array is not interrupted by ionization chambers in a different orientation. This dose profile shows a slightly higher dose response for the centre three ionization chambers. When the panel is moved along the inplane axis, the deviating results remain at the same ionization chambers. This confirms the hypothesis that the deviation is linked to specific ionization chambers. Previous studies [71] have shown that this effect is present in other multi-axis ionization chamber arrays as well. Our current recommendation is to exclude the signal of these specific ionization chambers from analysis.

5.5 Conclusion

The purpose of this study was to characterize the performance of the STARCHECK^{TM} detector array in a 1.5 T magnetic field. We have shown that the STARCHECK^{TM} is suited for dose profile measurements in a transverse 1.5 T magnetic field. The ionization chambers are affected by the magnetic field, but this only affects the performance of the panel in a very limited manner. Because of a difference in ionization chamber orientation between axes, caution must taken when comparing the un-normalized values of ionization chambers on more than one axis. The availability of a multi-axis ionization chamber array greatly speeds up measurements in the MR-linac.

Acknowledgements

The authors would like to thank PTW for providing us with a magnetic field compatible STARCHECK^{TM}. Part of this research is financially supported by the Dutch Technology Foundation STW.

6

Integrated MegaVoltage portal imaging with a 1.5 T MRI linac.

This chapter has been published as:
B.W. Raaymakers, J.C. de Boer, C. Knox, K. Smit, S.P. Crijns, M.K. Stam, M.R. van den Bosch, J.G.M. Kok and J.J.W. Lagendijk. Integrated megavoltage portal imaging with a 1.5 T MRI linac. *Physics in Medicine and Biology*. 2011. **56**(19):N207–14.

Abstract
The feasibilty of complementing our hybrid 1.5 T MRI linac (MRL) with a MV portal imager is investigated. A standard aSi Megavoltage (MV) detector panel is added to the system and both qualitative and quantitative performance are determined.
Simultaneous MR imaging and transmission imaging can be done without mutual interference. The MV image quality is compromised by beam transmission and larger isocenter distance, still, the field edges and bony anatomy can be detected at very low dose levels of 0.4 cGy.
MV imaging integrated with the MRL provides an independent and well established position verification tool, a field edge check and a calibration for alignment of the coordinate systems of the MRI and the accelerator. The portal imager can also be a valuable means for benchmarking MRI guided position verification protocols on a patient specific basis in the introductory phase.

Chapter 6

6.1 Introduction

At the UMC Utrecht, the Netherlands, we have, in collaboration with Elekta, Crawley, U.K. and Philips, Best, The Netherlands, developed and built an MRI linac (MRL). The system consists of a modified 1.5 T Philips Achieva MRI with a modified 6 MV Elekta accelerator next to it and allows independent and unhampered imaging and beam delivery [40]. The aim of this system is to facilitate MRI guided Radiotherapy (MRIgRT) [57]. Now the proof of concept of simultaneous MRI and radiation delivery has been given, the system is currently upgraded to a clinical prototype with a continuous rotating ring-mounted accelerator including a MLC collimator which will be installed in August 2011.

The MRI provides exquisite soft-tissue contrast imaging of the tumour and its surroundings during radiation delivery. However, it cannot visualise the treatment beam relative to the patient. So to define the spatial relation between the coordinate system of the accelerator and the coordinate system of the MRI one has to rely on pre-treatment calibration. This can be done using a MegaVoltage (MV) portal imaging device mounted opposite to the accelerator on the ring gantry to generate beam transmission images independent of the MR images.

Besides the possibilities for calibrating the coordinate systems, MV portal imaging can also be used as is already commonly done in the radiotherapy practice such as fiducial marker detection for position verification, IMRT segment shape validation, exit dosimetry but potentially also MV CBCT [18], [72], [16], [73] and [74]. Furthermore, MV imaging is valuable in introducing MRIgRT in the clinic. For selected tumour sites such as spinal bone metastases, the MRI guidance can be benchmarked against the MV imaging for individual patients.

In this paper we demonstrate the technical feasibility of a MV detector panel for portal imaging in the MRL.

6.2 Methods

6.2.1 Setup of static prototype

The current set-up of the MRL is presented in detail by Raaymakers et. al. [40]. In summary, it is a static 6 MV Elekta (Crawley, U.K.) accelerator mounted on a stand that is placed lateral to a modified 1.5T Achieva Philips MRI with an isocenter distance of 1.5m. The mid transversal section of the MRI has been optimised for beam transmission. Both the magnet and the gradient coil

are homogeneous and minimized with respect to mass [75]. This region allows a 24 cm field in axial direction at isocenter while the total amount of mass in the beam portal is the equivalent of 10 cm of aluminium. Additionally the radiofrequency quadrature bodycoil (QBC) is in the beam. This is the innermost cylinder in the MRI and is not optimised for radiation transmission. The QBC is relatively transparant but does induce some heterogeneity as will be seen in section 8.3.

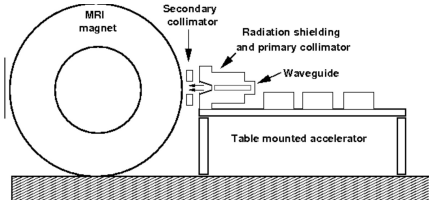

Figure 6.1: A schematic of the static set-up as used in this work. The accelerator is positioned static next to the MRI, the portal imager is positioned at 2.58 m at the distal side of the MRI, shown in red.

6.2.2 Position of the panel in the MRL

A ring gantry in which the accelerator is mounted will be built around the MRI scanner and is currently under construction. Opposite to the accelerator in the ring is a beam stopper that also acts as a counterbalance. On top of this beam stopper a Megavoltage detector panel can be mounted. For the present static beam set-up, the panel is 2.58 m from the target, see figure 8.1. Given the isocenter distance of 150 cm, the magnification factor is 1.72, i.e. a 10x10 cm^2 field at the isocenter will be projected as 17.2x17.2 cm^2 at the panel. Since the portal imager is 40x40 cm^2, the panel is limiting the maximum field size that can be detected to 23.3x23.3 cm^2 at isocenter. Before the beam hits the panel it has to travel through the MRI twice, so through the equivalent of 20 cm aluminium, plus twice through the QBC. The magnetic stray field outside the MRI, at the location of the panel is approximately 0.08 T, this work investigates the performance of the panel in this set-up.

6.2.3 The Megavoltage detector panel

The panel is a amorf Silicium flatpanel for imaging Megavoltage radiation beams (Elekta, Crawley, U.K.). Data was acquired with the standard frame rate of 433 ms per frame. This corresponds to 0.4 cGy per frame at the isocenter.

The images for qualitative purposes were acquired using the XIS software (Heimann Imaging Systems) where the offset or dark current is corrected and the gain per pixel can be calibrated. The images used in quantitative analysis were acquired and analysed using the Theraview NT software (Theraview Technology, Cablon Medical).

6.2.4 Perfomance tests

The performance of the panel is evaluated in several ways:

Feasibility The first feasibility test is acquisition of the offset and gain images to see if the panel works in the close vicinity of the 1.5 T MRI system. This is done for a 10x10 cm^2 field at the isocenter.

Simultaneous MV and MR imaging The feasibility of simultaneous portal imaging and MRI is investigated by irradiating a small, plastic bottle of 6 cm diameter and 14 cm height, filled with water doped with copper sulphate for MRI contrast, with a 10x10cm^2 radiation field. The portal images are the average of 50 frames, the MRI sequence is a T1 weighted gradient echo. Also the MRI data is the average of 32 consecutive images to make sure the MRI is constantly running during portal imaging.

Qualitative image quality The qualitative performance is demonstrated by lateral transmission images through the Alderson phantom (Radiology Support devices inc.) for vertebrae and a hip joint. The latter imaging is also done with a 3 cm and 1.1 mm diameter Visicoil marker (RadioMed Corporation) positioned at the proximal side of the Alderson phantom. The average of 1, 10, 25 and 50 frames is presented.

Quantitative image quality The quantitative performance is analysed using the QC3 phantom (Standard Imaging inc.) and the Las Vegas phantom (Elekta, Crawley, U.K.). The analysis of these phantom images is automatically performed in the Theraview software. Both phantoms are placed at the isocenter, i.e. 1.5 m from the target. For the QC3 phantom the F50 in line pairs per mm will be determined at isocenter, as well as the contrast to noise ratio, see [76] for details. This will be done as function of the number of averaged frames. For the Las Vegas phantom contrast-detail curves are generated as function of the number of averaged frames. Whether a circle is detected is determined using a student t-test on the difference between the signal from the object in question and the direct surroundings, see [77] for details.

6.3 Results

The first feasibility test is acquiring the gain and offset images for a open beam. Later, these images will be used to correct for the heterogeneity from beam transmission through the MRI system. As mentioned in section 7.2 the magnet and the gradient coil are optimised for beam transmission, the RF body coil (QBC) is not. In figure 6.2(a) the transmission image through the system is shown. Clearly the copper rods from the QBC can be recognised, together with electronic print boards. If the transmission image is used as a gain correction, a flat open field is the result, see figure 6.2(b). Note that also the penumbra region is accounted for by the gain correction, yielding a sharply bordered field for imaging. The panel functions properly in the presence of a 0.08 T field.

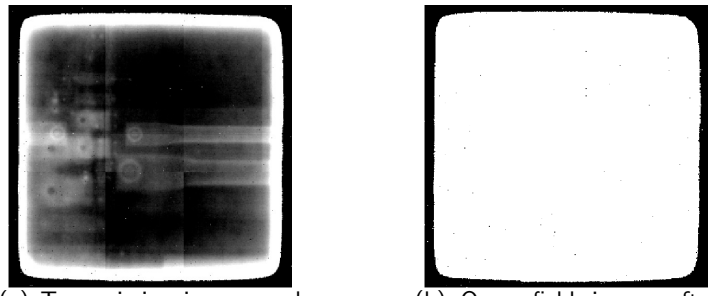

(a) Transmission image used for gain correction

(b) Open field image after gain correction

Figure 6.2: MV images of transmission before and after gain correction.

The simultaneous performance of the portal imager and MRI is shown in figure 6.3. There is no difference between the portal image with and without simultaneous MRI acquisition, when subtracting the images, only noise remains.

In figure 6.4 the lateral portal images through the Alderson phantom at the level of the upper torso are shown. Already for a single frame the vertebrae can be distinghuished, the vertical stripes are from the gaps in between the slices of the Alderson phantom. Averaging over more frames yields less noisy images, as expected.

In figure 6.5 the lateral portal images through the Alderson phantom at the level of the pelvis are shown. Again, already for a single frame the pelvic structure can be distinghuished.

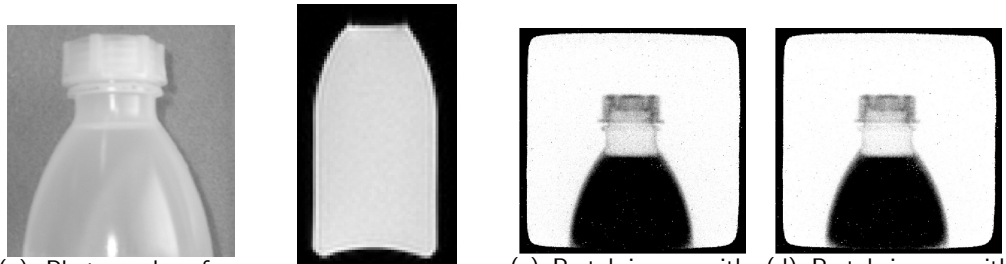

(a) Photograph of a small water bottle (b) MRI during beam on (c) Portal image without MRI acquisition (d) Portal image with MRI acquisition

Figure 6.3: Photograph(a), T1FFE MRI (b) and portal images of a small water bottle without (c) and during MRI scanning (d).

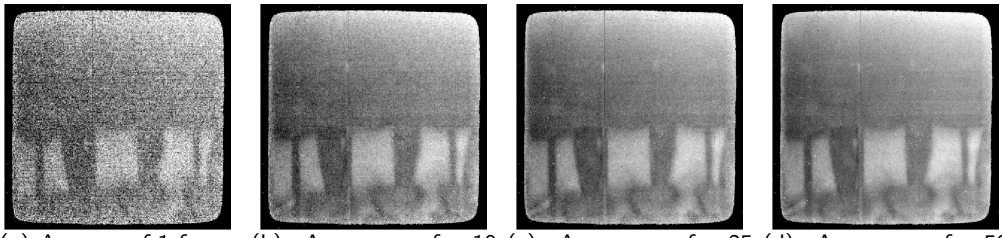

(a) Average of 1 frame (b) Average of 10 frames (c) Average of 25 frames (d) Average of 50 frames

Figure 6.4: Portal images of the Alderson phantom at the level of the upper torso with an increasing number of frames averaged to increase the signal to noise ratio.

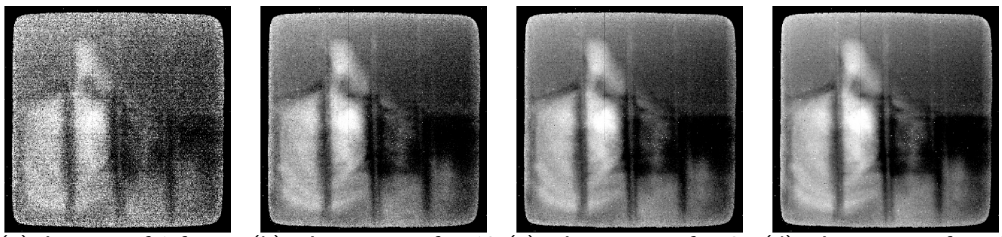

(a) Average of 1 frame (b) Average of 10 frames (c) Average of 25 frames (d) Average of 50 frames

Figure 6.5: Portal images of the Alderson phantom at the level of the pelvis with an increasing number of frames averaged to increase the signal to noise ratio.

Figure 6.6 shows the same anatomy as figure 6.5, but now with a Visicoil marker taped at the proximal side of the Alderson phantom. The marker can be seen on the average of 10 frames and more in the bottom middle section of the image.

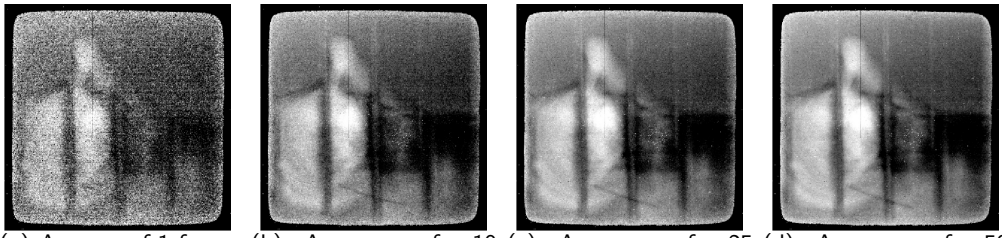

(a) Average of 1 frame (b) Average of 10 frames (c) Average of 25 frames (d) Average of 50 frames

Figure 6.6: Portal images of the Alderson phantom at the level of the pelvis with an increasing number of frames averaged to increase the signal to noise ratio.

A more quantitative performance evaluation is done using the QC3 phantom, figure 6.7(a) and the Las Vegas phantom, figure 6.7(b). The F50 found from the QC3 phantom is 0.31 line pairs per mm and is independent on the number of averaged frames. The contrast-to-noise ratio (CNR) is plotted as function of the number of frames averaged in figure 6.7(c). The CNR value is around 25 for a 20 frame image. The contrast-detail curve for the average of 20 frames is shown in figure 6.7(d). This curve shows that for instance a contrast of 0.25 % can be detected for cylindrical objects of more than 10 mm diameter. Detection success is also indicated in figure 6.7(b) by the green and red circles. Note that objects not detected at all are not indicated.

6.4 Discussion

The flat panel portal imaging device does work in the direct vicinity of the MRI. So an object can be visualised on MV transmission images, together with the radiation field edges, while simultaneous an MR image of the same object can be made, as seen in figure 6.3.

The image quality of the portal images is less than conventional portal images. Clearly this is due to the large distance of the panel from the focus, but also due to the limited beam transmission through the MRI system. The CNR of

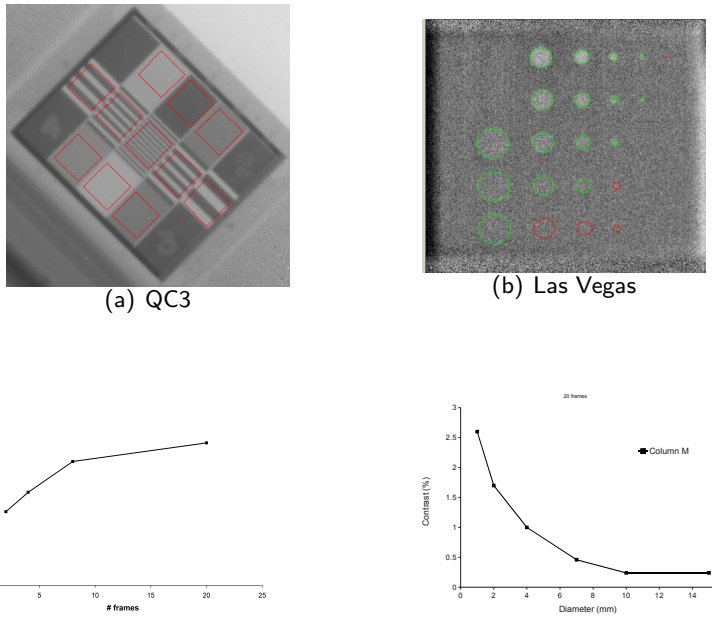

(a) QC3

(b) Las Vegas

(c) Contrast-to-noise ratio for QC3

(d) Contrast detail curve for Las Vegas

Figure 6.7: Portal images of the QC3 and the Las Vegas phantom for an average of 20 frames. In the lower row the contrast-to-noise versus the number of averaged frames as determined for the QC3 phantom and the contrast-detail curve for the Las Vegas phantom using the average of 20 frames.

approximately 25 for the average of 20 frames (approximately 8 MU on a clinical accelerator) is low. When using the same phantom on a regular 6 MV linac (Elekta), with a standard flat panel EPID at source to detector distance of 150 cm, a value of 106 is measured for an exposure of 10 MU. However, if we assume that quantum noise dominates the noise contribution, we can correct this value for the transmission through the MRI and the source to detector distance of 258 cm. Then the CNR of the clinical panel would drop to 19, which is in the same range as the CNR in the MRL configuration. This suggests that panel performance on the MRI linac is comparable to that of a portal imager on a standard linac.

The spatial resolution, in this case expressed by the F50, is 0.31 line pairs per mm at isocenter. This is somewhat lower than F50 values found in current standard radiotherapy setup but not dramatically so. Typical F50 values are in the range 0.30-0.40 as seen in the PIPSpro technical note on the QC3 phantom (Standard Imaging inc, WI, USA). The value is a little lower because of the relatively large magnification factor (1.72). The result is the combined effect of image blurring due to the finite source size and the improved spatial resolution due to the magnification factor. In fact, using fundamental equations regarding the modulation transfer function of the EPID system, the estimated source size is 3.0 mm FWHM. This value is fully consistent with published values in the range of 2.5-3.3 mm for Elekta-manufactured linacs, see e.g. [78].

Consequently, the image quality allows easy detection of field edges from a single frame of 0.433 ms. This allows for dynamic quality assurance of the radiation field geometry. Because we also obtain the detailed anatomical information from the MRI scanner, accurate in-vivo dose reconstruction based on EPID images becomes feasible. Since the accelerator and the MV panel will be mounted on a continuous rotating gantry as of August 2011, projections from multiple gantry positions can be acquired. By proper design of a phantom, e.g. a ball bearing in a water phantom, the exact isocenter location of the accelerator can be determined while the isocenter of the MRI can be determined from the MR image. This allows for fast and accurate calibration of the coordinate systems of the accelerator and the MRI. Note that the MRI images should first be corrected for both patient induced and hardware induced geometric errors [79] [80].

Alternatively, MRI geometrical correction schemes can be independently verified by using the MV images of the bony anatomy. For instance, during the clinical introduction of the MRL for spinal bone metastases, position verification can be done using MV but also using MR imaging. MV imaging is a well established technology that can be used for benchmarking MRI based position verification strategies. One can interpret figure 6.6, which shows a Visicoil gold marker on MV imaging in the same context: for initial patient studies one can use such a clinically accepted method for position verification against which a MRI based position verification schedule can be benchmarked. Once MRI guided radiotherapy, including dedicated image sequences are established, MV portal imaging for clinical purposes will probably become rapidly obsolete on this system. However, for fast and accurate dosimetrical and geometrical beam QA, the portal imager may have a lasting role to play.

6.5 Conclusion

The hybrid 1.5 T MRL can be complemented with a MV portal imager. This allows simultaneous MR imaging and transmission imaging without mutual interference. Although the MV image quality is compromised by beam transmission and larger isocenter distance, the field edges and bony anatomy can be detected at very low dose levels of 0.4 cGy.

MV imaging integrated with the MRL provides an independent and well established position verification tool, a field edge check and a calibration for alignment of the coordinate systems of the MRI and the accelerator. The portal imager can also be a valuable means for benchmarking MRI guided position verification protocols on a patient specific basis in the introductory phase.

7

Performance of the ArcCHECK-MR QA system in a transverse 1.5 T magnetic field

In preparation for submission
A.C. Houweling, W. de Vries, J.W. Wolthaus, J.G.M. Kok, B. van Asselen, K. Smit, A. Bel, J.J.W. Lagendijk and B.W. Raaymakers

Abstract

At the UMC Utrecht, a linear accelerator with integrated magnetic resonance imaging (MRI) has been developed, the MR-linac. Routine quality assurance (QA) of treatment plans for MRI-based image guided radiotherapy requires QA systems compatible with a 1.5 T magnetic field. The purpose of this study was to examine the performance characteristics of the ArcCHECK-MR QA system in a transverse 1.5 T magnetic field. To this end, the short-term reproducibility, dose linearity, dose rate dependence, field size dependence, dose per pulse dependence and inter-diode variation of the ArcCHECK-MR diodes were evaluated on a conventional linac and on the MR-linac. The ArcCHECK-MR diodes performed well for all tests on both linacs, no significant differences in performance characteristics were observed. Differences in the maximum dose deviations between both linacs were less than 1.5%. Therefore, we conclude that the ArcCHECK-MR can be used in a transverse 1.5 T magnetic field.

Chapter 7

7.1 Introduction

At the UMC Utrecht, a linear accelerator with integrated magnetic resonance imaging (MRI) has been developed, the MR-linac. This prototype MR-linac is an upgraded version of the machine described by Raaymakers et. al. [40] and consists of an 8 MV linac (Elekta Limited Crawley, Crawley, UK) integrated with a 1.5 T MR-scanner (Philips Medical Systems, Best, The Netherlands). This combination allows for simultaneous irradiation and high-precision image guidance with soft-tissue contrast [81].

Dose deposition, dosimetry and quality assurance (QA) of the linac is affected by the presence of the 1.5 T magnetic field. Smit et. al. [66] have demonstrated that reference dosimetry using a Farmer-type ionization chamber is feasible in a 1.5 T magnetic field. Furthermore, QA of the linac can be performed using an ionization chamber array [71], a water tank [82] or an EPID panel [83].

For the clinical use of the MR-linac, routine QA of patient-specific treatment plans is required. Several QA systems [84] are available for 3D dose measurements of patient-specific treatment plans. To perform QA of patient-specific treatment plans, such QA systems must have a reproducible dose response that is independent of the applied dose, dose rate and field size.

An MRI-compatible version of the ArcCHECK QA system (ArcCHECK-MR ^{TM}, Model 1220-MR, Sun Nuclear Corporation, Melbourne, USA) has been developed recently. The performance characteristics of the ArcCHECK without the presence of a magnetic field have been evaluated [85].

The purpose of this study was to examine the performance characteristics of the ArcCHECK-MR in a transverse 1.5 T magnetic field. Therefore, the short-term reproducibility, dose linearity, dose rate dependence, field size dependence and dose per pulse dependence were evaluated on a conventional linac and on the MR-linac according to the measurement framework described by Li et. al. [85]. Additionally, the ArcCHECK-MR diodes show an orientation dependence [85], which could be influenced by the magnetic field. Therefore, the inter-diode variation was also investigated.

7.2 Materials and methods

The ArcCHECK-MR (ArcCHECK-MR ^{TM}, Model 1220-MR, Sun Nuclear Corporation, Melbourne, USA) is a cylindrical water-equivalent phantom with

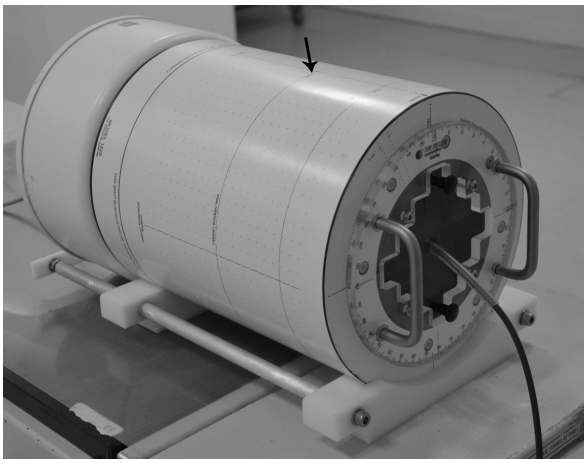

Figure 7.1: The ArcCHECK-MR with the MultiPlug^{TM} and NE2571 Farmer ionization chamber inserted at the conventional linac. Diode A (indicated by the black arrow) is located at the top of the ArcCHECK-MR .

an array of diodes, which are arranged in a spiral pattern with 10 mm diode spacing. An insert (ArcCHECK PMMA MultiPlug^{TM}, Model 1220000-3, Sun Nuclear Corporation, Melbourne, USA) can be placed in the 15cm-wide center cavity to accommodate an ionization chamber for reference dosimetry.

To examine the effect of a 1.5 T magnetic field on the performance of the ArcCHECK-MR QA system (Figure 7.1), several basic tests, as described by Li et. al. [85], were performed on both a conventional linac and on the MR-linac. The measurements on the conventional linac (Precise Treatment System, Elekta, Stockholm, Sweden) were carried out using a 6 MV photon beam. The multi-leaf collimator (MLC) has 80 leafs with a projected leaf width of 1 cm at the isocenter, which is located 100 cm from the target. The MR-linac is an upgraded version of the machine described by Raaymakers et. al. [40]. The unflattened photon beam has a nominal beam energy of almost 8 MV and the magnetic field strength is 1.5 T. The isocenter is located 142.7 cm from the target, inside the MRI bore. The MLC has 160 leafs, with a projected leaf width at the isocenter of 0.72 cm, and the field size is restricted in the feet-head direction by MRI-scanner structures to a maximum of 22 cm at the isocenter. Both accelerators are calibrated to deliver 1 Gy per 100 MU at dose maximum.

Unless mentioned otherwise, the following reference setup conditions were applied to all measurements. The MultiPlug^{TM} was inserted in the ArcCHECK-MR to enable stable positioning of a NE2571 Farmer ionization chamber (NE Technology Limited, Berkshire RG7 5PR, England) at the isocenter [66]. All measurements were performed with a field size of 20 x 20 cm^2, gantry and collimator angle of 0°, a dose rate of 128-148 MU/min and 100 MU per measurement.

The raw ArcCHECK-MR diode readings were corrected for background. Relative sensitivity differences between the detectors were adjusted using the factory array calibration. The ionization chamber reading was used to correct for any variation in linac output. All measurements were performed in threefold to reduce uncertainties and the average reading was calculated. In accordance with [85], the average reading of one of the diodes (diode A, coordinates: -5 mm, 0 mm; Figure 7.1) was evaluated for all tests.

7.2.1 Short term reproducibility

The effect of the magnetic field on the short term reproducibility of the ArcCHECK-MR diode was examined by calculating the standard deviation and maximum deviation of 10 consecutive readings of diode A under reference setup conditions on both linacs. For each linac, the reading of diode A was normalized to the average reading of the 10 measurements.

7.2.2 Dose linearity

Dose linearity differences of the ArcCHECK-MR diode due to the magnetic field were evaluated by applying different MUs per measurement. The delivered MUs per measurement were 2, 5, 10, 20, 50, 100, 200 and 500 MU. For each linac, the reading of diode A was normalized to the average reading at 100 MU per measurement.

7.2.3 Dose rate dependence

The dose rate dependence of the ArcCHECK-MR diode was evaluated by changing the dose rate per measurement. The available dose rates were 31, 62, 128, 259 and 519 MU/min at the conventional linac, and 10, 38, 82 and 148 MU/min at the MR-linac. The reading of diode A was normalized to the average reading at 128 MU/min for the conventional linac and to 148 MU/min for the MR-linac.

7.2.4 Field size dependence

Field size dependence of the ArcCHECK-MR diode was evaluated by measuring the reading of diode A using different field sizes. In correspondence with [85], the ArcCHECK reading was corrected using ionization chamber measurements in a solid-water slab phantom. On both linacs, the source-to-detector distance (SDD) in the ArcCHECK-MR setup (diode A) and in the slab phantom setup (Farmer ionization chamber) was 132.3 cm, which was identical to the reference condition at the MR-linac.

The applied field sizes were 5 x 5, 10 x 10, 16 x 16, 20 x 20 and 22 x 22 cm^2 at 142.7 cm from the target. For each linac, the reading of diode A was normalized to the average reading at field size 20 x 20 cm^2.

7.2.5 Dose per pulse dependence

Dose per pulse dependence was measured on the conventional linac as described by [85] using different SDDs. The used SDDs, defined as the distance from the target to diode A, were 79.2, 89.6, 100, 112.9, 122.9 and 132.9 cm. The reading of diode A was corrected to ionization chamber measurements in a solid-water slab phantom, using identical SDDs. The reading of diode A was normalized to the average reading at SDD 89.6 cm, which was the reference setup.

At the MR-linac, a fixed table height is preventing the use of different SDDs. To evaluate the effect of the 1.5 T magnetic field on the dose per pulse dependence, the ratio between diode A and the opposing diode was evaluated on both linacs under reference conditions. To rule out inter-diode dependence, this measurement was repeated with the ArcCHECK-MR rotated 180° over its longitudinal axis to position diode A at the bottom side of the ArcCHECK-MR .

7.2.6 Inter-diode variation

The inter-diode variation was evaluated by comparing the average reading of each diode on both linacs, using a field size of 20 x 30 cm^2 (FH x LR). The calculated dose was used to correct for differences in field profile and in dose deposition due to the presence of the magnetic field.

Dose distributions were calculated using a Monte Carlo algorithm [86], taking the magnetic field into account for the MR-linac dose distribution. The dose distributions were calculated with a voxel size of 2 x 2 x 2 mm^3.

The average reading of each diode was divided by the calculated dose at that diode location for both linacs. To enable comparison, for each linac, the resulting maps of the corrected diode reading were normalized to the 90^{th} percentile value of that map. The absolute difference between the corrected diode reading of the MR-linac and the conventional linac was calculated for each diode.

7.2.7 Statistical analysis

A Kolmogorov-Smirnov test (Matlab, version R2012a, The Mathworks Inc., USA) was used to evaluate if the performance of the ArcCHECK-MR diode on the MR-linac was different from the performance on the conventional linac.

7.3 Results

7.3.1 Short term reproducibility

No significant difference was observed in the short term reproducibility of the ArcCHECK-MR diode on the conventional linac and the MR-linac (p=0.7). At the conventional linac, the standard deviation over the 10 consecutive measurements was 0.05% and the maximum deviation was 0.2%. At the MR-linac, these deviations were 0.06% and 0.2%, respectively.

7.3.2 Dose linearity

The maximum dose response difference (Figure 7.2) was 2.1% at the conventional linac, and 0.7% at the MR-linac (p=0.5). The largest dose response errors were observed for the 2 and 5 MU measurements. If we evaluated the measurements of 10 MU or more, the maximal dose response difference was 0.4% at the conventional linac, and 0.1% at the MR-linac (p=0.8).

7.3.3 Dose rate dependence

The varying dose rate resulted in maximal dose differences of 1.0% for both linacs. No significant difference was observed between the linacs (Figure 7.3, p=0.4).

7.3.4 Field size dependence

The maximum dose response difference for varying field sizes was 2.6% at the conventional linac, which was in correspondence with the dependence reported by [85], and 1.0% at the MR-linac (Figure 7.4, p=0.7).

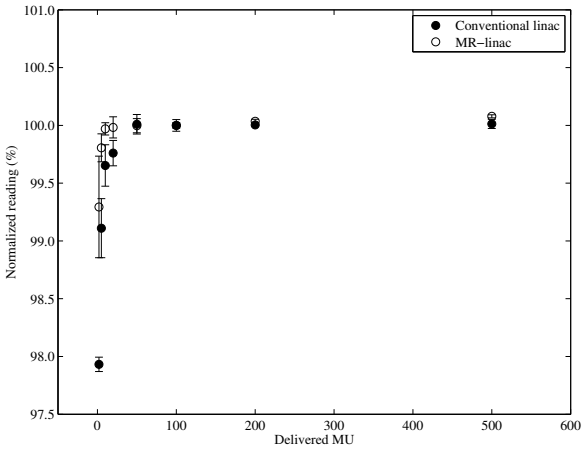

Figure 7.2: Dose linearity of diode A. For each linac, the average reading of diode A was normalized to the average reading of the 100 MU measurement. Error bars indicate the standard deviation of the average reading.

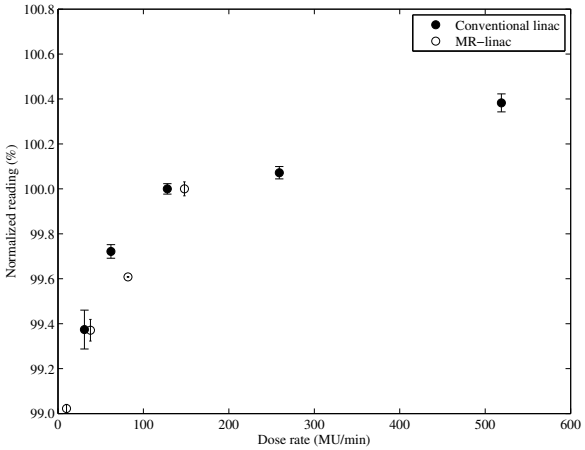

Figure 7.3: Dose rate dependence of diode A. The average reading of diode A was normalized to the average reading at 128 MU/min for the conventional linac and to 148 MU/min for the MR-linac. Error bars indicate the standard deviation of the average reading.

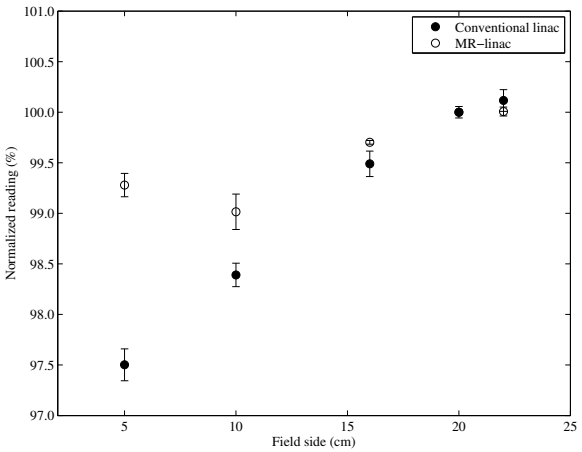

Figure 7.4: Field size dependence of diode A. For each linac, the average reading of diode A was normalized to the average reading of a field size of 20 x 20 cm^2. Error bars indicate the standard deviation of the average reading.

7.3.5 Dose per pulse dependence

The maximum dose difference due to the dose per pulse dependence was 1.0%, as measured using the varying SSD technique on the conventional linac. This was well in accordance to Li et. al. [85]. The ratio between the reading of diode A and the opposing diode was 2.7 at the conventional linac, and 2.9 at the MR-linac and no inter-diode differences were observed.

7.3.6 Inter-diode variation

The corrected diode reading maps showed a similar behavior on both linacs (Figure 7.5). The difference between the corrected diode reading on both linacs had a random variation, with a median difference of -1.5 % (25^{th} - 75^{th} percentile: -5.0 - 1.7 %).

7.4 Discussion

We investigated the performance characteristics of the ArcCHECK-MR in a transverse 1.5 T magnetic field at the MR-linac and compared that to the performance characteristics on a conventional linac. The performance of this MR-compatible version of the ArcCHECK^{TM} was similar (within 1%) to the

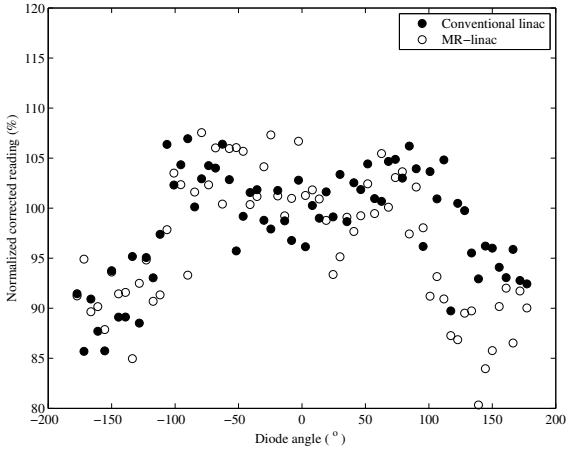

Figure 7.5: The corrected diode reading (average diode reading/calculated dose), normalized to the 90^{th} percentile value of all diodes, on the central axial line on the ArcCHECK-MR for both linacs. The diode angle represents the location on the axial axis, where 0° is top of the ArcCHECK-MR (location of diode A).

performance described by [85]. No significant differences between the performance on the MR-linac and the conventional linac were observed in the short-term reproducibility, dose linearity, dose rate dependence, field size dependence, dose per pulse dependence and inter-diode variation. Hence, the suitability of the ArcCHECK-MR for clinical IMRT and VMAT plan verification is not influenced by the presence of a transverse 1.5 T magnetic field.

At this moment, the ArcCHECK-MR is the only commercially available MR-compatible array-based system for patient-specific QA. The results could therefore not be compared to other systems [84].

Besides the difference in the presence of the magnetic field, there were other variations between the conventional linac and the MR-linac. First of all, the MR-linac has an unflattened field profile [71], while the conventional linac has a flattened field. However, we believe the performance characteristics of diode A, which was positioned at the field maximum, were not influenced by the field profile. Secondly, the nominal beam energy is 6 MV at the conventional linac and almost 8 MV at the MR-linac. Finally, the source-axis-distance (SAD) at the conventional linac is 100 cm, while this is 142.7 cm at the MR-linac.

Measurements were performed with the ionization chamber positioned at the isocenter, resulting in different SDDs at each linac. Because the results were reported relative to the reference setup, this issue can be neglected. The field size and dose per pulse dependence, however, were evaluated using the same SDD at both linacs to ensure identical field sizes at the ionization chamber and diode A.

The dose linearity test showed the largest dose response differences for the 2 and 5 MU measurements, up to 2.1% for the conventional linac. A dose linearity check, according to NCS 18[49] (data not shown), was performed prior to these measurements, which showed a 0.1% difference in linac output. Although the dose response error measured using the ArcCHECK-MR was larger, this difference is best explained by the diode performance and unavoidable alignment difficulties.

The field size dependence at the conventional linac was corresponding to the values described by Li et. al.[85] (a maximum dose difference of 2.6% in this paper, and 2.7% reported by [85]. Due to the difference in leaf width, the field sizes were not exactly the same on both linacs and the rounded values of the field sizes were reported. The maximum dose difference at the MR-linac was smaller than at the conventional linac, mainly due to the relatively small dose response error for the 5 x 5 cm^2 field. The remaining difference could be explained by the difference in beam energy, since the field size dependence of the ArcCHECK-MR decreases with increasing beam energy. Because the ArcCHECK-MR software uses a beam energy specific field size correction factor for analyzing patient treatments plans, an additional field size correction factor for the MR-linac is useful.

The inter-diode variation showed a similar behavior of the diode reading corrected for the calculated dose on both linacs and is not influenced by the magnetic field. The observed behavior (Figure 7.5) is a result of the measurement and alignment errors and the rotational dependence of the ArcCHECK-MR diodes. Li et. al. [85] reported a similar behavior with a maximum variation in diode response of 14% due to the irradiation angle, which is in accordance with our results.

The ArcCHECK-MR is approved for use in a 0.35 T static magnetic field, i.e. the MRIdian^{TM}system (ViewRay Inc., Ohio, USA). Given that the impact of the magnetic field reduces with decreasing field strength, our results at 1.5 T confirm the suitability of using the ArcCHECK-MR in magnetic fields with a

strength up to 1.5 T. Additionally, the impact of the magnetic field is expected to be maximum when it is oriented transverse to the beam. Therefore, the use of the ArcCHECK-MR seems also safe in systems using a beam orientation parallel to the magnetic field [37] [87].

7.5 Conclusion

The short-term reproducibility, dose linearity, dose rate dependence, field size dependence, dose per pulse dependence and inter-diode variation of the ArcCHECK-MR diodes were not influenced by the presence of a transverse 1.5 T magnetic field.

Acknowledgements

The authors would like to thank Sun Nuclear Corporation and Elekta for providing us with a ArcCHECK-MR ™and a MultiPlug™.

8

The impact of beam transmission through a closed bore MRI on several beam characteristics for a prototype MR-linac system

In preparation for submission
K Smit, DA Roberts, JGM Kok, JJW Lagendijk and BW Raaymakers

Abstract
The MR-linac is a hybrid MRI radiotherapy system allowing dose delivery in a 1.5 T magnetic field. This paper investigates the influence of irradiating through a closed bore MRI scanner on several radiation beam characteristics for squared fields of sizes 5.6, 9.8 and 23.8 cm. For this purpose the MR-linac set-up was implemented into a Monte Carlo simulation environment facilitating dose profile simulations in a 1.5 T magnetic field with and without MRI scanner structures. The results of the Monte Carlo simulations will be validated against scanning water phantom measurement results obtained in the MR-linac for the PDD and lateral profiles. The MRI scanner structures attenuate the irradiation beam by a factor between 3.5, for a 5.6 cm squared field and 2.9 for a 23.8 cm squared field. Because of the MRI scanner structures the photon energy spectrum of the irradiation beam is hardened significantly. This results in an 1.9, 1.4 and 0.5% increase in dose at a depth of 5 cm for squared fields of sizes 5.6, 9.8 and 23.8 respectively. In the lateral dose profile direction, the penumbra shape is changed slightly due to the magnetic field. The largest effect is found for the low scatter dose regions, at a distance of 5 cm from the field edge the scatter dose is increased by 0.5%, 1.7% and 4.4% for the 5.6, 9.8 and 23.8 cm fields, respectively. Since the impact of the beam transmission decreases for smaller radiation field sizes,

the impact for patient radiotherapy is limited and the new beam characteristics can be implemented into the treatment planning system.

8.1 Introduction

The University Medical Center Utrecht, The Netherlands, has developed a prototype MR-linac in collaboration with Elekta (Elekta AB, Stockholm, Sweden) and Philips (Philips Medical Systems, Best, The Netherlands). This prototype MR-linac is an upgraded version of the set-up described by [40] and consists of an 8 Me V linac integrated with a 1.5 T MR-scanner.

In this ring-based gantry design, the irradiation beam axis is perpendicular to the permanent 1.5 T field of the MRI scanner. Because the systems share a common isocenter, the set-up allows simultaneous irradiation and imaging of the patient. On-line imaging enables escalation of the dose to the tumour while sparing surrounding healthy tissues [57]. The linac is equipped with a 160 leaf Elekta Agility based MLC, with a projected leaf width at the isocenter of 7 mm. In the direction of the leaf travel, the irradiation field is restricted to a maximum size of 24 cm due to MRI scanner structures.

The MR-imaging system influences the beam characteristics on two levels. Firstly, the dose at the isocenter is delivered in the presence of a magnetic field. The effect of the magnetic field on the dose distribution (e.g. [46] and [42]) as well as the dosimetry equipment (e.g. [66] and [71]) have been subjects of investigation. Secondly, although the MRI scanner is optimized for beam transmission, the irradiation beam travels through the equivalent of 11.50 cm aluminium before reaching the isocenter. When the beam passes through the scanner structures the photons will interact with the matter, attenuating the beam. This will decrease the radiation dose and the energy spectrum of the beam will change because lower energy photons are more likely to interact i.e. beam hardening. In addition the photons scattered in the material can reach the isocentric plane, creating an MRI scanner originated scatter contribution at the isocentric plane. Before patients can be treated in the MR-linac, it is of vital importance to know the consequences of irradiation through a closed bore MRI to investigate if this would hamper the use of IMRT in the MR-linac set-up.

In this work we will use a validated Monte Carlo environment to calculate the influence of the MRI scanner structures on several important radiation beam characteristics. The correct implementation of the MR-linac set-up in

the Monte Carlo environment will be verified by comparing simulated dose distribution profiles with dose profiles measured in the MR-linac. Once the simulation environment is validated, it can be used to investigate the consequence of irradiating though the structures of the closed bore MRI scanner on the beam energy spectrum and scatter levels. In addition the attenuation caused by the MRI scanner will be investigated.

8.2 Materials and methods

8.2.1 Measurements

A scanning water phantom is available for measurements in the MR-linac ([82]). This phantom facilitates dose profile measurements within a scanning volume of 24 x 40 x 11.5 cm^3. The profile measurements were performed using the CC13 air filled ionisation chamber(IBA dosimetry, Germany) for field sizes larger than 9.5 x 9.5 cm^2 field sizes and the CC04 ionisation chamber for smaller radiation field sizes. An additional reference CC13 ionisation chamber, placed in the irradiation beam above the phantom, was used to correct for possible linac output variations. A tandem electrometer (PTW, Freiburg, Germany) was used for simultaneous signal readout of the scanning and reference ionization chambers.

8.2.2 Monte Carlo Simulations

For all simulations the Monte Carlo code Pegasus (Elekta Ltd) has been used. The Monte Carlo code allows import of the CAD geometry of the MR-linac system and modelling of radiation transport via the Penelope ([88] or [89]) physics engine. A mono energetic electron beam of 7.2 MeV was used in the simulations. The cryostat was modelled as several cylinders of various materials which could be removed from modelling to determine the effect of the cryostat on the beam physics. The precise internal geometry of the cryostat is propriety, but the total material in the beam portal equates to 115.5 mm equivalent of aluminium. Inside the magnet bore, at an SSD of 133.5 cm, a 40 x 40 x 30 cm^3 water phantom was positioned.

Two different set-up configurations can be implemented. The first set-up includes the MRI scanner structures as specified by the manufacturer. The magnetic field is assumed to be present only in the bore of the MRI scanner. The second set-up omits the MRI scanner structures, but the 1.5 T magnetic field remains.

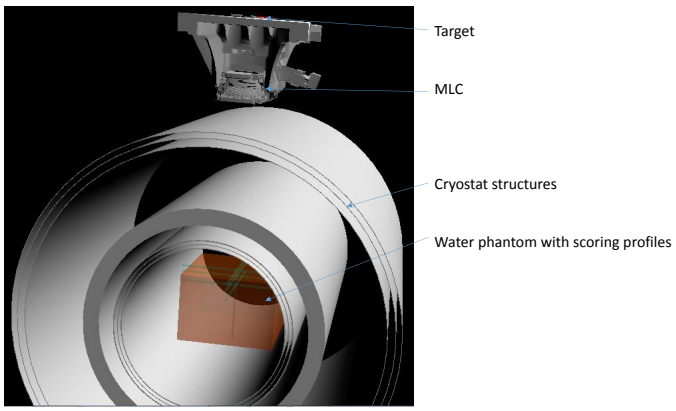

Figure 8.1: An overview of the MR-linac set-up implemented into the Monte Carlo simulation environment.

8.2.3 Validation of the Monte Carlo Simulations

Three different squared fields of sizes 5.6, 9.8 and 23.8 cm^2 were used for validation of the Monte Carlo calculations. Lateral dose profiles were measured and simulated along the major axes at d_{max} (1.5 cm), 5 cm and 10 cm deep. Additionally, the PDD profiles were measured and simulated for each field size. The simulations were performed with a sampling of 1 mm in the profile direction and 10 mm in all other directions. The measurements were obtained by measuring the dose every 2 mm in the direction of the profile.

For all field sizes the inline and crossline lateral dose profiles will be measured and simulated. The influence of the magnetic field ([41] is expected to be present in the crossline direction. The measured and simulated percentage depth dose (PDD) profiles were compared to investigate correct implementation of the irradiation beam spectrum.

For the comparison, the measured and simulated profiles were normalized to their maximum dose value. The simulated dose profiles are convolved with a moving average filter to account for the ionization chamber measuring volume. To account for the effective point of measurement for the ionization chamber, the depth of the simulated profiles was decreased by 0.6 times the diameter of

the ionization chamber. The agreement between the simulated and measured profiles was evaluated by performing a gamma analysis, as described by [90], using a 1%/1mm gamma criterium.

8.2.4 Influence of the MRI scanner structures on the PDD profiles

The influence of the MRI scanner structures on the PDD profile at the isocenter was investigated for all three radiation field sizes. The PDD profiles were simulated for the situations with and without the scanner structures. The maximum difference in the total PDD profile, as well as the difference in dose at a depths of 5, 10 and 20 cm were calculated to gain insight into the quantitative dose difference. The difference in PDD originates in a difference in radiation beam spectrum, which will be investigated using the Monte Carlo simulations. The energy of the photons that pass through the centre 2 x 2 cm^2 of the isocentric plane perpendicular to the beam axis is scored for the situations with and without MRI scanner structures.

8.2.5 Attenuation due to the MRI scanner structures

The scanner structure attenuation can be determined from the un-normalized simulation results with and without the scanner structures. The maximum dose was determined for the inline and crossline profiles. The ratio between these maximum dose values is the attenuation coefficient.

8.2.6 Influence of the MRI scanner structures on the scatter outside the field

The lateral dose profiles were simulated with and without the MRI scanner structures present. The difference between the lateral dose profile with and without the MRI scanner structures will be calculated. The difference in dose at 5 cm from the field edge will be determined, this is a measure for the additional dose caused by the photons that have scattered in the MRI scanner structures.

8.3 Results

8.3.1 Validation of the Monte Carlo simulations

Figure 8.2 shows the measured and simulated lateral dose profiles for a 9.8 x 9.8 cm^2 field at a depth of 5 cm.

For all the investigated lateral profiles more than 99.4% of the points pass the 1%/1 mm gamma criterium.

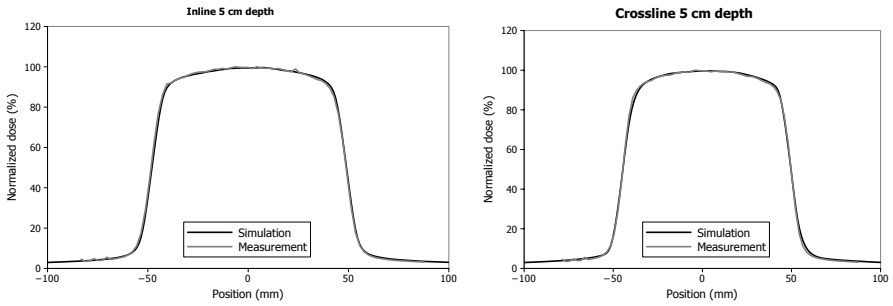

Figure 8.2: Results of the measurements and simulations. Figure a and b show the results for the inline and crossline directions at a depth of 5 cm.

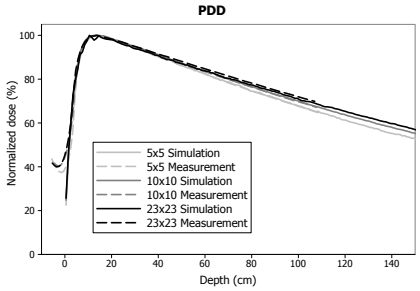

Figure 8.3: Results of the PDD measurements and simulations for the three investigated field sizes.

For the PDD profiles a total 100% of the investigated points passes the 1%/1 mm gamma criterium. The first 2 mm of the dose profiles were excluded from the comparison because of ionization chamber measurement characteristics.

8.3.2 Influence of the MRI scanner structures on the PDD profiles

The irradiation beam spectrum with and without the MRI scanner structures present is visualized in figure 8.4(a). The energy spectrum with the MRI scanner structures shows significant hardening of the beam spectrum. The peak of the photon energy spectrum, i.e. the most common photon energy, is found at 0.3 MeV for the situation without the MRI scanner. Including the MRI scanner in the simulations shifts the peak to 0.96 MeV.

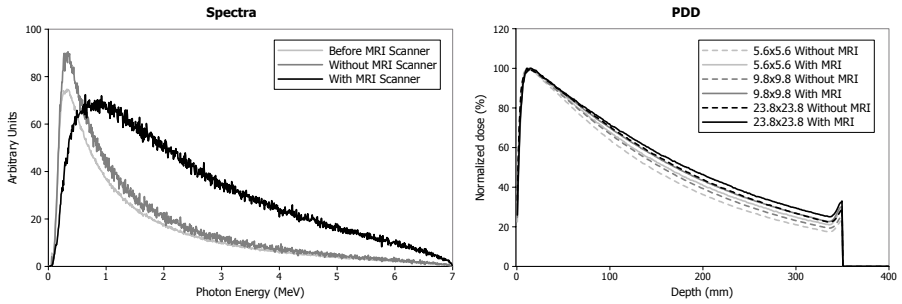

(a) (b)

Figure 8.4: Results of the simulations. Figure a shows the simulated photon energy spectra at the isocenter for the situations with and without the MRI scanner. Figure b shows the simulated PDD profiles with and without the MRI scanner, for squared field of sizes 5.6, 9.8 and 23.8 cm.

The difference in energy spectrum translates to a difference in the PDD shape as visualized in figure 8.4(b) and presented in table 8.1.

Table 8.1: Overview of the difference in PDD profile due to the MRI scanner structures. The maximum difference over the profile, difference at a depth of 5, 10 and 20 cm.

	5.6	9.8	23.8
Difference at 5 cm (%)	1.92	1.37	0.48
Difference at 10 cm (%)	3.82	3.04	0.94
Difference at 20 cm (%)	4.53	3.96	2.49
Maximum difference (%)	5.69	5.10	4.46

8.3.3 Attenuation due to the MRI scanner structures

The ratios between the maximum doses found with and without the MRI structures are presented in table 8.2.

The attenuation coefficient appears to decrease with increasing measurement depth due to the beam hardening.

8.3.4 Influence of the MRI scanner structures on the lateral dose profiles

The difference at 5 cm from the field edge are presented in table 8.3. A positive value indicates a dose increase due to the scanner structures.

Table 8.2: Overview of the dose attenuation factors due to the MRI scanner structures for the different depths.

	5.6		9.8		23.8	
	Inline	Crossline	Inline	Crossline	Inline	Crossline
1.5 cm	3.57	3.56	3.09	3.08	2.89	2.87
5 cm	3.52	3.52	3.05	3.06	2.88	2.88
10 cm	3.38	3.38	2.98	2.98	2.85	2.86

Table 8.3: Overview of the absolute difference in normalized dose in the lateral profiles due to the MRI scanner structures. The maximum difference, found in the penumbra region, and the difference at 5 cm from the field edge.

	5.6		9.8		23.8	
	Inline	Crossline	Inline	Crossline	Inline	Crossline
1.5 cm	0.63	0.63	1.82	1.75	4.61	4.58
5 cm	0.65	0.47	1.68	1.60	4.33	4.12
10 cm	0.42	0.36	1.30	1.31	3.81	3.71

The additional scatter dose at 5 cm from the field edge increases as the field size increases. The relation between the increase in scatter dose and the field size is visualized in figure 8.5

8.4 Discussion

The agreement between the measured and simulated dose profiles indicate that the MR-linac set-up is implemented correctly into the Monte Carlo simulation environment. The influence of the MRI scanner structures on the energy spectrum is clearly visible. However, at a depth of 5 cm the PDD differences are limited to 1.92% and 1.37% for the 5.6 and 9.8 cm squared fields, respectively. For the squared 23.8 cm field, the difference is decreased to 0.48%. The influence of the MRI scanner structures on the PDD profile decreases as the field size increases.

Since the SSD for the measurements in the MR-linac is increased, the divergence in the phantom differs from a standard clinical set-up. This already influences the shape of the PDD with a magnitude similar to the effect of the beam hardening due to the MRI scanner structures. The combined effect of the MRI scanner structures and the increased SSD yield the 7.2 MeV MR-linac

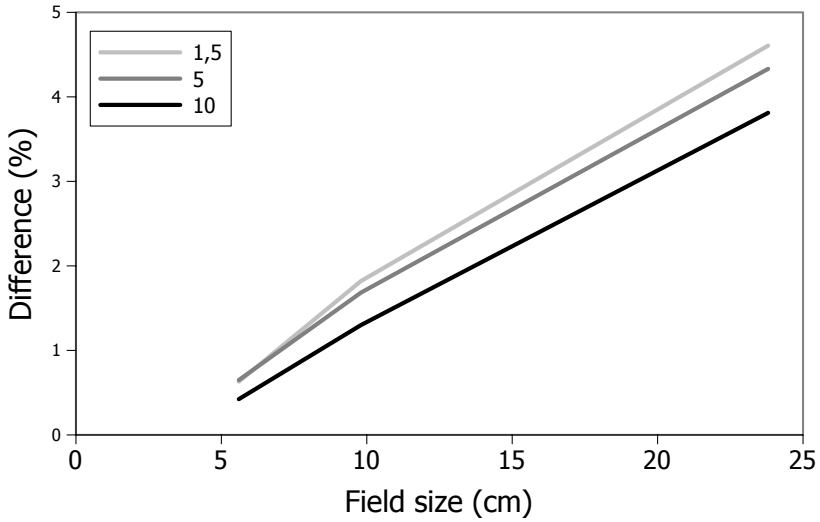

Figure 8.5: An overview of the MR-linac set-up implemented into the Monte Carlo simulation environment.

PDD slope after the dose maximum is comparable to a clinical set-up using a 10 MeV irradiation beam and an SSD of 100 cm.
The PDD is influenced by the transmission through the MRI scanner structures, but the new shape is similar to another type of radiation beam used in clinical practice. The exact shape of the PDD can therefore be implemented in the treatment planning system and will therefore automatically be taken into account in patient treatment.

The lateral profiles are influenced by the presence of the cryostat. The increased scatter dose at 5 cm from the field edge is 1.6% for a 9.8 x 9.8 cm^2 field at a depth of 5 cm. This contribution is directly related to the surface of the irradiation field. Since a field size comparable to the squared 23.8 cm field is rarely used in the clinic, the expected influence of the MRI scanner structures on the scatter dose contribution is limited. Since the scatter contribution on average has a lower energy, the relative contribution is larger for the lower measurement depths. This scatter dose contribution is hypothesised to be an

'offset' found throughout the whole phantom, but is most noticeable in the low dose regions.

Compared to the attenuation coefficient one might expect a larger scatter contribution. The relatively low scatter contribution is most likely due to a self shielding effect of the MRI scanner. Photons that have once interacted with the scanner structures are more likely to interact again because each interaction decreases the photon energy. Therefore mainly the photons that have had their first interaction in the inner MRI scanner structures or in the phantom can contribute to the scatter dose. The secondary electrons created during photon scattering in the MRI scanner structures will not contribute to dose in the phantom. These electrons will be deflected by the Lorentz force and move back to the MRI scanner structures [41].

The simulations in this paper were performed on the geometry described by [40]. A new MR-linac design has been developed and is being installed. The new design includes a new MRI scanner with an optimization in the amount of material in de radiation beam. Less material in the radiation beam, will cause less beam attenuation and therefore less scatter and beam hardening.

8.5 Conclusion

Monte Carlo simulations can be used to perform dose distribution calculations for the MR-linac set-up. This facilitates dose calculations for possible upgraded MR-linac systems before actual installation of the system. The influence of the MRI scanner structures on the irradiation beam properties is influenced by the field size and measurement depth. For a reference 9.8 x 9.8 cm^2 field, the MRI scanner increases the scatter by 1.6%, this additional scatter decreases as the field size decreases. The scatter contribution is limited for the clinically relevant field sizes and can be accounted for in the treatment planning system. The irradiation beam is attenuated by the MRI scanner structures by a factor of 3.1 for the reference field size at maximum dose depth. In addition the MRI scanner structures cause a hardening of the beam energy spectrum, resulting in a dose increase of 1.37% at 5 cm depth for a 9.8 x 9.8 cm^2 field. In conclusion, the influence of the MRI scanner structures on the irradiation beam characteristics must not be ignored, but can easily be implemented in a treatment planning system and the influence on a standard IMRT radiation treatment is minimal.

9

Summary and general discussion

9.1 Reference dosimetry in the MR-linac

Chapter 2 investigated the feasibility to correct the ionisation chamber reading for the magnetic field within the dosimetry calibration method described by the AAPM [50]. Firstly, the feasibility of using an ionisation chamber in an MR-linac was assessed by investigating possible influences of the magnetic field on NE2571 Farmer type ionisation chamber characteristics: linearity, repeatability, orientation in the magnetic field; and correction factors for voltage polarity and ion recombination. The measurement results show that the correction factors for the NE2571 chamber were not influenced by the magnetic field. Secondly, the influence of the permanent 1.5 T magnetic field on the NE2571 chamber reading was quantified. The reading was influenced by the magnetic field, therefore an additional magnetic field correction coefficient has been added. For the standardised set-up used in this paper, the NE2571 chamber reading increases by 4.9% ($\pm$ 0.2%) due to the transverse 1.5 T magnetic field. Dosimetry measurements in an MR-linac are feasible, if the setup specific magnetic field correction factor ($k_{1.5\ T}$) for the ionisation chamber reading is introduced. For the set-up investigated in this paper, the $k_{1.5\ T}$ has a value of 0.953.

When this magnetic field correction factor would be added to the standard equations from the NCS 18 [49], the absorbed dose can be calculated from the measured ionisation chamber reading using equation 9.1 and 9.3.

Firstly, the IC reading M_{raw} is corrected for the measurement conditions using equation 9.1.

$$M = M_{raw} \times k_{TP} \times k_{ion} \times k_{pol} \times k_{elec} \qquad [C] \tag{9.1}$$

The correct measurement value M is calculated by correcting the M_{raw} for variations in ambient conditions including temperature and air pressure (k_{TP}), and non-ambient influences including incomplete ion collection (k_{ion}), polarity effects (k_{pol}) and electrometer calibration factor (k_{elec}).

The introduction of the magnetic field correction coefficient ($k_{1.5\ T}$) to equation 9.1 allows minimal influence on the standard reference dosimetry protocol. However, if any of the correction coefficients in equation 9.1 are influenced by the magnetic field this will also affect the accuracy of dose measurements in the MR-linac. Therefore, the other correction coefficients should not be influenced by the transverse 1.5 T magnetic field. The magnetic field correction coefficient is defined as:

$$k_{1.5\ T} = \frac{M_{corr1.5\ T}}{M_{corr0\ T}} \tag{9.2}$$

If the correction coefficients for the ionization chamber reading are influenced by the magnetic field, this would automatically be taken into account by the magnetic field correction factor. That would still yield correct results, but only if the relevant measurement conditions are the same as for the situation where the magnetic field correction factor was determined. For the ionisation voltage and the polarity this is easily achieved, the air temperature in the treatment room can also be kept constant (within $\pm$ 0.1°). But the air pressure and humidity are less easily controlled. As a first estimation, the influence of the magnetic field on these correction coefficients is negligible for the variations found in clinical practice. However the precise effect of the magnetic field on the correction factors is something that can be investigated in future studies.

The corrected ionisation chamber reading (M) can then be used to calculate the absorbed dose (D_w^Q) in water for the clinical beam quality (Q) using equation 9.3.

$$D_w^Q = M \times k_Q \times N_{D,w,Q0} \qquad [Gy] \tag{9.3}$$

Where the $N^{60}Co_{D,w}$ is the absorbed dose to water calibration coefficient for an ionisation chamber at the beam quality used in the reference set-up. The beam quality correction factor k_Q, used in [49], is determined as the ratio between the absorbed dose to water coefficients ($\mathrm{N_{D,w,Q}}$) for the clinical beam quality, and the reference beam quality.

$$k_Q = \frac{N_{D,w,Q}}{N_{D,w,Q0}} \tag{9.4}$$

Since the $\mathrm{N_{D,w,Q}}$measurement requires a ^{60}Co radiation source, it is not possible to perform this measurement in a lateral 1.5 T magnetic field. This means the k_Q factor cannot be determined for the MR-linac specifically. However, this can be mitigated by the fact that the current designs of the MR-linac use a single beam quality. Therefore, if the $\mathrm{N_{D,w,Q}}$factor can be determined in the MR-linac set-up for that beam quality and the k_Q factor in equation 9.3 can be omitted.

The $\mathrm{N_{D,w,Q}}$factor can be determined using a water calorimeter, figure 9.1, a measurement method where the rise in temperature of a volume of water is monitored. This rise in temperature correlates to a deposition of energy by photons of the irradiation beam. Critical in the measurements with a water calorimeter is the determination of a small temperature rise of 0.24 to 0.48 mK with an uncertainty less than 1 μK for a dose between 1 and 2 Gy. The calorimeter has been be used as the primary standard for radiation dosimetry by the Van Swinden Laboratory (VSL) since 2001. Additionally, it is also the foundation for the new NCS-18 dosimetry protocol [49], which is commonly applied by medical physicists in the Netherlands and Belgium.

The VSL has developed a new primary standard calorimeter which is compatible with the magnetic field [91]. Using extensive multi-physics simulations the final design was simulated to test whether the strict specifications were met. At the end of 2013 the new primary standard water calorimeter, figure 9.1, was delivered. Currently the characterization and commissioning of the calorimeter is taking place and the calorimeter will be compared to the existing calorimeter. After the commissioning, the calorimeter is ready for accurate dosimetry in standard clinical settings as well as new advanced radiotherapy modalities.

Chapter 9

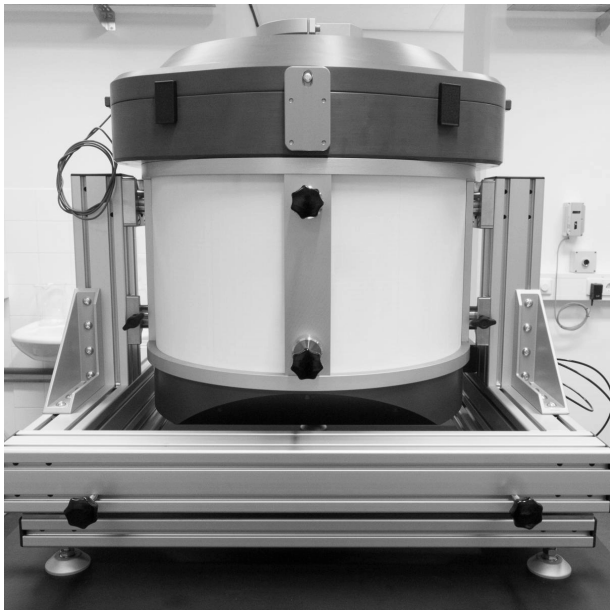

Figure 9.1: A picture of the MR compatible calorimeter developed by the Van Swinden Laboratory.

The primary standard can be implemented into clinical reference dosimetry using the current protocol. A water proof Farmer type chamber can be inserted in the geometry after the initial calorimetric dose measurement. The relation between the dose delivered and the ionisation chamber reading is then known for a water proof Farmer type ionisation chamber. This water proof ionisation chamber can then be used for cross calibration of other (non-water proof) ionisation chambers.

Because the calorimeter is magnetic field compatible, direct absolute dosimetry in the MR-linac can be done. Using this method a direct reading to dose in water factor for a water proof farmer type ionization chamber in a transverse 1.5 T magnetic field can be determined. This allows verification of the reference dosimetry ionization chambers via cross calibration and NCS 18 [49]

9.2 Radiation beam commissioning

Chapter 3 presents the design and performance of a prototype MR-linac compatible scanning water phantom. Since a scanning water phantom requires dose detectors, the performance of air filled ionisation chambers in the magnetic field was characterised. The linearity and reproducibility of an ionisation chamber are unaffected by the magnetic field. Also, moving the ionisation chambers in a magnetic field during irradiation does not affect the dose response. When scanning in-plane profiles, the change in irradiation orientation can influence the ionisation chamber dose response by up to 0.4% in the most unfavourable setting. However, this effect can be eliminated by rotating the ionisation chamber 90° before measuring the in-plane profile. There was no significant difference between the dose profiles measured with a standard clinical scanning water phantom and the profiles measured with the MR-linac compatible scanning water phantom. The performance of the MR-linac scanning water phantom in the MR-linac was validated using Gafchromic EBT2 film. There was no significant difference in dose profiles between the MR-linac scanning water phantom and the radiochromic film. These results show that automated scanning water phantom measurements using ionisation chamber detectors are feasible in the MR-linac.

This scanning water phantom has the potential to be used for radiation beam commissioning prior to using a linac for clinical practice. The beam characteristics measured with the scanning water phantom are then imported into the treatment planning system to be taken into account in the calculations of the patient treatment plan. For future measurements the water phantom design can be optimized, e.g. optimize scanning volume dimensions to increase the PDD measurement possibilities or scanning speed optimization.

9.3 Routine radiation beam quality assurance

Chapter 4 investigates the performance of the IC PROFILER^{TM} (Sun Nuclear Corporation, Melbourne, FL USA) in a 1.5 T magnetic field, a multi-axis ionisation chamber arrays panel. The influence of the magnetic field on the IC PROFILER^{TM} short term reproducibility, dose response linearity, pulse rate frequency dependence, power to electronics, panel orientation and ionisation chamber shape were investigated. The linearity, reproducibility, pulse rate frequency dependence, panel orientation and ionisation chamber shape

were unaffected by the magnetic field. When measurements were normalised to the centre reference chamber, the measurements can commence unaltered. Orientation of the ionisation chambers in the magnetic field is of importance, therefore caution must be taken when comparing or normalising results from several different axes. Dose profiles obtained with the IC panels were compared with radiochromic film dose profiles obtained simultaneously in the MR-linac. There were no systematic differences between the dose profiles measured with film and the IC panel, indicating correct performance of the panel in the transverse 1.5 T magnetic field.

Chapter 5 investigates the influence of the 1.5 T magnetic field on the STARCHECK^{TM}. The linearity, pulse rate frequency dependence, panel orientation and ionisation chamber shape were unaffected by the magnetic field. The magnetic field increases the standard deviation during 1 minute of measurement was increased significantly by 0.03%, but this increase is not considered to be clinically relevant. The difference in ionization chamber orientation between axes does not influence the individual measured dose profiles when the central ionization chambers are excluded from analysis.

All IC panels with the star-shaped ionisation chamber configuration only have one detector in the centre position, the signal of this detector is then used to complete the profiles in the other directions. Unless the IC is perfectly symmetrical, the orientation of an ionisation chamber in the magnetic field influences the dose response. Therefore the relative dose response of the central detector will deviate slightly from the dose response of the other detectors on the profile for all but one of the measurement profiles.

At the centre of these types of panels, many ionisation chambers are placed close together. Without a magnetic field the disturbance in dose distribution due to these air cavities is less than inside a magnetic field [43]. Therefore an actual different dose can be present for the centre few ionisation chambers. The reading of these ionization chambers can be used e.g. for normalization since the dose relative to other measurement locations is constant, but not for measuring the exact dose in the centre of the radiation field. In the future it would be desirable to implement the IC configuration in a Monte Carlo environment. Using this simulation environment the previous statement can be

checked and the exact dose change in the central region of the panel can be calculated as is done (e.g. [51] [45] [92]).

Both ionization chamber panels are similarly affected by the magnetic field. Therefore the choice of panel to use for routine radiation beam quality assurance in a magnetic field is similar to the choice for the situation without a magnetic field.

9.4 Machine quality assurance

Chapter 6 shows that electronic portal imaging device (EPID) panels can be mounted on the gantry opposite to the linac in the relatively low magnetic field region. A standard aSi Megavoltage (MV) detector panel is added to the MR-linac system and both qualitative and quantitative performance of the panel were investigated. Simultaneous MR imaging and transmission imaging can be done without mutual interference. The MV image quality is compromised by beam transmission and larger isocenter distance, but the field edges and bony anatomy can be detected at very low dose levels of 0.4 cGy. The MV imaging integrated with the MR linac provides an independent and well established position verification tool, a field edge check and a calibration for alignment of the coordinate systems of the MRI and the accelerator.

The EPID can be used to assess machine parameters for sufficiently small radiation fields. In addition to functioning correctly in the low magnetic field region, the EPID has now been tested inside the MR-linac itself in the 1.5 T magnetic field. This enables the use of the EPID for instance for MLC calibration. If the EPID needs to be used for time resolved dose reconstruction the images should be time stamped in synchrony with the MRI and linac time stamps.

9.4.1 EPID in the MR-linac

In vivo dosimetry based on EPID panel measurements has been a subject of investigation for external beam radiation therapy set-ups (e.g. [93] [94]. For this type of dosimetry, the radiation exiting the patient during treatment is detected by the EPID panel. Via back projection the difference between the expected dose at the EPID panel, and the measured dose can give insight into the actual dose delivered to the patient. This dosimetry method can provide an independent verification of the overall treatment procedure. It enables identification of potential errors in dose calculation, data transfer, dose delivery, patient set-up, and changes in patient anatomy.

EPID dosimetry for the MR-linac might seem interesting. However, for the MR-linac set-up, the image quality of the EPID is less than in a standard setup due to the double passage of the beam through the MR scanner structures. Additionally, the surface of the panel that can be used for measurement is limited by the beam portal in the MR scanner. But most importantly, the standard back projection method used for the dose calculations cannot be used. Because this method does not take into account the influence of the magnetic field on the dose distribution surrounding air-tissue interfaces. One needs to identify the orientation of all tissue/air interfaces in the anatomy and apply a forward dose calculation on it to assess the actual distribution of the delivered dose.

Because of these limitations, the EPID cannot be used to visualize 3D patient anatomy or to generate dose distributions and therefore it cannot be used for plan adaptations. The MRI can be used to generate the 3D anatomy and combine that with the fluence settings taken from the machine logs [95].

9.5 Patient treatment plan quality assurance

Chapter 7 examines the performance characteristics of the ArcCHECK-MR (Sun Nuclear Corporation, Melbourne, FL USA) treatment plan QA system in a transverse 1.5 T magnetic field. This device was designed for pre-treatment patient plan QA and consists of a cylindrical phantom with 1386 diodes embedded in the phantom. The dose at each diode location is compared to the dose predicted for that location by the treatment planning system. To ensure this functionality is also possible in the MR-linac; the short-term reproducibility, dose linearity, dose rate dependence, field size dependence, dose per pulse dependence and inter-diode variation of the ArcCHECK-MR diodes were evaluated on a conventional linac and on the MR-linac. The ArcCHECK-MR diodes performed well for all tests on both linacs, no significant differences in performance characteristics were observed. Differences in the maximum dose deviations between both linacs were less than 1.5%. Therefore, we concluded that the ArcCHECK-MR can be used in a transverse 1.5 T magnetic field.

There are alternative 3D patient QA devices, e.g. the Delta^4 phantom (Scandidos AB, Uppsala, Sweden) or the Octavius 4D (Physikalische Technische Werkstätten, Freiburg, Germany). An MR compatible Delta^4 phantom will be available for testing in the MR-linac soon. This phantom has 1069 p-type

diodes arranged in a matrix along two orthogonal planes. The Octavius 4D uses a detector plane which rotates with such that it is constantly perpendicular to the radiation beam. Movement in a magnetic field using electronic motors requires attention but can be done as shown in chapter 3 of this thesis.

Another option is to use radiation sensitive gels. These gels can be radiochromic, and need to be scanned using an optical CT scanner. Another option is polymer gels, e.g. [96], these types of gels can be scanned in an MRI. The advantage of gel based measurement is that they provide full 3D dose distributions, unfortunately the measurement process is more labor intensive than the QA devices. The use of radiation sensitive gels is not easy, extensive knowledge about gel dosimetry is required before it can be attempted. However, this field is under constant development especially now with the commercially available TrueView gels (Modus Medical Devices Inc., London, Canada), which can be scanned using an optical CT as well as an 1.5 T MRI scanner.

9.6 On-line quality assurance for adaptive radiotherapy

Patient treatment plan QA described in the previous paragraph is based on a perfectly reproducible patient positioning. However, in clinical practice discrepancies between the pre-treatment CT patient anatomy and the daily patient anatomy can occur. These discrepancies can be minimized by performing couch translations and/or small rotations. Full compensation of, in particular, rotation is usually not possible. During a radiation treatment, the MRI provides images to enable on-line plan adaptation or full re-planning.

A first and rather simple example of this is introduced by Bol et. al. [97], the online 'virtual couch shift (VCS)'. During this process the pre-treatment dose distribution is translated and/or rotated to compensate for the changes in patient anatomy. A new radiation treatment plan is generated which delivers the transformed dose distribution automatically. The VCS is the first step toward compensating these anatomical changes, including deformations, by online re-optimization of the IMRT dose distribution.

This next step in adaptive radiotherapy is accounting for all anatomical changes, but this requires full re-optimisation. Such an approach creates an entirely new dosimetry challenge; on-line QA. Initially this type of on-line QA will be limited to calculating the dose delivered during each treatment. In the future the

on-line imaging functionality of the MR-linac can be used for intra-fraction radiation motion management. The same type of QA can be used to assess the delivered dose during the radiation treatment. However, an additional type of QA will need to be designed and developed to ensure correct motion management during the radiation treatment.

One option to verify the online generated dose distribution is forward dose calculation based on machine parameters.

9.6.1 Forward dose calculation based on machine parameters

Since the MR-linac can obtain images during radiation treatment, the patient anatomy during each time point in the treatment is known. This information can be combined with the machine parameters as a function of time to calculate the exact dose delivered to each tissue as a function of time. This type of dose QA has been under investigation at the UMC Utrecht. For this method, the relevant machine parameters (i.e. gantry angle, pulse repetition frequency, pulse duration, MLC leaf positions) are recorded at any time point during the radiation treatment. The delivered dose can then be calculated from these parameters when combined with the 3D anatomy, measured using the MRI scanner, as stated in section 9.4.1. The forward dose calculation method requires correct feedback from the linac, but does not require any additional hardware to be present on the MR-linac. The drawback is that this method relies heavily on the accuracy of the dose calculations. This warrants new additional QA on the treatment planning system and possibly a need for an independent dose calculation method. The first radiation treatments potentially using this type of online QA will be spinal bone metastasis as these can be visualized on the EPID as well as the MRI scanner. This site was preferred as starting point because of the possiblity for an independent imaging check using the EPID panel.

Dose calculations on MR images

An additional point of attention for such online dose calculation purposes is that in clinical practice dose distribution calculations are done based on a pre-treatment CT image. The electron density information obtained using a CT scan is essential for the dose calculations. An MR image can be weighted for many different types of contrast, but no contrast type gives exact contrast obtained by a CT-scan. There are several possible ways to tackle this challenge.

A first solution can be obtained by restricting the number of tissue types; e.g. a pseudo-CT can be created with bulk densities for the tissue types (e.g. [98], [99], [100]). Another option would be to register the pre-treatment CT scan to the MR scan using the deformable registration methods (e.g. [101], [102]). Before the forward dose calculation method can be implemented in the clinical practice, this challenge needs to be addressed.

9.7 MR-linac design

9.7.1 Current MR-linac design

Chapter 8 describes the influence of de closed bore MRI scanner on several radiation beam characteristics for squared fields of sizes 5.6, 9.8 and 23.8 cm. The MRI scanner structures attenuate the irradiation beam by a factor between 3.5, for a 5.6 cm squared field and 2.9 for a 23.8 cm squared field. This attenuation creates a hardened beam spectrum, which results in an increase in dose of 1.9, 1.4 and 0.5% at a depth of 5 cm for squared fields of sizes 5.6, 9.8 and 23.8, respectively. The largest effect of irradiating through the closed bore MRI scanner is found for the low scatter dose regions, at a distance of 5 cm from the field edge the scatter dose is increased by 0.5%, 1.7% and 4.4% for the 5.6, 9.8 and 23.8 cm fields, respectively. These new beam characteristics need to be implemented into the treatment planning system by using an appropriate beam model.

9.7.2 New MR-linac design

The first prototype closed bore MR-linac integration has been operational for several years. The MRI scanner has been adapted for beam transmission; but the irradiation beam still has to travel through an equivalent of 11.5 cm of aluminium. In recent years there have been new insights in the design of a linac compatible MRI scanner, and this has lead to optimizations to the design.

A new closed bore MR-linac combination, visualized in figure 9.2, has been installed in the UMC Utrecht in 2014. This new MR-linac comprises a 70 cm diameter bore. The RF coil used for MR imaging that is integrated in the system, is homogeneously transparent to irradiation. The amount of material in the path of the irradiation beam has been optimized. This decreases the beam attenuation and therefore the hardening in the PDD profile.

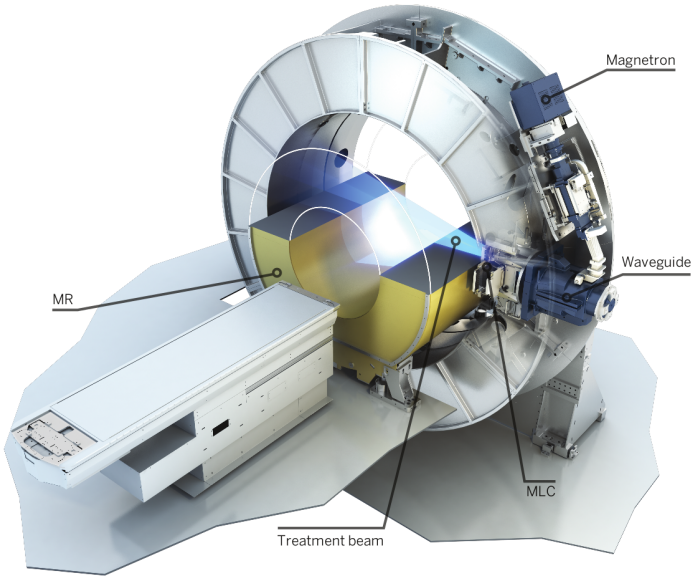

Figure 9.2: A visualization of the new MR-linac design.

9.8 Concluding remarks

In this thesis we have shown that reference dosimetry in the MR-linac is possible using an air filled ionization chamber. The dosimetry protocol is something that will need to be addressed in the future. For relative dosimetry there are several different methods. Many of these methods use their own specialized equipment. The magnetic field must be taken into account, e.g. during the equipment selection and the actual measurement procedure. But for all types of required dosimetry measurements, there is a magnetic field compatible option that can be used. Therefore, the magnetic field does not limit the standard dosimetry measurements options. Irradiating through the structures in the closed bore MRI scanner does influence the beam, but these can be accounted for in the beam model of the MR linac.

We expect that the future work wil expand on different devices in the MR-linac and also defining the procedures and requirements for the dosimetry and on-line QA in the MR-linac.

References

[1] Khan FM. The physics of radiation therapy. 3rd ed, 2003. *Williams and Wilkins*.

[2] ICRU 50. Prescribing, recording and reporting photon beam therapy. 1993. *ICRU Bethesda Maryland*.

[3] ICRU 62. Prescribing, Recording and Reporting Photon Beam Therapy (Supplement to ICRU Report 50). 1999. *ICRU Bethesda Maryland*.

[4] Burnet NG, Thomas S, E BK, Jefferies SJ. Defining the tumour and target volumes for radiotherapy. *Chancer Imaging* 2004;4:153–61.

[5] AAPM 166. The use and QA of biologically related models for treatment planning. 2012. *American Association of Physicists in Medicine*.

[6] van Herk M, Remeijer P, Rasch C, Lebesque JV. The probability of correct target dosage: dose-population histograms for deriving treatment margins in radiotherapy. *Int. J. Radiat. Oncol. Biol. Phys.* 2000;47:1121–1135.

[7] Stroom J, Gilhuijs K, Vieira S, *et al.* Combined recepe for clinical target volume and planning target volume margins. *Int. J. Radiat. Oncol. Biol. Phys.* 2014;88:708–714.

[8] Verellen D, Ridder MD, Linthout N, Tournel K, Soete G, Storme G. Innovations in image-guided radiotherapy. *Nat Rev Cancer* 2007;7:949–960.

[9] Colgan R, McClelland J, McQuaid D, *et al.* Planning lung radiotherapy using 4D CT data and a motion model. *Phys. Med. Biol.* ;53.

[10] Differding S, Hanin FX, Grégoire V. PET imaging biomarkers in head and neck cancer. *Eur. J. Nucl. Med. Mol. Imaging* ;.

[11] Sergieva S, Mihailova I, Zahariev Z, Dimcheva M, Bozhikov S. Role of SPECT-CT in radiotherapy. *J BUON.* 2014;3:831–835.

[12] van der Meer S, Bloemen-van Gurp E, Hermans J, *et al.* Critical assessment of interamodality 3D ultrasound imaging for prostate IGRT compared to fiducial markers. *Med. Phys.* 2013;40.

[13] Groenendaal G, Moman MR, Korporaal JG, *et al.* Validation of functional imaging with pathology for tumor delineation in the prostate. *Radiother. Oncol.* 2010;94:145–150.

[14] Bentzen SM. Theragnostic imaging for radiation oncology: dose-painting by numbers. *Lancett Oncology* 2005;6:112–117.

[15] Ling CC, Humm J, Larson S, *et al.* Towards multidimensional radiotherapy (MD-CRT): biological imaging and biological conformality. *Int. J. Radiat. Oncol. Biol. Phys.* 2000; 47:551–560.

[16] Heijmen BJ, Pasma KL, Kroonwijk M, *et al.* Portal dose measurement in radiotherapy using an electronic portal imaging device (EPID). *Phys. Med. Biol.* 1995;40:1943–55.

[17] Nederveen AJ, Dehnad H, Van der Heide UA, Van Moorselaar RJA, Hofman P, Lagendijk JJW. Comparison of megavoltage position verification for prostate irradiation based on bony anatomy and implanted fiducials. *Radiother. Oncol.* 2003;68:81–88.

[18] Van der Heide UA, Kotte ANTJ, Dehnad H, Hofman P, Lagendijk JJW, Van Vulpen M. Analysis of fiducial marker-based position verification in the external beam radiotherapy of patients with prostate cancer. *Radiother. Oncol.* 2007;82:38–45.

[19] Uematsu M, Fukui T, Shioda A, *et al.* A dual computed tomography linear accelerator unit for stereotactic radiation therapy: a new approach without cranially fixated stereotactic frames. *Int. J. Radiat. Oncol. Biol. Phys.* 1996;35:587–592.

[20] Jaffray DA, Siewerdsen JH, Wong JW, Martinez AA. Flat-panel cone-beam computed tomography for image-guided radiation therapy. *Int. J. Radiat. Oncol. Biol. Phys.* 2002; 53:1337–1349.

[21] McNair HA, Mangar SA, Coffey J, *et al.* A comparison of CT-and ultrasound-based imaging to localize the prostate for external beam radiotherapy. *Int. J. Radiat. Oncol. Biol. Phys.* 2006;65:678–687.

[22] de Boer HC, van Sörnsen de koste JR, Creutzberg CL, Visster AG, Levendag PC, Heijmen BJ. Electronic portal image assisted reduction of systematic set-up errors in head and neck irradiation. *Radiother. Oncol.* 2001;61:299–308.

[23] Murthy V, Master Z, Adurkar P, *et al.* 'plan of the day' adaptive radiotherapy for bladder cancer using helical tomotherapy. *Radiother. Oncol.* 2011;99:55–60.

[24] Heijkoop ST, Langerak TR, Quint S, *et al.* Clinical implementation of an online adaptive plan-of-the-day protocol for nonrigid motion management in locally advanced cervical cancer IMRT. *Int. J. Radiat. Oncol. Biol. Phys.* 2014;90:673–979.

[25] Ahunbay EE, Peng C, Godley A, Schultz C, Li XA. An on-line replanning method for head and neck adaptive radiotherapy. *Med. Phys.* 2009;36:4776.

[26] Mohan R, Zhang X, Wang H, *et al.* Use of deformed intensity distributions for on-line modification of image-guided IMRT to account for interfractional anatomic changes. *Int. J. Radiat. Oncol. Biol. Phys.* 2005;61:1258–66.

[27] Kitamura K, Shirato H, Seppenwoolde Y, *et al.* Tumor location, cirrhosis, and surgical history contribute to tumor movement in the liver, as measured during stereotactic irradiation using a real-time tumor-tracking radiotherapy system. *Int. J. Radiat. Oncol. Biol. Phys.* 2003;56:221–228.

[28] Van Sörnsen de Koste JR, Senan S, Kleynen CE, Slotman BJ, Lagerwaard FJ. Renal mobility during uncoached quiet respiration: An analysis of 4DCT scans. *Int. J. Radiat. Oncol. Biol. Phys.* 2006;64:799–803.

[29] Wolthaus JWH, Sonke JJ, van Herk M, *et al.* Comparison of different strategies to use four-dimensional computed tomography in treatment planning for lung cancer patients. *Int. J. Radiat. Oncol. Biol. Phys.* 2008;70:1229–1238.

[30] Seppenwoolde Y, Berbeco RI, Nishioka S, Shirato H, Heijmen B. Accuracy of tumor motion compensation algorithm from a robotic respiratory tracking system: a simulation study. *Med. Phys.* 2007;34:2774–2784.

[31] Hugo GD, Agazaryan N, Solberg TD. The effects of tumor motion on planning and delivery of respiratory-gated IMRT. *Med. Phys.* 2003;30:1052–2525.

[32] George R, Chung TD, Vedam SS, *et al.* Audio-visual biofeedback for respiratory-gated radiotherapy: impact of audio instruction and audio-visual biofeedback on respiratory-gated radiotherapy. *Int. J. Radiat. Oncol. Biol. Phys.* 2006;65:924–933.

[33] Poulsen PR, Cho B, Ruan D, Sawant A, Keall PJ. Dynamic multileaf collimator tracking of respiratory target motion based on a single kilovoltage imager during arc radiotherapy. *Int. J. Radiat. Oncol. Biol. Phys.* 2010;77:600–607.

[34] Karlsson M, Karlsson MG, Nyholm T, Amies C, Zackrisson B. Dedicated magnetic resonance imaging in the radiotherapy clinic. *Int. J. Radiat. Oncol. Biol. Phys.* 2009; 74:644–651.

[35] Jaffray DA, Carlone MC, Milosevic MF, *et al.* A facility for magnetic resonance-guided radiation therapy. *Semin. Radiat. Oncol.* 2014;24.

[36] Raaymakers BW, Raaijmakers AJE, Kotte ANTJ, Jette D, , Lagendijk JJW. Integrating a MRI scanner with a 6 MV radiotherapy accelerator: dose deposition in a transverse magnetic field. *Phys. Med. Biol.* 2004; 4109–4118.

[37] Fallone BG, Murray B, Rathee S, *et al.* First MR images obtained during megavoltage photon irradiation from a prototype integrated linac-MR system. *Med. Phys.* June, 2009;36:2084–2088.

[38] Fallone BG. The rotating biplanar linac-magnetic resonance imaging system. *Semin. Radiat. Oncol.* 2014;24:200–2.

[39] Low DA, Stark R, Dempsy JF. Adaptive Motion Compensation in Radiotherapy. Imaging in Medical Diagnosis and Therapy. CRC Press, 2011; 115–128.

[40] Raaymakers BW, Lagendijk JJW, Overweg J, *et al.* Integrating a 1.5 T MRI scanner with a 6 MV accelerator: proof of concept. *Phys. Med. Biol.* 2009;54:N229–237.

[41] Raaijmakers AJ, Raaymakers BW, Lagendijk JJW. Integrating a MRI scanner with a 6MV radiotherapy accelerator: dose increase at tissue-air interfaces in a lateral magnetic field due to returning electrons. *Phys. Med. Biol.* 2005;7:1363.

[42] Raaijmakers AJ, Raaymakers BW, van der Meer S, Lagendijk JJW. Integrating a MRI scanner with a 6MV radiotherapy accelerator: impact of the surface orientation on the entrance and exit dose due to the transverse magnetic field. *Phys. Med. Biol.* 2007; 4:929.

[43] Raaijmakers AJ, Raaymakers BW, Lagendijk JJW. Magnetic-field-induced dose effects in MR-guided radiotherapy systems: dependence on the magnetic field strength. *Phys. Med. Biol.* 2007;4:909.

[44] Kirkby C, Murray B, Rathee S, Fallone BG. Lung dosimetry in a linac-MRI radiotherapy unit with a longitudinal magnetic field. *Med. Phys.* 2010;37:4722–32.

[45] Reynolds M, Fallone BG, Rathee S. Dose response of selected ion chambers in applied homogeneous transverse and longitudinal magnetic fields. *Med. Phys.* 2013;10.

[46] Raaijmakers AJ, Raaymakers BW, Lagendijk JJW. Experimental verification of magnetic field dose effects for the MRI-accelerator. *Phys. Med. Biol.* 2007;14:4283.

[47] Oborn BM, Metcalfe PE, Butson MJ, Rosenfeld AB. Monte Carlo characterization of skin doses in 6 MV transverse field MRI-linac systems: effect of field size, surface orientation, magnetic field strength, and exit bolus. *Med. Phys.* 2010;37:5208–17.

[48] Oborn BM, Metcalfe PE, Butson MJ, Rosenfeld AB, Keall PJ. Electron contamination modeling and skin dose in 6 MV longitudinal field MRIgRT: Impact of the MRI and MRI fringe field. *Med. Phys.* 2012;39:874–90.

[49] NCS 18. Code of Practice for the absorbed dose determination in high energy photon and electron beams. 2012. *Nederlandse Commissie voor Stralingsdosimetrie*.

[50] AAPM 51. AAPM's TG-51 protocol for clinical reference dosimetry of high-energy photon and electron beams. 1999. *American Association of Physicists in Medicine*.

[51] Meijsing I, Raaymakers BW, Raaijmakers AJ, *et al.* Dosimetry for the MRI accelerator: the impact of a magnetic field on the response of a Farmer NE2571 ionization chamber. *Phys. Med. Biol.* 2009;54:2993–3002.
[52] O'Neill MJ, Lam WC, Partowmah M, Khalifeh A. External beam profiles measured with film or ionization chamber. *Med. Dosim.* 1988;13:167–9.
[53] AAPM 106. Accelerator beam data commissioning equipment and procedures: Report of the TG-106 of the Therapy Physics Committe of the AAPM. 2008. *American Association of Physicists in Medicine*.
[54] AAPM 13. Physical aspects of quality assurance in radiation therapy. 1994. *American Association of Physicists in Medicine*.
[55] NCS 8. Kwaliteitscontrole van Medische Lineaire Versnellers, methoden voor kwaliteitscontrole. 1995. *Nederlandse Commissie voor Stralingsdosimetrie*.
[56] AAPM 46. Comprehensive QA for radiation oncology. 1994. *American Association of Physicists in Medicine*.
[57] Lagendijk JJW, Raaymakers BW, Raaijmakers AJE, *et al.* MRI/linac integration. *Radiother. Oncol.* 2008;86:25–29.
[58] IAEA 398. Absorbed dose determination in external beam radiotherapy. 2000. *International Atomic Energy Agency*.
[59] Lillicrap SC, Owen B, Williams JR, Williams PC. Code of practice for high-energy photon therapy dosimetry based on the NPL absorbed dose calibration service. *Med. Phys.* 1990;35:1355–1360.
[60] Tessier F, Kawrakow I. Effective point of measurement of thimble ion chambers in megavoltage photon beams. *Med. Phys.* 2010;37:96–107.
[61] Weinhous MS, Meli JA. Determining P_{ion}, the correction factor for recombination losses in an ionization chamber. *Med. Phys.* 1984; 846–849.
[62] Bedford RE, J QT. Techniques for approximating the international temperature scale of 1990. *Working group 2 of the Comité Consultatief de Thermométrie* 1993; 253–260.
[63] Boag JW. The saturation curve for ionization measurements in pulsed radiation beams. *Br. J. Radiol.* 1952;25:649–650.
[64] Boag JW. Ionization chambers. *Br. J. Radiol.* 1966;2:968–976.
[65] Jaffé G. On the theory of recombination. *Phys. Rev.* 1940;58:193–195.
[66] Smit K, van Asselen B, Kok JGM, Aalbers AHL, Lagendijk JJW, Raaymakers BW. Towards reference dosimetry for the MR-linac: magnetic field correction of the ionization chamber reading. *Phys. Med. Biol.* 2013;58:5945–5957.
[67] Wijlemans JW, Bartels LW, Deckers R, *et al.* Magnetic resonance-guided high-intensity focused ultrasound (MR-HIFU) ablation of liver tumours. *Cancer Imaging* 2012;12:387–394.
[68] Mellenberg DE, Dahl RA, Blackwell CR. Acceptance testing of an automated scanning water phantom. *Phys. Med. Biol.* 1990;17:311–314.
[69] Simon TA, Kozelka J, Simon WE, Kahler D, Li J, Liu C. Characterization of a multi-axis ion chamber array. *Med. Phys.* 2010;37:6101–6111.
[70] Micke A, Lewis DF, Yu X. Multichannel film dosimetry with nonuniformity correction. *Med. Phys.* 2011;38:2523–2534.
[71] Smit K, Kok JGM, Lagendijk JJW, Raaymakers BW. Performance of a multi-axis ionization chamber array in a 1.5 T magnetic field. *Phys. Med. Biol.* 2014;59:1845–1855.

[72] Lee L, Mao W, Xing L. The use of epid-measured leaf sequence files for imrt dose reconstruction in adaptive radiation therapy. *Med. Phys.* 2008;35:5019–29.
[73] Essers M, Hoogervorst BR, van Herk M, Lanson H, Mijnheer BJ. Dosimetric characteristics of a liquid-filled electronic portal imaging device. *Int. J. Radiat. Oncol. Biol. Phys.* 1995;33:1265–72.
[74] Ford EC, Chang J, Mueller K, *et al.* Cone-beam CT with megavoltage beams and an amorphous silicon electronic portal imaging device: potential for verification of radiotherapy of lung cancer. *Med. Phys.* 2002;29:2913–24.
[75] Overweg J, Raaymakers BW, Lagendijk JJW, Brown K. System for MRI guided radiotherapy. *In Proceedings ISMRM* 2009; Abstr. 593.
[76] Rajapakhe R, Luchka K, S S. A quality control test for electronic portal imaging devices. *Med. Phys..* 1996;23:1237–44.
[77] Dong L, Boyer AL. An objective method for evaluating electronic portal imaging devices. *Med. Phys.* 1994;21:755–60.
[78] De Boer JCJ, Barnhoorn JC, Heijmen BJM. RankingEPID image quality: standard methods and their clinical relevance. *Radiother. Oncol.* 2004;73:S139.
[79] Moerland MA, Beersma R, Bhagwandien R, Wijrdeman HK, Bakker CJG. Analysis and correction of geometric distortions in 1.5 T magnetic resonance images for use in radiotherapy treatment planning. *Phys. Med. Biol.* 1995;40:1651–1664.
[80] Crijns SPM, Raaymakers BW, Lagendijk JJW. Real-time correction of magnetic field inhomogeneity-induced image distortions for MRI-guided conventional and proton radiotherapy. *Phys. Med. Biol.* 2011;56:289–297.
[81] Lagendijk JJW, Raaymakers BW, van Vulpen M. The magnetic resonance imaging-linac system. *Semin. Radiat. Oncol.* 2014;24:207–209.
[82] Smit K, Sjöholm J, Kok JGM, Lagendijk JJW, Raaymakers BW. Relative dosimetry in a 1.5 T magnetic field: an MR-linac compatible prototype scanning water phantom. *Phys. Med. Biol.* 2014;59:4099–4109.
[83] Raaymakers BW, J dJC, Knox C, *et al.* Integrating a 1.5 T MRI scanner with a 6 MV accelerator: proof of concept. *Phys. Med. Biol.* 2011;56:N207–N214.
[84] Hussein M, Rowshanfarzad P, Ebert MA, Nisbet A, Clark CA. A comparison of the gamma index analysis in various commercial IMRT/VMAT QA systems. *Radiother. Oncol.* 2013;109:370–376.
[85] Li G, Zhang Y, Jang X, *et al.* Evaluation of the ArcCHECK QA system for IMRT and VMAT verification. *Phys. Med.* 2013;29:295–303.
[86] Bol GH, Hissoiny S, Lagendijk JJW, Raaymakers BW. Fast online Monte Carlo-based IMRT planning for the MRI linear accelerator. *Phys. Med. Biol.* 2012;57:1375–85.
[87] Keall PJ, Barton M, Crozier S. The Australian magnetic resonance imaging-linac program. *Med. Phys.* 2014;24:203.
[88] Salvat F, Fernandez-Varea JM, Sempau J. PENELOPE-2006 A code system for Monte Carlo simulation of electron and photon transport. *OECD/Nuclear Energy Agency Issy-les-molineaux* 2006;.
[89] Baro J, Sempau J, Fernandez-Varea JM, Salvat F. PENELOPE: An algorithm for monte carlo simulation of the penetration and energy loss of electrons and positrons in matter. *Nucl. Instrum. Meth B* 995;100:31–46.
[90] Low DA. Gamma dose distribution evaluation tool. *Journal of Physics: Conference series* 2011;250:012071.

[91] Van Swinden Laboratory. *http://www.vsl.nl/en/new-vsl-water-calorimeter-ready-future* 2015;.
[92] Gargett M, Oborn B, Metcalfe P, Rosenfeld A. Monte Carlo simulation of the dose response of a novel 2D silicon diode array for use in hybrid MRI-LINAC systems. *Med. Phys.* 2015;42:856.
[93] Mans A, Wendling M, McDermott LN, *et al.* Catching errors with in vivo EPID dosimetry. *Med. Phys.* 2010;37:2638–44.
[94] Mijnheer B, Beddar S, Izewska J, Reft C. In vivo dosimetry in external beam radiotherapy. *Med. Phys.* 2013;40.
[95] Fast M F, Nill S, Bedford JL, Oelfke U. Dynamic tumor tracking using the Elekta Agility MLC. *Med. Phys.* 2014;41.
[96] Ceberg S, Lepage M, Bäck Sr, Gustafsson H, Ceberg C. Modelling the dynamic dose response of an nMAG polymer gel dosimeter. *Phys. Med. Biol.* 2008;57:4845–53.
[97] Bol GH, Lagendijk JJW, Raaymakers BW. Virtual couch shift (VCS): accounting for patient translation and rotation by online IMRT re-optimization. *Phys. Med. Biol.* 2013;58:2989–3000.
[98] Hoogcarspel SJ, van der Velden JM, Lagendijk JJW, van Vulpen M, Raaymakers BW. The feasibility of utilizing pseude CT-data for online MRI based treatment plan adaptation for stereotactic radiotherapy treatment of spinal bone metastases. *Phys. Med. Biol.* 2014;59:7383–91.
[99] Gurdur MS, Hara W, Le QT, Wang L, Xing L, Li R. A unifying probabilistic bayesian approach to derive electron density from MRI for radiation therapy treatment planning. *Phys. Med. Biol.* 2014;59:6595–606.
[100] Lee YK, Bollet M, Charles-Edwards G, *et al.* Radiotherapy treatment planning of prostate cancer using magnetic resonance imaging alone. *Radiother. Oncol.* 2003; 66:203–216.
[101] Roujol S, Ries M, Moonen C, de Senneville BD. Automatic nonrigid calibration of image registration for real time MR-guided HIFU ablations of mobile organs. *IEEE Trans. Med. Imaging.* 2011;30:1737–45.
[102] Bolme DS, Beveridge JR, Draper Ba, Lui YM. Visual object tracking using adaptive correlation filters. *IEEE conference on computer vision and pattern recognition* 2010; 2544.

10

Publications

Published papers

Relative dosimetry in a 1.5 T magnetic field: an MR-linac compatible prototype scanning water phantom K. Smit, J. Sjöholm, J.G.M. Kok, J.J.W. Lagendijk and B.W. Raaymakers *Physics in Medicine and Biology* 2014 **59** 4099–109

Performance of a multi-axis ionization chamber array in a 1.5 T magnetic field K. Smit, J.G.M. Kok, J.J.W. Lagendijk and B.W. Raaymakers *Physics in Medicine and Biology* 2014 **59** 1845–55

Towards reference dosimetry for the MR-linac: magnetic field correction of the ionization chamber reading K. Smit, J.G.M. Kok, A.H Aalbers, J.J.W. Lagendijk and B.W. Raaymakers *Physics in Medicine and Biology* 2013 **58** 5945–57

Integrated megavoltage portal imaging with a 1.5 T MRI-linac B.W. Raaymakers, J.C. de Boer, C. Knox, S.P. Crijns, K. Smit, M.K. Stam, M.R. van den Bosch, J.G.M. Kok and J.J.W. Lagendijk *Physics in Medicine and Biology* 2011 **56** N207–14

Proceedings and abstracts

Characterization of a multi-axis ionization chamber array in a 1.5 T magnetic field K. Smit, J.G.M. Kok, J.J.W. Lagendijk, and B.W. Raaymakers *2nd ESTRO Forum 2013, Geneva, Switzerland*

Reference Dosimetry for an MRI-linac: the magnetic field correction factor K. Smit, B. Asselen, J.G.M. Kok, J.J.W. Lagendijk and B.W. Raaymakers *AAPM annual meeting 2012, Charlotte, NC*

Dosimeter characterisation in a magnetic field: dosimetry for a 1.5 T MRI-linac hybrid K. Smit, J.G.M. Kok, B.W. Raaymakers and J.J.W. Lagendijk *ESTRO Anniversary Congress 2011, London, England*

Initial scatter characterization for a 1.5 T MRI accelerator: Geant4 Monte Carlo simulations and measurements K. Smit, A.J.E. Raaijmakers, J.W. Wolthaus, J.G.M. Kok, B.W. Raaymakers and J.J.W. Lagendijk *ESTRO annual meeting 2010, Barcelona, Spain*

Beam characterization for an MRI-radiotherapy system: measurements and Monte Carlo simulations K. Smit, A.J.E. Raaijmakers, J.G.M. Kok, B.W. Raaymakers and J.J.W. Lagendijk *ICCR 16th Scientific Meeting, Amsterdam, The Netherlands*

11

Nederlandse Samenvatting

Radiotherapie en MRI

Tijdens een radiotherapie behandeling worden maligne cellen bestraald met fotonen. Deze fotonen maken tijdens interactie met weefsels elektronen vrij die moleculen in weefsels kunnen ioniseren. DNA moleculen kunnen op deze manier beschadigd raken. In gezonde cellen zijn mechanismen om het DNA weer te herstellen, maar in tumorcellen zijn deze mechanismen vaak niet meer intact, waardoor de cel afsterft. Met behulp van medische beelden kan het behandelsucces van een radiotherapeutische behandeling vergroot worden. De informatie kan gebruikt worden om de tumorkarakteristieken te bepalen en de precieze locatie en vorm van de tumor te bepalen. MRI is hiervoor vanwege het hoge contrast in de zachte weefsels de beste afbeeldingsmodaliteit.

De mogelijke voordelen van beeldvorming in de radiotherapie worden nog groter wanneer de beeldvorming gedaan kan worden tijdens de behandeling. Hiervoor zijn verschillende ontwerpen die een MRI scanner en een radiotherapie modaliteit combineren. Het UMC Utrecht heeft in samenwerking met Elekta (Elekta AB, Stockholm, Sweden) en Philips (Philips Medical Systems, Best, Nederland) een prototype gerealiseerd waarin het een 6 MV staande golf lineaire versneller gecombineerd wordt met een 1.5 T MRI scanner. De lineaire versneller is geplaatst op een ring om de MRI heen, waardoor het isocentrum van de lineaire versneller overeen komt met dat van de MRI scanner. De geometrie in de MRI scanner is aangepast hierdoor ontstaat een 'raam' waar slechts het equivalent van 11.5 cm aluminium aan materiaal in de stralingsbundel aanwezig is.

Het combineren van de MRI met een lineaire versneller beïnvloed de afgegeven dosis op 2 manieren. Ten eerste wordt de stralingsdosis afgegeven in een sterk magnetisch veld. De fotonen in de stralingsbundel hebben hier geen last van, maar de elektronen worden tijdens hun beweging afgebogen door de Lorentzkracht. Daarnaast moet de straling door verschillende structuren van de MRI heen voordat deze bij het isocentrum aankomt. Hierdoor verminderd de hoeveelheid fotonen, maar wordt de gemiddelde energie van de fotonen hoger doordat fotonen met een lage energie een grotere kans hebben om een interactie te hebben in de MRI structuren.

Referentie dosimetrie in de MR-linac

Hoofdstuk 2 beschrijft onderzoek naar de mogelijkheid om het signaal van een ionisatiekamer te corrigeren voor het magnetisch veld van de MRI scanner, binnen de (inter) nationale referentie dosimetrie protocollen. Ten eerste wordt de invloed van het magneetveld op het functioneren van de NE2571 ionisatiekamer onderzocht. De lineariteit, reproduceerbaarheid en de invloed van de oriëntatie in het magneetveld worden onderzocht. Daarnaast wordt de invloed van het magneetveld op de correctiefactoren voor de ion recombinatie en polariteit van de ionisatiekamer onderzocht. De metingen laten zien dat de correctiefactoren en het functioneren van de NE2571 niet beïnvloed worden door het magnetisch veld. Ten tweede wordt de invloed van het magneetveld op de gemeten waarde onderzocht. Hieruit blijkt dat de gemeten waarde met ongeveer 4.9% toeneemt door de aanwezigheid van een transvers 1.5 T magnetisch veld. Deze invloed kan gecorrigeerd worden met een correctiefactor voor het magnetisch veld ($k_{1.5\ T}$), welke een waarde van 0.953 zal hebben voor de onderzochte setup.

Relatieve dosimetrie in de MR-linac

In hoofdstuk 3 wordt een scannend water fantoom gepresenteerd die in de MR-linac gebruikt kan worden. Omdat dit type fantoom ionisatiekamers gebruikt voor de dosismetingen wordt het functioneren van de lucht gevulde ionisatiekamers onderzocht in de MR-linac. De lineariteit en reproduceerbaarheid van de ionisatiekamers worden niet beïnvloed door het magneetveld. Daarnaast wordt onderzocht of het bewegen en de oriëntatie van aanstralen in een magneetveld invloed heeft op de gemeten waarden. Alhoewel het bewegen geen invloed heeft, wordt een maximale mogelijke invloed van 0.4% gevonden voor de oriëntaties van aanstralen. Dit effect kan teniet gedaan worden door de ionisatiekamer 90° te draaien voor aanvang van de meting. Een vergelijking van klinische dosisprofielen gemeten met een standaard water fantoom en het MR-linac water fantoom laat geen significante verschillen zien. In de MR-linac worden de dosisprofielen gemeten met het MR-linac water fantoom vergeleken met profielen gemeten met radiochromische film, ook hier waren geen significante verschillen te zien. Deze resultaten laten zien dat metingen met lucht gevulde ionisatiekamers in een scannend water fantoom mogelijk zijn in de MR-linac.

Hoofdstuk 4 onderzoekt het functioneren van een IC PROFILER™ (Sun Nuclear Corporation, Melbourne, FL USA) ionisatiekamer panel in de MR-linac. Dit type panel bevat arrays van ionisatiekamers die op meerdere assen geplaatst zijn. De lineariteit, reproduceerbaarheid, invloed van PRF van de versneller en de opwarmtijd zijn vergelijkbaar voor de situatie met en zonder magneetveld. De oriëntatie van de ionisatiekamers in het panel, en daarmee in het magneetveld, is van belang. Hiermee moet rekening gehouden worden wanneer de waarden van ionisatiekamers gelegen op verschillende assen vergeleken worden. Een vergelijking van dosisprofielen gemeten met de IC PROFILER™ en profielen gemeten met radiochromische film laat geen significante verschillen zien.

In hoofdstuk 5 wordt een vergelijkbaar panel als in hoofdstuk 4 onderzocht. Ook voor dit STARCHECK™ panel word de lineariteit, invloed van PRF van de versneller en de opwarmtijd niet beïnvloed door het magneetveld. De reproduceerbaarheid tijdens een 1 minuut lang durende meting is significant verhoogd met 0.03%, maar dit is geen klinisch relevante waarde.

Ook hier heeft de oriëntatie van de ionisatiekamer in het magneetveld invloed op de gemeten waarden, dit effect moet meegenomen worden bij het vergelijken en/of samenvoegen van signalen gemeten op meerdere assen. Voor dit STARCHECK^{TM} panel wordt aanbevolen om de ionisatiekamers in de centrale 2 x 2 cm2 niet mee te nemen in verdere analyse.

Hoofdstuk 6 laat zien dat het mogelijk is om een standaard aSI electonic portal imaging device (EPID) op de gantry te monteren tegenover de lineaire versneller. MR beeldvorming en EPID beeldvorming kan gedaan worden zonder interferentie De kwaliteit van de EPID beeldvorming is beperkt door de transmissie van de stralingsbundel door de MRI structuren heen en de vergrote afstand. Het meetbare gebied is verkleind door het stralings 'raam' in de MRI scanner. Door de integratie van deze EPID in de MR-linac is een onafhankelijk positie-verificatie, bijvoorbeeld voor veld rand metingen en/of uitlijning van de coördinatensystemen beschikbaar.

Hoofdstuk 7 onderzoekt het functioneren van de ArcCHECK-MR (Sun Nuclear Corporation, Melbourne, FL USA) in de MR-linac. Dit cilindrische fantoom omvat 1386 diodes die de afgegeven dosis meten. De gemeten dosis kan dan vergeleken worden met de dosis die berekend is door het TPS. De lineariteit, reproduceerbaarheid, dose rate afhankelijkheid, bundel grootte afhankelijkheid, inter diode variatie en de invloed van de dosis per pulse worden onderzocht bij een klinische versneller en in de MR-linac. Geen significante verschillen in functionaliteit worden gevonden. De grootste verschillen in gemeten dosis tussen de beiden lineaire versnellers zijn minder dan 1.5% daarom concluderen wij dat de ArcCHECK-MR gebruikt kan worden in het transverse magnetische veld van de MR-linac.

Het ontwerp van de MR-linac

Hoofdstuk 8 beschrijft computer simulaties over de invloed van de structuren in de MRI scanner op verschillende eigenschappen van de stralingsbundel voor verschillende veldgroottes. De Monte Carlo simulaties zijn geverifiëerd met metingen in de MR-linac. De MRI scanner structuren verzwakken de bundel met een factor van 3.5 (voor een 'klein' vierkant 5.6 cm veld) tot 2.9 (voor een 'groot' vierkant 23.8 cm veld). Deze verzwakking creeert ook een opharding van het energiespectrum, dit wordt terug gezien in de PDD profielen als een maximale verhoging van 1.9% van de dosis op 5 cm diep. De hoeveelheid scatter buiten de bundel wordt verhoogd door de structuren in de MRI, met 0.5%, 1.7% en 4.4% voor de 5.6, 9.8 en 23.8 cm bundels, respectievelijk.

Korte conclusie

In dit proefschrift hebben we aangetoond dat referentie dosimetrie in de MR-linac mogelijk is, maar dat het exacte protocol nog uit gezocht moet worden in de toekomst. Er zijn verschillende mogelijkheden voor relatieve dosimetrie in the MR-linac, veel van deze methoden gebruiken specifieke apparatuur. Het magneet veld moet tijdens de selectie van de apparatuur en het dagelijks gebruik in acht genomen worden. Maar dit proefschrift laat zien dat er voor veel dosimetrie procedures apparatuur beschikbaar is die veilig en correct gebruikt kan worden in het magneetveld. Het bestralen door de structuren van de MRI scanner heen beïnvloed de eigenschappen van de stralingsbundel, maar dit kan meegenomen worden in de bundel berekeningen.

12

Dankwoord

Promotieonderzoek doe je niet alleen, er zijn dan ook vele mensen die ik wil bedanken voor hun bijdrage. Als eerste mijn twee promotoren, Bas en Jan. Jan, jij vond het altijd zo jammer als we alleen bij je binnenkwamen voor een handtekening op een of ander formulier. Als hoofd van de afdeling kwam je dan ook regelmatig tussen het 'gewone volk' koffiepauze houden waarbij soms wat dingen boven de tafel kwamen die wij daarna fluisterend op onze kamer besproken: "Hadden we dat al mogen weten?". Schijnbaar zonder moeite zet je een MRI versneller en vervolgens een CBOI neer met een flink tal onderzoekslijnen. Dat je tussen al die bezigheden ook nog altijd tijd had om een artikel of abstract van goed (en kritisch) commentaar te voorzien is geweldig, waar je de tijd vandaan haalt voor al die bezigheden zal ik waarschijnlijk nooit snappen.
Bas, aan het begin van mijn promotietraject was je nog co-promotor nu al mijn promotor. Zelf ben je ontzettend druk geweest meer dan eens moest jij 1 of meerdere keren per week naar het buitenland. Toch kon ik altijd bij je aankloppen als ik hulp nodig had. En toen mijn contract afgelopen was, kon ik zonder aarzeling in het weekend bij jou thuis terecht om de feedback op mijn geschreven werk door te nemen. Jij hebt me de vrijheid gegeven om binnen het project mijn eigen richtingen te kiezen, natuurlijk met wat sturing door kritische vragen op de juiste momenten. Dit was voor mij een ontzettende leerzame ervaring die niet in een boekje of ceremonie te meten is, maar waar ik de rest van mijn leven plezier van zal hebben.

Sjoerd, zonder jouw goede voorbeeld was ik waarschijnlijk nooit aan een promotie begonnen, en zonder jouw therapie sessies op en naast de squashbaan had ik het waarschijnlijk niet afgemaakt. Daarnaast zijn er natuurlijk nog de nodige spelletjesmiddagen en andere bijeenkomsten geweest waarbij promoties altijd nog even besproken werden.
Anette, dank je wel voor de vliegende start van mijn promotie, ik heb met name dat eerste jaar zo ontzettend veel geleerd. Je hebt de lat ongelofelijk hoog gelegd voor de kamergenoten die jou opvolgden. Ik ben heel blij dat we elkaar nog steeds regelmatig zien, ook nu we niet meer samen werken. Zelfs na maanden aan de andere kant van de wereld is he in de eerste minuut weer als vanouds.
Frank en Mariska bedankt voor alle liedjes die ik nooit meer uit mijn hoofd krijg, maar natuurlijk het meest voor alle gezellige momenten in de jaren dat wij een kamer gedeeld hebben.

Hebben de haai en de achtbaan al een huis gevonden? Alle (ex-)OiOs van de radiotherapie wil ik graag bedanken voor de gezellige lunches, koffiepauzes en andere bijeenkomsten.

Arna bedankt voor de gezellige sportavonden, met afstand de leukste manier om spierpijn te kweken. Alle verschillende spelletjesmiddag-gangers bedankt voor de gezellige tijden en voor de leuke gesprekken, met name WC-borstel werpen en de Gesaboteerde-Saboteur zijn ware toppers. Een datum vinden waarop zo veel mogelijk mensen kunnen komen zal niet makkelijker worden, maar we blijven ons best doen!

Jan, met gemengde gevoelens kijk ik terug op de tijd waar je, na een paar MU stralen, de modulator moest resetten om vervolgens 15 minuten te moeten wachten. Het meten ging extreem traag maar met jou erbij was het altijd gezellig! Ook je vele knutselprojectjes zal ik zeker gaan missen. De leden van de beoordelingscommissie wil ik graag bedanken voor het kritisch lezen van dit proefschrift. De versneller technici en fysisch medewerkers wil ik bedanken voor hun mee-denken, mee-meten en geduld als ik weer met een leuk projectje of vraag aanklopte. De medewerkers van mijn nieuwe werk bij het functiecentrum van de KNO wil ik graag bedanken voor de leuke werksfeer en alle mooie momenten die nog komen gaan.

Mam en Pap, jullie wil ik graag bedanken voor alles wat jullie mij geleerd hebben. Dat ik dit promotietraject af kan ronden komt door de goede basis die jullie (met veel pijn en moeite) aan mij geleerd hebben. Ik kan altijd even bellen voor advies of een goede raad, of om gewoon even bij te kletsen. Michiel, ik ben en blijf altijd je kleine zusje, maar ook kleine zusjes kunnen ontzettend trots zijn op hun grote broer!
Eugenie, bedankt voor alle gezellige filmavonden en het bedenken van de outfits voor de thema-avonden. Hopelijk heb ik nu meer tijd om ook achter de naaimachine te kruipen De hele familie Snel wil ik bedanken dat ze mij zo geweldig opgenomen hebben in de familie.

Isabelle, je weet iedereen om je heen op te vrolijken met je mooie lach en ondeugende ogen. Zonder jouw oneindige voorraad vrolijkheid (en goede slaapgewoontes) had dit boekje veel langer op zich laten wachten.
Egbert, ik ben nog nooit zoooo blij geweest dat ik een trein gehaald heb. Door jouw steun eeuwige optimisme is dit boekje waarheid geworden. Als we nagenoeg probleemloos in 1 jaar een huis verkopen, verhuizen, bij je ouders inwonen, een nieuw huis afmaken, nog een keer verhuizen, een promotie afronden, een nieuwe baan zoeken, een wietkwekerij op kunnen rollen én een baby kunnen krijgen; dan weet ik dat we samen alles aankunnen. Ik heb zin in onze toekomst samen!

Kimmy